Title
ELECTRONIC AND NUCLEAR PROPERTIES OF SOME RADIOACTIVE RARE-EARTH ELEMENTS

Author
Cabezas, Amado Y.

Publication Date
1960-08-09

UNIVERSITY OF CALIFORNIA

Ernest O. Lawrence Radiation Laboratory

BERKELEY, CALIFORNIA

DISCLAIMER

UCRL-9346
UC-4 Physics and Mathematics
TID-4500 (15th Ed.)

UNIVERSITY OF CALIFORNIA

Lawrence Radiation Laboratory
Berkeley, California

Contract No. W-7405-eng-48

ELECTRONIC AND NUCLEAR PROPERTIES OF SOME RADIOACTIVE RARE-EARTH ELEMENTS

Amado Y. Cabezas

(Thesis)

August 9, 1960

ELECTRONIC AND NUCLEAR PROPERTIES OF SOME RADIOACTIVE RARE-EARTH ELEMENTS

Contents

ELECTRONIC AND NUCLEAR PROPERTIES OF SOME RADIOACTIVE RARE-EARTH ELEMENTS

Amado Y. Cabezas

Lawrence Radiation Laboratory
University of California
Berkeley, California

August 9, 1960

ABSTRACT

Ground-state nuclear spins of thirteen radioactive rare earths (lanthanides) have been measured by the atomic-beam magnetic-resonance method. Ground levels (J) and corresponding g values of four rare earths have been determined. Ground-state electronic configurations have been inferred for the following elements:

Atomic number	Element	Observed ground levels	Ground-state electronic configuration
61	promethium	$^6H_{(5/2),\,7/2,\,9/2}$	$4f^5\,6s^2$
66	dysprosium	$^5I_8$	$4f^{10}\,6s^2$
67	holmium	$(^4I_{15/2})$	$(4f^{11}\,6s^2)$
68	erbium	$^3H_6$	$4f^{12}\,6s^2$

The configuration assigned to holmium is tentative in view of the measurement $I = 0$ for Ho^{166}, which does not allow an unambiguous determination of the J levels. The basis of the assumption is the close agreement between the measured g_J and the pure Russell-Saunders value for $^4I_{15/2}$.

In addition, these electronic properties have also been verified for the following rare earths:

Atomic number	Element	Observed ground levels	Ground-state electronic configuration
59	praseodymium	$^4I_{9/2}$	$4f^3\ 6s^2$
60	neodymium	$^5I_4$	$4f^4\ 6s^2$
62	samarium	$^7F_{(0),1,2}$	$4f^6\ 6s^2$
64	gadolinium	$^9D_{2,3,4,5}$	$4f^7\ 5d\ 6s^2$
65	terbium	$^6H_{15/2}$ and $([^7F_6, {}^2D_{3/2}]_{15/2, 13/2, 11/2})$	$4f^9\ 6s^2$ and $(4f^8\ 5d\ 6s^2)$
69	thulium	$^2F_{7/2}$	$4f^{13}\ 6s^2$

The following isotopes were used in these investigations. The half lives, nuclear ground-state spins, and J and g_J values are also stated:

Pr^{142} ($T_{1/2}$ = 19 hr) I = 2
with J = 9/2,* g_J = -0.7311(3)
$|a|$ = 67.5(1.0) Mc, $|\mu_I|$ = 0.30(2) n m
$|b|$ = 7(2) Mc, $|Q|$ = 0.035(15) barns

Nd^{147} ($T_{1/2}$ = 11.6 d) I = 5/2
with J = 4* g_J = - 0.6032(1)*

Pm^{147}	($T_{1/2}$ = 2.6 yr)	I = 7/2
	with J = 5/2,	g_J = - 0.286 (not observed)
	J = 7/2,	g_J = - 0.831(5)
	J = 9/2,	g_J = - 1.068 (4)
Sm^{153}	($T_{1/2}$ = 47 hr)	I = 3/2
	with (J = 0)	(not observed)
	J = 1*	g_J = - 1.495(15)
	J = 2*	g_J = - 1.497(15)
Gd^{159}	($T_{1/2}$ = 18 hr)	I = 3/2
	with J = 2*	g_J = - 2.6514(3)*
	J = 3*	g_J = - 2.0708(2)*
	J = 4*	g_J = - 1.8392(2)*
	J = 5*	g_J = - 1.725(7)*
Tb^{160}	($T_{1/2}$ = 72 d)	I = 3
	with J = 15/2*	g_J = - 1.3225*
	J = 15/2*	g_J = - 1.4563*
	J = 13/2*	g_J = - 1.4633*
	J = 11/2*	g_J = - 1.5165*
Dy^{165}	($T_{1/2}$ = 2.3 hr)	I = 7/2
Dy^{166}	($T_{1/2}$ = 82 hr)	I = 0
	with J = 8	g_J = - 1.2415(3)
Ho^{166}	($T_{1/2}$ = 27 hr)	I = 0 or I ≠ 0 with very small hfs (a<100 kc)
	with (J = 15/2)	g_J = - 1.1956(12)

Er^{169} ($T_{1/2}$ = 9.4 d) I = 1/2

Er^{171} ($T_{1/2}$ = 7.5 hr) I = 5/2

with J = 6 g_J = - 1.164(5)

Tm^{170} ($T_{1/2}$ = 129 d) I = 1

with J = 7/2* g_J = - 1.1412(2)

$|a|$ = 200(3) Mc, $|\mu_I|$ = 0.26(2) n m

$|b|$ = 1,010(15)Mc, $|Q|$ = 0.61(5) barns

Tm^{171} ($T_{1/2}$ = 1.9 yr) I = 1/2.

The quantities measured elsewhere, but verified and directly involved in the experimental observations are marked by an asterisk. Our original results are unmarked. The numbers enclosed in the parenthesis denote the uncertainty in the last places of the figures quoted.

The magnetic dipole and electric quadrupole moments of the two odd-odd nuclei Pr^{142} and Tm^{170} are calculated from measurements of the hyperfine-structure separations.

I. INTRODUCTION

The purpose of this research is to investigate those electronic and nuclear properties of the radioactive rare earths which may be determined by atomic-beam magnetic-resonance spectroscopy. The rare earths are the elements between lanthanum (Z = 57) and lutetium (Z = 71). The main characteristic of this transition series, also known as the lanthanides, is that the unfilled 4f subshell resides well within closed electronic shells. The striking similarity between these elements and the actinides with respect to electronic structure and its general behavior throughout the series is discussed. The similarities are exposed in view of recent results obtained using the atomic-beam method with isotopes of both series.

The nuclear properties specifically studied are the nuclear ground-state spin angular momenta and the nuclear electric- and magnetic-multipole moments.

The shape of the nucleus in this region of the isotope chart (atomic mass number between 150 and 175) is expected to depart considerably from spherical symmetry. This is found to be true for most of the thirteen nuclei investigated here as part of the research program.[1-10] The applicability of the collective-model theory is tested in its interpretation of the measured spins.

It is also of interest to test the other major existing theory of nuclear models, the single-particle shell-model theory. In order to analyze the validity of this model in the early part of the lanthanides (atomic mass number less than 150), theoretical estimates based on this model are made for the nuclear magnetic-dipole and electric-quadrupole moments of the odd-odd nucleus, praseodymium-142. These estimates are then compared with calculations of the nuclear moments based on the measurements obtained in the experiment.

Magnitudes of the electronic magnetic moments are measured. This is directly proportional to the electronic g value. The accuracies of these measurements range from 5 parts in 100 up to 2 parts in 10,000.

For the g values measured with high accuracy, the deviations of the experimental values from the theoretical Landé value are explained on the basis of present theories.

For some of the elements studied, the electronic ground levels with their corresponding g values are determined for the first time. From this information, an attempt is made to infer the ground-state electronic configurations of the elements.

The part of atomic spectral theory that is directly connected with the experimental method is reviewed in the next chapter. A description of the experimental technique is included, together with the experimental results and observations.

II. THEORY

A. Electron-Electron and Electron-Nuclear Interactions

One of the main features of the atomic system is the high degeneracy of its energy levels. To understand the magnitudes of the energy separations between the levels actually observed in nature, we must analyze the causal electron-electron and electron-nuclear forces. The removal of these degeneracies is discussed below.

One may start this investigation by immediately looking at the best available Hamiltonian that describes the quantum-mechanical system. This approximate Hamiltonian is[11]

$$\mathcal{H} = \sum_i \frac{p_i^2}{2m} - \sum_i \frac{Z e^2}{r_i} + \sum_{i>j} \frac{e^2}{r_{ij}} + \sum_i \xi(r_i)\, \vec{l}_i \cdot \vec{s}_i + \mathcal{H}(\text{hfs}). \tag{1}$$

The first term is the kinetic energy of the electrons, which are assumed to move around a fixed heavy nucleus. Relativistic effects are neglected above but are treated in a later chapter. The second summation is carried over a term which is the attraction energy between the nucleus and the ith electron located at a distance r_i from it. The third summation represents the repulsive energy between the several electrons separated by distances r_{ij}. The fourth term stands for the magnetic interactions between the electron spins and orbits, where $\xi(r_i)$ is the fine-structure energy constant. Finally, and most significant for our experiments, is the last interaction, denoted by $\mathcal{H}(\text{hfs})$. This represents the interaction of the nuclear multipoles with the electromagnetic fields set up by the electronic system.[12] Figure 1 is a schematic diagram of the energy levels and the corresponding degeneracies in each. The Coulomb interaction removes the degeneracy in the terms denoted by L and S, which are the total electronic-orbital-momentum and spin-angular-momentum quantum numbers, respectively. The levels J (the total electronic angular momentum is $J\hbar$) are separated by energies that are mostly affected by the spin-orbit interaction. The

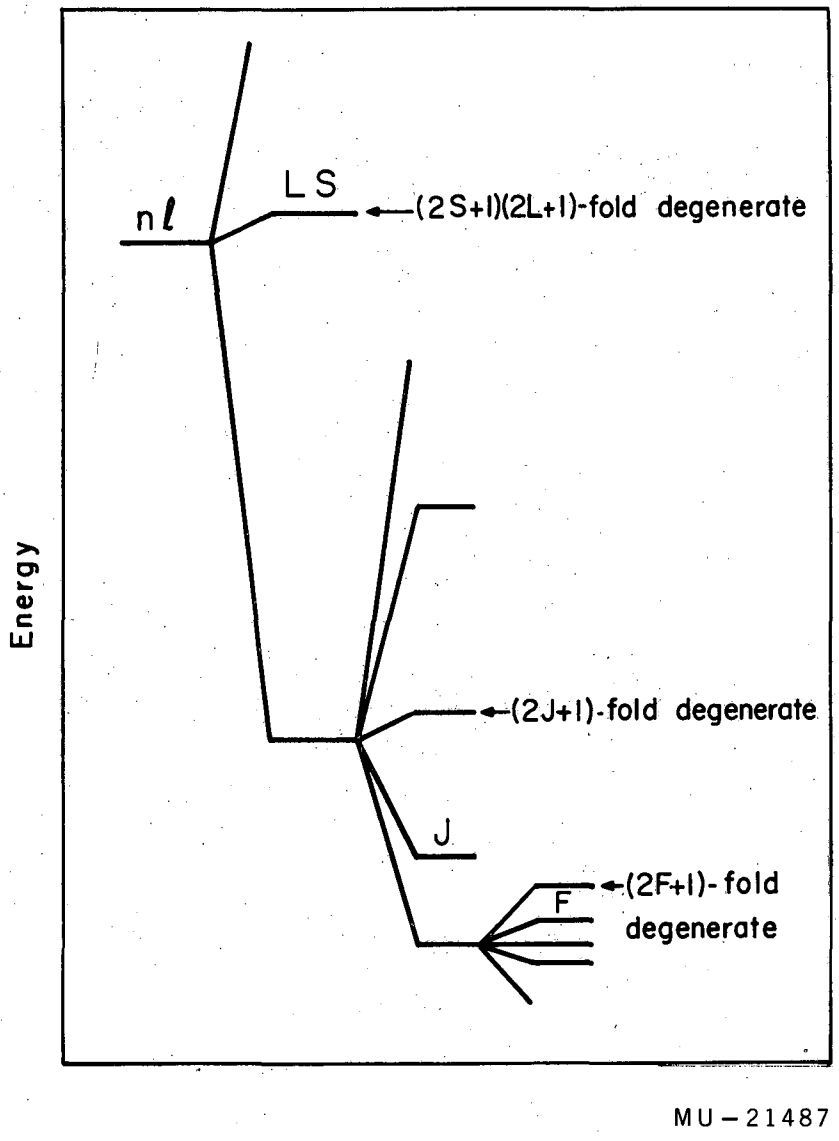

Fig. 1. Schematic diagram of the major degeneracies of the states of the atomic system.

$(2F+1)$-fold degeneracy of each F state is removed by the external magnetic field perturbation. A nonvanishing nuclear spin $\vec{I}$ combines vectorially with $\vec{J}$ to form $\vec{F}$, the total atomic angular-momentum quantum number.

It should be noted that other interactions present are the spin-spin, orbit-orbit, and spin-other-orbit effects. Interactions between configurations through some of the perturbations enumerated above are certainly possible. The energies of these interactions are usually neglected because they are much smaller compared to the other energies.

For many-electron spectra, the Hamiltonian of Eq. (1) as it stands is not practical for the evaluation of the energy eigenvalues. The term in r_{ij} prevents a separation of variables. A simplification is attained by assuming a screened potential $U(r_i)$, so that the remaining terms in the operator may be treated as perturbations. It seems that many spectral features may be obtained with this assumption.

Another factor that simplifies the energy operator arises when the electrostatic interaction is greater than the spin-orbit interaction. Then the latter is just neglected in the calculations, i.e.

$$\sum_{i>j} \frac{e^2}{r_{ij}} >> \sum_i \xi(r_i)\, \vec{l}_i \cdot \vec{s}_i \,. \tag{2}$$

This is called the Russell-Saunders limit, where the individual electron orbitals add up to L, while the electron spins add up to S.

The case of extreme j-j coupling applies when spin-orbit effects are much larger than electrostatic effects. Here, each electron-spin angular momentum $1/2\hbar$ and orbital angular momentum $\ell\hbar$ couple to form $j\hbar$. The total J is then the vector sum of the separate j's.

The choice of a representation in the evaluation of the matrix elements of the perturbations depends on the discovery of those angular-momentum operators that commute with the perturbation in question. This has the effect of diagonalizing the energy matrix with respect to the eigenvalues common to the operators. In cases where exact diagonalization is not possible, a perturbation theory in some convenient representation is carried out.

A set of four quantum numbers is found to be sufficient to completely specify the quantum state of an electron. The choice of the antisymmetric eigenfunction in the calculation of various atomic properties is equivalent to the application of the Pauli principle. Very simply, this means that no two electrons in the same atom may have the same set of quantum numbers. The fourth quantum number was a puzzling aspect before the discovery of electron spin by the Stern-Gerlach experiment.[13] This experiment which directly proved the idea of space quantization of angular momentum is considered to be one of the forerunners of the atomic-beam radiofrequency method.

The assignments of these quantum sets to the electrons lead to the periodicity of closed shells in the electronic system. A statement of these closed shells, together with the last unfilled shells, if any, is called the electronic configuration of the element.

B. Hyperfine-Structure Interactions

The electromagnetic fields at the nuclear site due to the electronic system interact with the electric and magnetic multipole moments. This interaction removes the $(2I+1)(2J+1)$-fold degeneracy of each substate denoted by I and J. The energy of this interaction is measured by several experimental methods which include paramagnetic resonance, microwave spectroscopy, optical spectroscopy, and atomic beams. In all of these methods, two assumptions are made about the nucleus. First, the nucleus has a spin angular momentum represented quantum-mechanically by $I\hbar$, where I is by definition the maximum projection of $\vec{I}$ in any direction. Secondly, the nuclear charge Ze is concentrated in a small region about 10^{-12} cm in diameter.

One way of expressing the electrostatic interaction between the nucleus and its electrons is to take the product of two infinitesimal nuclear and electronic charge densities located at a distance r apart, and integrating over both electronic and nuclear volumes.[11] Let $\vec{r}_n$ and $\vec{r}_e$ be radial vectors originating from the nuclear center, which locate the nuclear and electronic volumes respectively. Then the

assumption above is used, so that r_n/r_e is less than one. Now $1/r$ may be written in terms of the well-known power-series expansion in r_n, r_e and the Legendre polynomials $P_k(\cos\theta_{en})$, with θ_{en} as the angle between $\vec{r}_n$ and $\vec{r}_e$. The kth term in the expansion is referred to as the interaction energy between the electric field and the electric multipole of order 2^k.

A similar treatment for the magnetic multipole energies is performed by considering the magnetic interaction between a circulating current density and a magnetic vector potential arising from the electrons.

The following treatment uses the more elegant methods of Racah[14] and Schwartz.[15] The hyperfine structure (hfs) Hamiltonian is expressed as the scalar tensor product

$$\mathcal{H} = \sum_k T^k(e) \cdot T^k(n) = \sum_k \sum_q T^k_q(e)\, T^k_{-q}(n) . \qquad (3)$$

The tensor $T(e)$ is a function of electron coordinates alone. Similarly $T(n)$ is a function of nuclear coordinates alone. The tensor T^k has rank k, and its $2q+1$ components obey the following commutation relations with the angular momentum operators J_z, $J_x + iJ_y$, and $J_x - iJ_y$:

$$\left[J_z,\ T^k_q\right] = q\, T^k_q . \qquad (4)$$

$$\left[J_\pm,\ T^k_q\right] = \left[k(k+1) - q(q\pm1)\right]^{1/2} T^k_{q\pm1} .$$

In the absence of external magnetic fields, the I J F m representation is appropriate for finding the matrix elements of Eq. (3). These are

$$W^0_F = (I\ J\ F\ m \left| \sum_k T^k(e) \cdot T^k(n) \right| I\ J\ F\ m) . \qquad (5)$$

The superscript zero on W_F is written in order to emphasize that no external magnetic field perturbations are present. According to a

theorem due to Racah, the diagonal matrix elements in Eq. (5) may be separated into components of irreducible tensors. Thus we have

$$W_F^0 = \sum_k (-1)^{I+J-F} W(IJIJ;Fk)\ (I \| T^k(n) \| I)\ (J \| T^k(e) \| J)\ , \qquad (6)$$

where W is the Racah coefficient which is a function of six parameters. If one substitutes $a = c = I$, $b = d = J$, $e = F$ and $f = k$ in formulae (36) and (36') on page 444 of Racah,[14] the coefficient is evaluated as

$$W(IJIJ;Fk) = (I + J - F)!\,(I + F - J)!\ (J + F - I)!\,(k!)^2/(I + J + F + 1)!$$

$$\times \left[\frac{(2I - k)!\ (2J - k)!}{(2I + k + 1)!\,(2J + k + 1)!}\right]^{1/2}$$

$$\times \sum_z \frac{(-1)^z (2I + 2J + 1 - z)!}{z!\left[(I + J - F - z)!\,(F + k - I - J + z)!\right]^2 (2I - k - z)!\,(2J - k - z)!}\ .$$

Substituting this into Eq. (6) and extracting, one obtains

$$A_k = \frac{(2J)!\,(2I)!\,(J \| T^k(e) \| J)\ (I \| T^k(n) \| I)}{\left[(2J-k)!\,(2J+k+1)!\ (2I-k)!\,(2I+k+1)!\right]^{1/2}}\ .$$

The remaining factors in the summation are

$$M(IJ;F;k) = (2I-k)!\,(2J-k)!\,/(2I)!\,(2J)!$$

$$\times \frac{(I+J-F)!\,(J-I+F)!\,(I-J+F)!\,(k!)^2}{(I+J+F+1)!} \qquad (7)$$

$$\times \sum_z \frac{(-1)^{z+I+J+F}(2I+2J+1-z)!}{z!\ (2I-k-z)!\,(2J-k-z)!\left[(I+J-F-z)!\,(k+F-I-J+z)!\right]^2}\ .$$

Therefore the energy of each hfs level [Eq. (6)] is conveniently written in this representation as

$$W_F^0 = \sum_k A_k \, M(IJ;F;k) \, . \qquad (8)$$

The Racah coefficient W vanishes unless the following triads satisfy the triangular conditions.

$$(I, J, F), \quad (I, I, k) \quad \text{and} \quad (J, J, k) \, .$$

The first triad just repeats the statement that the only allowed values of F are between $|\vec{I}-\vec{J}|$ and $|\vec{I}+\vec{J}|$. The second and third triads govern the termination of the series [Eq. (8)]. In other words, the series ends at the value of k given by k(maximum) = 2I or 2J, whichever is smaller. From Eq. (7), the multipole coefficients up to and including octupole are:

<u>for k = 1 (dipole)</u>

$$M(IJ;F;1) = \frac{K}{2IJ} \, ,$$

where $K = F(F+1) - I(I+1) - J(J+1)$;

<u>for k = 2 (quadrupole)</u>

$$M(IJ;F;2) = \frac{6\left[K(K+1) - (4/3)I(I+1)J(J+1)\right]}{2I(2I-1)2J(2J-1)} \, ;$$

<u>for k = 3 (octupole)</u>

$$M(IJ;F;3) = 20\left\{\frac{K^3+4K^2+(4/5)K\left[-3I(I+1)J(J+1)+I(I+1)+J(J+1)+3\right]}{2I(2I-1)(2I-2)2J(2J-1)(2J-2)}\right.$$

$$\left.\frac{-4I(I+1)J(J+1)}{1}\right\} .$$

If the constants A_k are related to the more commonly used hfs interaction constants a, b, and c by

$$A_1 = IJa, \qquad A_2 = 1/4\, b \quad \text{and} \quad A_3 = c,$$

then the multipole interaction energy up to quadrupole is

$$W_F^0 = a(\vec{I}\cdot\vec{J}) + b\frac{3(\vec{I}\cdot\vec{J})^2 + (3/2)(\vec{I}\cdot\vec{J}) - I(I+1)J(J+1)}{2IJ(2I-1)(2J-1)}\ , \qquad (9)$$

with $\quad 2(\vec{I}\cdot\vec{J}) = F(F+1) - I(I+1) - J(J+1)\ .$

The matrix elements of the operator in Eq. (3) may also be obtained in the IJm_Im_J representation. This is useful when transitions of the type $\Delta m_I = 0$, $\Delta m_J = \pm 1$ are observed between hyperfine states. This is the case when I and J are completely "decoupled" by a strong external magnetic field. Transitions of this type have been observed in hfs measurements of americium-241 in the ground level.[16] By subtracting the part contributed to the transition energy by the effect of the external magnetic field, it was possible to make a direct estimate of the hfs constant a.

1. Generalized Nuclear Moments

A generalized concept of the electric and magnetic multipole moments may be stated by defining the following operators.[17] Let $g_L(i)$ be the orbital gyromagnetic ratio of the ith nucleon; g_L is unity for protons and zero for neutrons. Similarly let $g_S(i)$ be the spin gyromagnetic ratio such that g_S is 5.587 for protons and -3.826 for neutrons. Also write $\underset{\sim}{L}(i)$ and $\underset{\sim}{s}(i)$ as the orbital angular momentum and Pauli spin operators for the ith nucleon. Then if $P_k(\theta_i)$ is the Legendre polynomial of order k, the magnetic multipole operator of rank k is

$$M^k = \mu_N \sum_i^A \left[\frac{2}{k+1}\, g_L(i)\underset{\sim}{L}(i) + (1/2)g_S(i)\underset{\sim}{s}(i)\right] \cdot \nabla\left[r^k(i)P_k(\theta_i)\right], \qquad (10)$$

where μ_N is the nuclear magneton. The electric multipole operator of rank k is also defined in terms of these parameters by

$$Q^k = e \sum_i^A g_L(i)\, r^k(i)\, P_k(\theta_i)\,. \qquad (11)$$

Note that M^k has parity $(-1)^{k+1}$, while Q^k has parity $(-1)^k$. If it is assumed that the nuclear ground-state wave function has a definite parity, then only even-parity multipoles will have nonzero eigenvalues. It is for this reason that only nuclear magnetic multipole moments of odd order exist (2^k with odd k). By the same argument, only nuclear electric multipoles of even order exist (2^k with even k).

Therefore the magnetic dipole moment is defined from Eq. (10) with $k = 1$ as

$$\mu_I = (II \,|\, M^1 \,|\, II)$$

$$= \mu_N (II \,\Big|\, \sum_i^A \left[g_L(i)\, \underset{\sim}{L}(i) + (1/2)\, g_S(i)\, \underset{\sim}{s}(i)\right] \cdot \nabla \left[r(i) P_1(\theta_i)\right] \Big|\, II)$$

$$= \mu_N (II \,\Big|\, \Sigma \left[g_L(i)\, \underset{\sim}{L}(i) + (1/2) g_S(i)\, \underset{\sim}{s}(i)\right] \cdot \hat{k} \,\Big|\, II),$$

since

$$\nabla \left[r(i) P_1(\theta_i)\right] = \hat{k},$$ where $\hat{k}$ is the unit vector in the z direction.

The electric quadrupole moment, obtained from Eq. (11) with $k = 2$, is

$$Q = \frac{2}{e} (II \,|\, Q^2 \,|\, II)$$

$$= 2 \;(II \,\Big|\, \sum_i^A g_L(i)\, r^2(i)\, P_2(\theta_i) \,\Big|\, II)\,,$$

where the matrix element is evaluated for $m_I = I$.

The next significant multipole is the magnetic multipole moment Ω. Here again, the matrix element of the operator M^3 is evaluated for $m_I = I$:

$$\Omega = -\,(\mathrm{II}\,|\,M^3\,|\,\mathrm{II})$$

$$= -\,\mu_N(\mathrm{II}\,|\sum_i^A \left[\frac{2}{3}\,g_L(i)\underset{\sim}{L}(i) + \frac{1}{2}\,g_S(i)\underset{\sim}{s}(i)\right]$$

$$\cdot\,\nabla\left[r^3(i)P_3(\theta_i)\right]|\mathrm{II})\ .$$

Note that this has the dimension of nuclear magneton-barns.

2. Magnetic and Electric Fields at the Nucleus due to the Electronic System

The interaction energies between the electromagnetic fields with the nuclear moments are given by the hfs constants a, b, etc. For an s electron, the constant a is related to the nuclear dipole moment by the Fermi formula[18]

$$a = -\frac{8\pi}{3}\,\frac{\mu_I}{I}\,g_J\,\mu_0\,|\,\psi(0)\,|^2\ ,$$

where $\psi(0)$ is the electronic wave function evaluated at the nucleus.

For a single non-s electron, one of several derivations gives[19]

$$a = \frac{2\mu_I\mu_0}{I}\,\frac{\ell(\ell+1)}{j(j+1)}\left\langle\frac{1}{r^3}\right\rangle\mathcal{F} \qquad (12)$$

and

$$b = e^2Q\,\frac{2j-1}{2j+2}\left\langle\frac{1}{r^3}\right\rangle\mathcal{R}\ . \qquad (13)$$

Here $\mathcal{F}$ and $\mathcal{R}$ are relativistic correction factors which are close to unity. These corrections have been tabulated by Kopfermann.[20] The radial distance of the valence electron from the nucleus is given by r. These formulae are used in our calculations of the nuclear moments of Tm^{170}. Thulium ($4f^{13}$) has one electron missing from the closed shell $4f^{14}$, so that its electronic structure is effectively that of a single-electron atom.

Information from other isotopes is sometimes available from past experiments so that a simple comparison of relations (12) and (13) for two isotopes gives the ratios

$$g_I(1) = g_I(2)\ \frac{a(1)}{a(2)}$$

and

$$Q(1) = Q(2)\ \frac{b(1)}{b(2)}\ .$$

These relations are exact in the absence of hfs anomalies. The number 1 refers to the isotope under investigation, while 2 is the "comparison isotope".

For a many-electron system, these formulae are slightly more complicated. Under the following assumptions, the interaction constants are related to the nuclear moments μ_I and Q: (a) The electrons in the valence shell are equivalent; (b) Russell-Saunders coupling among the n electrons is a good approximation (the Coulomb interaction is much greater than the spin-orbit interaction). This leads to the Hund's-rule ground term[21] with the ground level $J = |L - S|$ for a shell that is less than half filled, $L + S$ for a shell that is more than half filled, and S for a half-filled shell. Thus if the magnetic field is calculated for the ground level $^{2S+1}L_J$, we have[22]

$$a(J) = \frac{\mu_I \mu_0}{IJ(J+1)} \left\langle \frac{1}{r^3} \right\rangle \left\{ J(J+1) + L(L+1) - S(S+1) \right.$$

$$\pm \frac{2(2L - n^2)}{n^2(2L - 1)(2\ell - 1)(2\ell + 3)} \left[L(L+1) \left[J(J+1) + S(S+1) - L(L+1) \right] \right.$$

$$\left. \left. - (3/2) \left[J(J+1) - L(L+1) - S(S+1) \right] \left[J(J+1) + L(L+1) - S(S+1) \right] \right] \right\}. \quad (14)$$

The quadrupole interaction constant b is related to the nuclear quadrupole moment Q and the expectation value of the electric field

gradient by[23]

$$b = - e^2 Q \left\langle \frac{1}{r^3} \right\rangle (SLJJ \left| \sum_i 3\cos^2 \theta_i - 1 \right| SLJJ) ,$$

where it is assumed that the angular part may be separated from the radial part. A derivation of the diagonal matrix element of the angular part for the ground level has been given by Nierenberg.[24] This result combined with the relation for b above gives

$$b = e^2 Q \left\langle \frac{1}{r^3} \right\rangle \left\{ \frac{3K(K+1) - 4L(L+1)J(J+1)}{2L(L-1)(J+1)(2J+3)} \times (\pm 1) \frac{2L(2L - n^2)}{n(2\ell - 1)(2\ell+3)} \right\}, \quad (15)$$

with $K = S(S+1) - L(L+1) - J(J+1)$. In Eqs. (14) and (15), the plus sign applies to a less-than-half-filled shell, while the minus sign refers to a more-than-half-filled shell. In the latter case, n is the number of electron holes.

An alternative method for the evaluation of the matrix elements of $\sum_i 3\cos^2 \theta_i - 1$ is carried out in Appendix A. This treatment uses the tensor-operator form $2\,C^2_0$ for the evaluation of the matrix elements for the state $\left| \ell^n \alpha\ SLJ \right)$.

When the ground-state electronic wave function $\left| \gamma\ SLJJ_z \right)$ describes a single pure ground state, formula (14) for the diagonal matrix elements is sufficient for the calculation of the magnetic field due to the electrons. In some cases however, it is necessary to estimate the effect on the magnetic-field calculation when the electronic wave function includes admixtures from excited terms in the configuration. The amount of admixture is dependent upon the magnitude of the spin-orbit energy connecting the excited levels with the ground level. Thus it is evident that in this case it is necessary to calculate off-diagonal elements of the magnetic-field operator.

This type of a calculation is performed for $Pr^{142}(4f^3)$ in a later section. The levels that perturb the ground level $^4I_{9/2}$ are $(210)(21)^2H_{9/2}$

and $(210)(11)^2H_{9/2}$, where the numbers in the parenthesis are additional quantum numbers necessary for the complete specification of the states.

The interaction constant a(J) is related to the magnetic field by

$$a(J) = \frac{2\mu_I\mu_0}{IJ} \left\langle \frac{1}{r^3} \right\rangle (\gamma\, JJ \,|\, \underset{\sim}{N} \,|\, \gamma\, JJ) , \qquad (16)$$

where

$$\underset{\sim}{N} = \sum_i \left[\underset{\sim}{\ell}_i - \underset{\sim}{s}_i + \frac{3\underset{\sim}{r}_i(\underset{\sim}{r}_i \cdot \underset{\sim}{s}_i)}{r_i^2} \right], \qquad (17)$$

and $|\gamma\, JJ)$ is the electronic wave function with admixtures for the level J with $J_z = J$. That is, we have

$$|\gamma\, JJ) = c_1\, |\gamma_1 JJ) + c_2 |\gamma_2 JJ) + c_3\, |\gamma_3\, JJ) + \cdots\cdots ,$$

where c_1, c_2, and c_3 are the amplitudes of the wave functions for each state. The remaining quantum numbers necessary to specify the state are denoted by γ.

The technique here is to convert $\underset{\sim}{N}$ to tensor-operator form. Then the matrix elements of this tensor operator are evaluated directly in the $SLJJ_z$ representation. The more conventional and lengthier method is to evaluate the single-particle operator of Eq. (17) in terms of determinantal product states. This means that each ket $|SLJJ_z)$ has to be expanded in terms of kets $|SLS_zL_z)$. Each of these are then further expanded in terms of single-particle wave functions $|sls_z l_z)$.

It may be shown that, in tensor-operator form we have[25, 26]

$$\underset{\sim}{N} = \sum_i \left[\underset{\sim}{\ell}_i - (10)^{1/2} (\underset{\sim}{s}\, \underset{\sim}{C}^2)^1_i \right], \qquad (18)$$

where $(\underset{\sim}{s}\, \underset{\sim}{C}^2)^1$ is a first-ranked tensor which results from the product of a tensor of rank 1 with a tensor of rank 2. This represents the interaction of $\underset{\sim}{\mu}_I$ with the magnetic field due to the electronic spins alone. The orbital contribution seems to constitute the larger part of the magnetic field.

For an n-electron system with n greater than two, the set of quantum numbers $SLJJ_z$ are not always sufficient to describe a state. Additional quantum numbers are needed to completely specify the states that occur more than once in the configuration. For example, all the terms for f^3 are listed as[11]

$$\underset{2222}{{}^2PDFGHIKL\ {}^4SDFGI}$$

The number below a term denotes the number of times that term occurs in the configuration.

In the two-electron system, the complications noted above do not arise because the terms in this system occur only once in the configuration. This case does not require the following concepts and is treated in Appendix D.

A method developed by Racah expresses the wave function of an n-electron system as the sum over a product of eigenfunctions for the (n-1)-system with the eigenfunction of the nth electron.[14] That is,

$$\left| \ell^n\ \psi\right) = \sum_{\overline{\psi}} \left(\psi \left\{ \left| \overline{\psi}\right.\right) \left| \ell^{n-1}\, \overline{\psi}\right) \left| \ell\right.\right)$$

where $\left(\psi \left\{ \left| \overline{\psi}\right.\right)\right.$ are the so-called coefficients of fractional parentage. The following matrix element of a general tensor U^k of rank k will be very useful for our purposes:[25]

$$\left(\ell^n \alpha\ SLJ \left\| U^k \right\| \ell^n \alpha' S' L' J'\right) = n\ \delta(S, S')\ (-1)^{S+J+L+L'+\ell}$$

$$\times \left[(2J+1)(2J'+1)\ (2L+1)(2L'+1)\right]^{1/2} \begin{Bmatrix} L & J & S \\ J' & L' & k \end{Bmatrix}$$

$$\times \sum_{\overline{\psi}} (-1)^{\overline{L}} \begin{Bmatrix} \ell & L & \overline{L} \\ L' & \ell & k \end{Bmatrix} \left(\psi \left\{ \left| \overline{\psi}\right.\right) \left(\psi' \left\{ \left| \overline{\psi}\right.\right) \left(\ell \left\| U^k \right\| \ell\right)\right.\right. . \qquad (19)$$

Where U^k depends on orbit alone. An analogous expression could be written if the tensor U^k operated on spin alone.

The matrix elements of a tensor product between two tensors U^{k_1} and V^{k_2} will also be extensively used in the following discussions. In this case, letting U^{k_1} act on spin alone while V^{k_2} acts on orbit alone, we have[25]

$$(\ell^n a\, SLJ \| \sum_i \{U^{k_1}(i)\, V^{k_2}(i)\}_K \| \ell^n a'S'L'J')$$

$$= n\left[(2K+1)(2J+1)(2J'+1)(2L+1)(2L'+1)(2S+1)(2S'+1)\right]^{1/2}$$

$$\times (-1)^{k_1+k_2+s+\ell+S+L} \begin{Bmatrix} S & S' & k_1 \\ L & L' & k_2 \\ J & J' & K \end{Bmatrix} \sum_{\bar{\Psi}} (\psi\{|\bar{\Psi})(\psi'\{|\bar{\Psi})$$

$$\times (-1)^{\bar{S}+\bar{L}} \begin{Bmatrix} s & S & \bar{S} \\ S' & s & k_1 \end{Bmatrix} \begin{Bmatrix} \ell & L & \bar{L} \\ L' & \ell & k_2 \end{Bmatrix} (s \| U^{k_1} \| s)(\ell \| V^{k_2} \| \ell). \tag{20}$$

The tensor resulting from the tensor product has rank K. The index i refers to electron i and the summation is taken over all the valence electrons. The curly brackets denote n-j symbols which are related to Racah's W-function. These symbols are defined in Appendix B. Numerical evaluations of these symbols are carried out in a recent publication by Rotenberg et al.[27]

The matrix elements of $\underset{\sim}{N}$ are expressed as

$$(\ell^n a\, SLJJ \Big| \sum_i \left[\underset{\sim}{\ell}_i - (10)^{1/2} (\underset{\sim}{s}\, \underset{\sim}{C}^2)^1\right]_i \Big| \ell^n a'S'L'J'J') \tag{21}$$

The J_z dependence of the matrix element of $\underset{\sim}{\ell}_i$ is removed by means of the Wigner-Eckart theorem:

$$(\ell^n a\, SLJJ \Big| \sum_i \underset{\sim}{\ell}_i \Big| \ell^n a' S' L' J' J') = (-1)^{J-J} \begin{pmatrix} J & 1 & J' \\ -J & 0 & J' \end{pmatrix}$$

$$\times (\ell^n\, a\, SLJ \Big\| \sum_i \underset{\sim}{\ell}_i \Big\| \ell^n\, a' S' L' J') \,. \qquad (22)$$

The figure in the large parenthesis is called a 3-j symbol which is related to the vector coupling coefficient $(j_1 m_1 j_2 m_2 | j_1 j_2 j_3 - m_3)$. This symbol is also defined in Appendix B. By using Eq. (22) and making the proper substitutions, we have

$$\begin{aligned}(\ell^n a\, SLJ \Big\| \sum \underset{\sim}{\ell}_i \Big\| \ell^n a' S' L' J') &= n\, \delta(S, S')\, (-1)^{S+L+J+L'+\ell} \\ &\times \left[(2J+1)(2J'+1)(2L+1)(2L'+1)\right]^{1/2} \begin{Bmatrix} L & J & S \\ J' & L' & 1 \end{Bmatrix} \\ &\times \sum_{\overline{\Psi}} (-1)^{\overline{L}} \begin{Bmatrix} \ell & L & \overline{L} \\ L' & \ell & 1 \end{Bmatrix} (\psi \{ | \overline{\Psi}) (\psi' \{ | \overline{\Psi}) (\ell \Big\| \sum \underset{\sim}{\ell}_i \Big\| \ell), \end{aligned} \qquad (23)$$

where $(\ell \Big\| \sum \underset{\sim}{\ell}_i \Big\| \ell) = \left[\ell(\ell+1)(2\ell+1)\right]^{1/2}$. The selection rules for the matrix elements of the orbit operator are seen from the 6-j symbol

$$\begin{Bmatrix} L & J & S \\ J' & L' & 1 \end{Bmatrix},$$

namely, $\Delta J = 0, \pm 1$ and $\Delta L = 0, \pm 1$. Therefore the diagonal matrix element of interest is

$$(a\, SLJ \Big\| \sum \underset{\sim}{\ell}_i \Big\| a\, SLJ) = n\, (-1)^{S+J+2L+\ell} (2J+1)(2L+1) \qquad (24)$$

$$\times \begin{Bmatrix} L & J & S \\ J & L & 1 \end{Bmatrix} \sum_{\overline{\Psi}} (-1)^{\overline{L}} \begin{Bmatrix} \ell & L & \overline{L} \\ L & \ell & 1 \end{Bmatrix} (\psi \{ | \overline{\Psi})^2 (\ell \Big\| \sum \underset{\sim}{\ell}_i \Big\| \ell) \,.$$

Note that Eq. (23) is non zero only for $S=S'$. Thus only the diagonal elements (24) are nonvanishing.

The spin part of the magnetic field operator $\underset{\sim}{N}$ has <u>off-diagonal</u> matrix components

$$-(10)^{1/2}(\ell^n a\ SLJJ\ \Big|\ \sum_i (\underset{\sim}{s}\ \underset{\sim}{C}^2)^1_i\ \Big|\ \ell^n\ a'S'L'JJ) \tag{25}$$

$$=-(10)^{1/2}\ (-1)^{J-J}\begin{pmatrix} J & 1 & J \\ -J & 0 & J \end{pmatrix}(\ell^n\ a\ SLJ\ \Big|\ \Sigma(\underset{\sim}{s}\ \underset{\sim}{C}^2)^1_i\Big|\ell^n a'S'L'J')$$

from the Wigner-Eckart theorem. Using Eq. (20) for the matrix elements of a tensor product, we have

$$(\ell^n a\ SLJ\ \Big\|\ \Sigma\ (s\ C^2)^1_i\ \Big\|\ \ell^n a'S'L'J)$$

$$= n\ (2J+1)\left[3(2S+1)(2S'+1)\ (2L+1)(2L'+1)\right]^{1/2} \tag{26}$$

$$(-1)^{3+s+\ell+S+L}\begin{Bmatrix} S & S' & 1 \\ L & L' & 2 \\ J & J & 1 \end{Bmatrix}\sum_{\Psi\overline{\Psi}}(\psi\{\ |\ \overline{\Psi})\ (\psi'\{\ |\ \overline{\Psi})$$

$$(-1)^{\overline{S}+\overline{L}}\begin{Bmatrix} s & S & \overline{S} \\ S' & s & 1 \end{Bmatrix}\begin{Bmatrix} \ell & L & \overline{L} \\ L' & \ell & 2 \end{Bmatrix}(s\ \Big\|\underset{\sim}{s}\Big\|\ s)(\ell\ \Big\|\underset{\sim}{C}^2\Big\|\ \ell),$$

where the reduced matrix elements are[25]

$$(s\ \Big\|\underset{\sim}{s}\Big\|\ s) = \left[s(s+1)(2s+1)\right]^{1/2}$$

and (27)

$$(\ell\ \Big\|\underset{\sim}{C}^2\Big\|\ \ell) = (-1)^{\ell}(2\ell+1)\begin{pmatrix} \ell & 2 & \ell \\ 0 & 0 & 0 \end{pmatrix}.$$

By referring to the equation in Appendix B for the 9-j symbol as the sum of products of three 6-j symbols, the triangular conditions on the 9-j symbol are obtained by considering the triangular conditions on the 6-j symbols appearing in the summation. It is seen that the three elements in each row and each column form the sides of a triangle. Therefore the selection rules for the spin part of the magnetic field operator are

$$\Delta S = 0, \pm 1, \qquad \Delta L = 0, \pm 1, \pm 2, \qquad \text{and} \quad \Delta J = 0, \pm 1.$$

The diagonal matrix elements $(\ell^n\ \alpha\ SLJJ \left| \Sigma_{\underline{m}_i} (-1)^{1/2} (\underline{s}\underline{C}^2)^1_i \right| \ell^n\ \alpha\ SLJJ)$ give exactly the same result obtained by using formula (14) derived by Brink et al.[22] This was checked for the state $|f^3\ ^4I_{9/2}\ 9/2)$.

C. Effect of an External Magnetic Field on the Atom

The effect of an external magnetic field on the electronic and nuclear moments is expressed by the Hamiltonian[12]

$$\mathcal{H}\ (\text{mag}) = -\vec{\mu}_J \cdot \vec{H} - \vec{\mu}_I \cdot \vec{H}\ , \tag{28}$$

where $\vec{H}$ is the external magnetic field, and we have

$$\vec{\mu}_J = g_J\ \mu_0\ \vec{J}$$

$$\vec{\mu}_I = g_I\ \mu_0\ \vec{I}.$$

Let us first consider the weak-field case (Zeeman effect of hfs). This is the case where $\vec{I}$ and $\vec{J}$ are tightly coupled to form $\vec{F}$, the total atomic angular momentum, i.e., $\vec{I}+\vec{J} = \vec{F}$. Then the components of $\vec{F}$ along the direction of quantization are given by m. This takes on quantized values between $\left|\vec{I} - \vec{J}\right|$ and $\left|\vec{I} + \vec{J}\right|$. The matrix element of the operator (28) in this IJFm representation is

$$W_{F,m} = (IJFm \left| \mathcal{H}(\text{mag}) \right| IJFm)$$

$$= \left[-g_J \frac{F(F+1) + J(J+1) - I(I+1)}{2F(F+1)} \quad -g_I \frac{F(F+1)+I(I+1)-J(J+1)}{2F(F+1)} \right] \mu_0 Hm. \tag{29}$$

When the atom is in the presence of a strong external magnetic field, the set of quantum numbers IJFm are no longer adequate for the description of the effect on the atomic energy levels. Now, $\vec{I}$ and $\vec{J}$ are completely decoupled and each angular momentum vector precesses about the quantization axis with projections m_I and m_J. This is known as the Paschen-Bach effect of hyperfine structure. Thus the appropriate quantum numbers are I, J, m_I and m_J. Then the additional energy due to this perturbation is

$$W_{m_I m_J} = (IJm_I m_J \left| \mathcal{H}(\text{mag}) \right| IJm_I m_J)$$

$$= - g_J \mu_0 H m_J - g_I \mu_0 H m_I . \tag{30}$$

The selection rules for allowed transitions are

$$\Delta m_J = \pm 1, \quad \text{and} \quad \Delta m_I = 0, \pm 1 . \tag{31}$$

In the case of magnetic fields intermediate with respect to the two extreme cases just considered, the procedure is to apply an ordinary perturbation calculation in a suitable representation. In the IJFm representation, the energy of a level up to third-order is[11]

$$W_{Fm} = W^0_F + (IJFm \left| V \right| IJFm)$$

$$+ \sum_{F'}{}' \frac{(IJFm \left| V \right| IJF'm)^2}{\Delta W^0(F, F')} .$$

$$+ \sum_{F'}{}' \frac{(IJF'm|V|IJF'm)(IJFm|V|IJF'm)^2}{\left[\Delta W^0(F,F')\right]^2}$$

$$- (IJFm|V|IJFm) \sum_{F'}{}' \frac{(IJFm|V|IJF'm)^2}{\left[\Delta W^0(F,F')\right]^2} , \qquad (32)$$

with $V = \mathcal{H}_{mag}$. The prime over Σ indicates that the summation is not carried over $F = F'$, W^0 is the zero-field energy of an hfs level, and $\Delta W^0(F, F')$ is the hfs energy separation between the hfs states F and F'. The only nonvanishing matrix elements are those with $\Delta F = 0, \pm 1$ and $\Delta m = 0$. Off-diagonal matrix elements in J give a negligible contribution in view of the large separation $\Delta W(J, J')$ compared to a typical $\Delta W(F, F')$.

The off-diagonal terms connecting states of the same m but with F differing by ± 1 are, from Condon and Shortley,[11]

$$(IJFm|-\mu_J \cdot H|IJF-1,m) = \left\{\frac{\left[F^2-(J-I)^2\right]\left[(I+J+1)^2+F^2\right](F^2-m^2)}{4F^2(4F^2-1)}\right\}^{1/2} \mu_0 H. \qquad (33)$$

By replacing F with $F+1$ in Eq. (33), one obtains

$$(IJFm|-\mu_J \cdot H|IJF+1,m) = \left\{\frac{\left[(F+1)^2-(J-I)^2\right](I+J+2+F)(I+J-F)\left[(F+1)^2-m^2\right]}{4(F+1)^2(2F+1)(2F+3)}\right\}^{1/2} \mu_0 H .$$

III. EXPERIMENTAL METHOD

A. Source Production

The radioactive source is produced by irradiating the pure metal with low-energy neutrons. With these thermal neutrons, the predominant reaction proceeds as

$$\text{element-A } (n, \gamma) \text{ element-(A+1)},$$

where A is the atomic mass number of the target isotope. The nuclear piles employed for the irradiations were the Livermore Pool-Type Reactor in Livermore, Calif., the Vallecitos General Electric Test Reactor in Pleasanton, Calif., and the Materials Testing Reactor in Arco, Idaho. Table I is a summary of the irradiation times, resulting radioactivity, amount of target material, etc. for each of the isotopes investigated. The target material was vacuum-sealed in a quartz capsule which was then inserted into an aluminum capsule of high purity. The 99.99 (4 $\rightarrow$ 9) % purity of the aluminum is convenient for avoiding unnecessary radioactivity from any possible contaminants.

The target was then delivered to Berkeley by the Health Chemistry Division of the Radiation Laboratory. The capsule was then transferred to a "cave" which is lined with lead in order to protect the researcher from the beta and gamma rays emitted by the source (see Fig. 2). Some of the capsules were opened in an inert gas, usually argon, in order to prevent the oxidation of the metallic source. The material was then transferred to another cave which is attached to the apparatus. The oven-loading procedure can be done by remote control through the use of tongs and manipulators if the high level of radioactivity demands it.

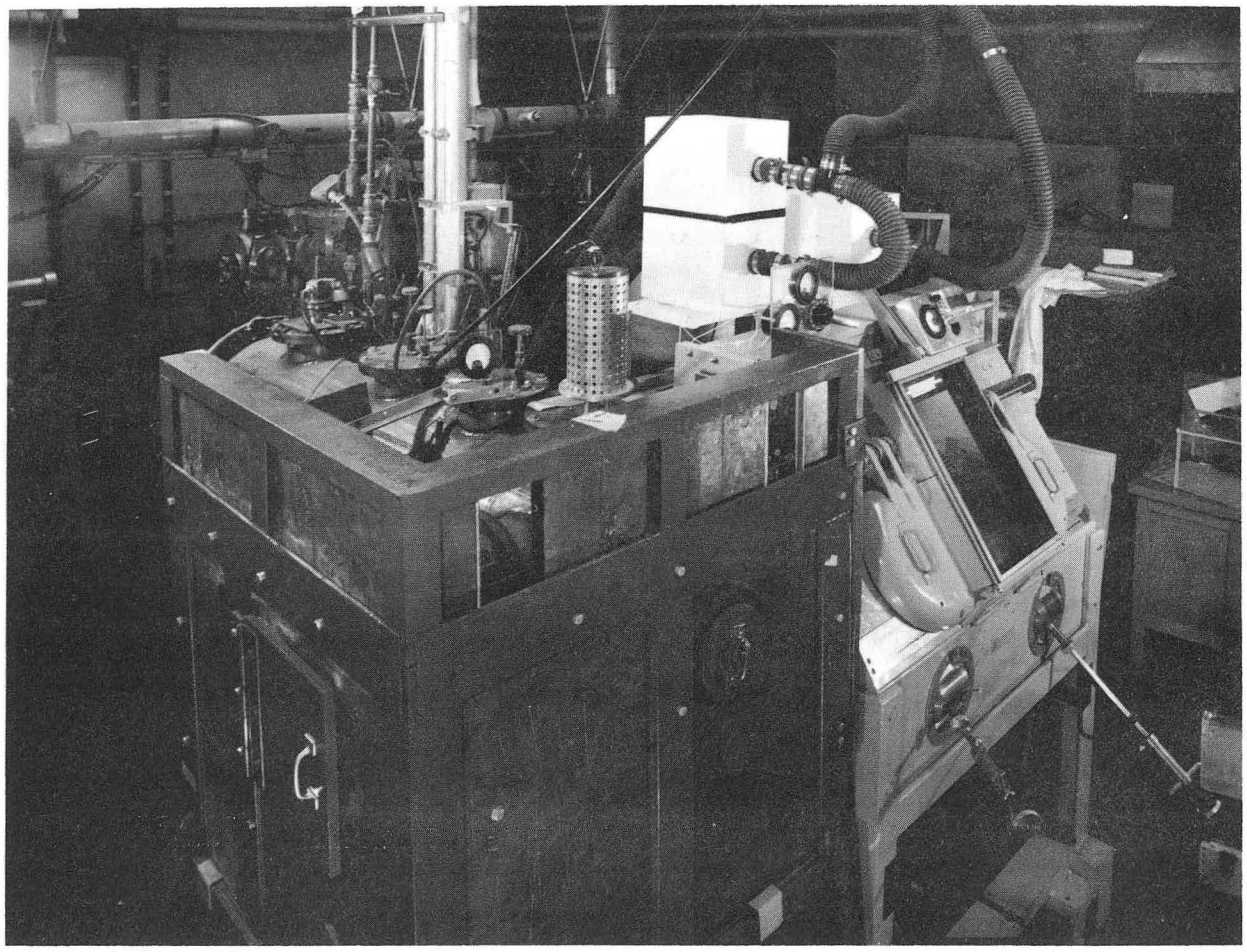

ZN-2590

Fig. 2. The oven end of the atomic-beam apparatus, which is enclosed by the lead shield. Note the "cave" on the right where the source is loaded into the "oven loader" before insertion into the apparatus.

Table I. Data for radioactive-source production

Target isotope	Isotopic abundance	Neutron capture σ (barns)	Amount of target (mg)	Typical irradiation time	Reactor[a] used	Isotope produced	Approximate Radioactivity (curies)	$T_{1/2}$
Ce^{142}	11.1	1	100	72 hr	V	Ce^{143}	0.2	33.0 hr
Pr^{141}	100.0	11	50	10 hr	V	Pr^{142}	2.6	19.1 hr
Nd^{146}	17.2	2	100	7 d	M	Nd^{147}	0.5	11.6 d
Sm^{152}	26.8	140	100	16 hr	L	Sm^{153}	2.5	47.0 hr
Gd^{158}	24.9	4	100	16 hr	L	Gd^{159}	0.2	18.0 hr
Tb^{159}	100.0	45	50	2 d	V	Tb^{160}	0.6	72.0 d
Ho^{165}	100.0	64	100	16 hr	L	Ho^{166}	8.0	27.2 hr
Er^{168}	27.1	2	100	4 d	V	Er^{169}	0.2	9.4 d
Er^{170}	14.9	9	100	8 hr	V	Er^{171}	1.3	7.5 hr
Tm^{169}	100.0	125	200	2 d	L	Tm^{170}	0.8	129.0 d
Er^{170}	14.9	9	100	45 d	L	Tm^{171}	0.1	1.9 yr

[a]V--Vallecitos G. E. Test Reactor (8×10^{13} neutrons per sec-cm^2)
L--Livermore Pool-Type Reactor (2×10^{13} neutrons per sec-cm^2)
M--Materials Testing Reactor, Arco, Idaho (2×10^{14} neutrons per sec-cm^2)

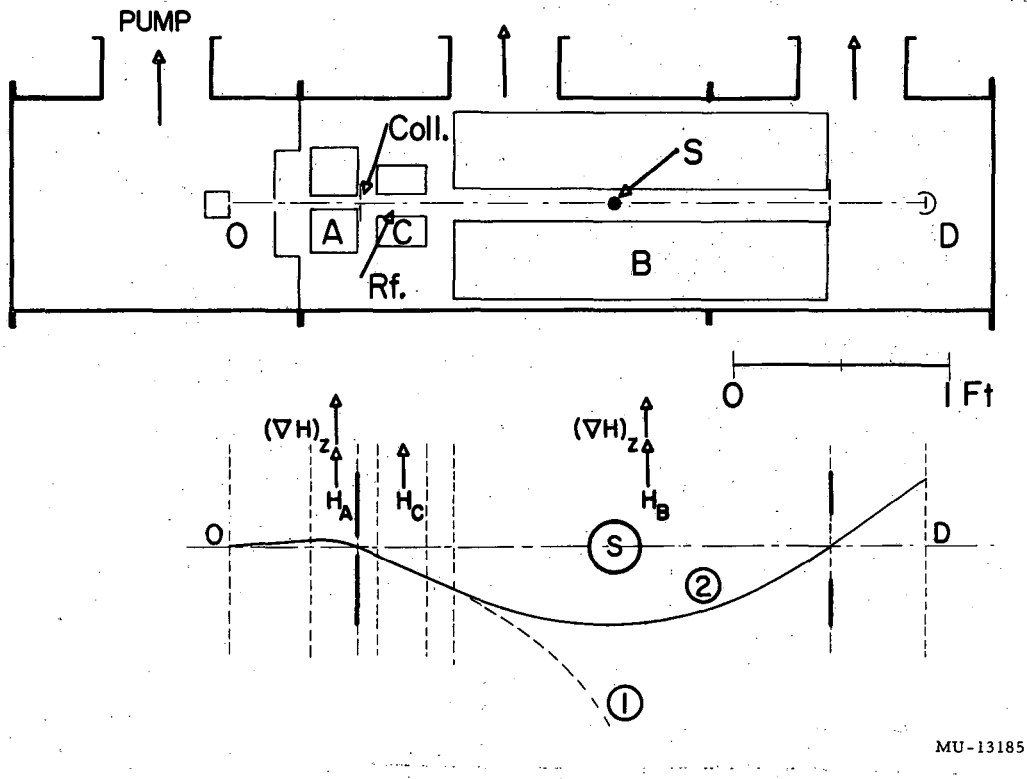

Fig. 3. Schematic diagram of atomic-beam trajectories.

B. Apparatus and Experimental Technique

The apparatus used in the experiments is a conventional atomic-beam magnetic-resonance machine. The A and B inhomogenous magnetic fields are set in the same direction so that the resonance atoms "flop-in" at the detector.[28] Thus at resonance, the effect is registered as an increase in intensity of the atomic beam. A detailed description of this apparatus has appeared in previous papers;[22, 29] therefore, only the parts of the machine necessary for the discussion of the resonance process will be mentioned.

The beam of neutral atoms emerges from a cylindrical tantalum oven with a press-fit tantalum cap. Tantalum plates are spot-welded on the oven in order to provide a rectangular aperture for the atomic beam. An inner-liner container, also made of tantalum is machined with a sharp lip in order to prevent the phenomenon known as "creep". It has been observed that this effect, where the liquid material creeps up the containing walls and spills out of the aperture, is present in some of the lanthanides. The source oven is heated by electron bombardment by setting the oven at a high positive voltage (0.5 to 4.0 kv) near a current-carrying filament. Temperatures ranging up to about $3{,}000^{\circ}K$ are easily attained.

The atomic beam is collimated as it enters the A-magnet region. Figure 3 is a schematic diagram of typical atomic trajectories. The first inhomogenous magnetic field serves to deflect some of the atoms with nonzero moments, which emerge at different angles with respect to the symmetry axis of the machine. These atoms now enter the C-magnet region, where they may undergo transitions. In the resonance process, approximately only one in 10^5 atoms eventually reach the detector. The rest are lost in the machine and contribute to "machine background". If the interaction potential W is equal to $-\vec{\mu} \cdot \vec{H}$, where μ is a constant with respect to H, then the force on the neutral atom is

$$\vec{F} = -\vec{\nabla} W = -\vec{\nabla} (-\vec{\mu} \cdot \vec{H}) = \mu_{eff} \vec{\nabla} H .$$

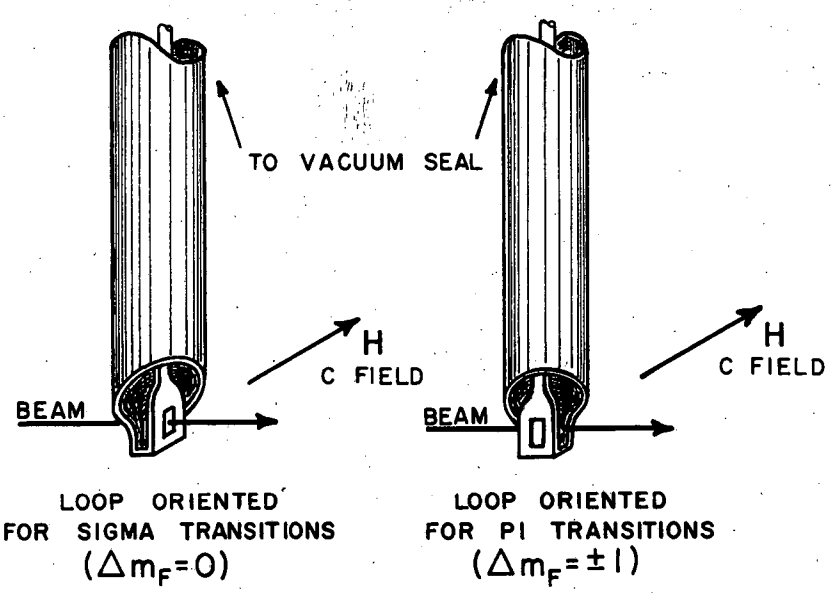

MU-18042

Fig. 4. Radio-frequency loop with two orientations with respect to the direction of the atomic beam.

It is seen from this equation that the force on the moving atom is directly proportional to the gradient of the magnetic field which it finds along its path. Referring back to Fig. 3, the trajectory numbered 1 shows an atom deflected by both magnets A and B when it meets no additional forces in the C-magnet region. Now suppose that a perturbation is applied to the atom so that the direction of its effective magnetic moment is completely reversed as it passes through the C-field region.[12] In this case, the B magnet can refocus the atom around a stop wire (S) and towards the detector (D), (trajectory No. 2). The torque that produces the sign reversal in the magnetic moment is caused by a small oscillatory magnetic field.

The stop wire intercepts the fast atoms which are not deflected by the magnetic fields. It is lifted out of the beam path whenever the total beam is checked for normalization purposes.

This oscillatory field located between the A and B magnets is due to an rf current passing through an rf loop (Fig. 4). One of the factors which govern the line width (full width at half-maximum intensity) of the resonace curve is the length of this loop in the direction of the beam. It is necessary that the rf loop be located in the most homogenous part of the static magnetic field. Most of the line broadening observed in our experiments is due to the inhomogeneity of this field. The other contributing factors to line broadening are the velocity distribution in the atomic beam, the Millman effect,[12] instability of the applied radio-frequency, doppler shifts, and the uncertainty principle. Figure 4 illustrates that, depending on which way the rf loop is oriented, the atoms are confronted by (a) an oscillating rf field directed perpendicular to the static C-field, and (b) an oscillating rf field directed parallel to the static C-field. Orientation (a) is used to observe transitions of the type

$$\Delta F = 0, \pm 1, \quad \Delta m = \pm 1 \qquad \text{(pi transitions)},$$

while (b) induces transitions of the type

$$\Delta F = \pm 1, \quad \Delta m = 0 \text{ (sigma transitions)}.$$

C. Calibration of the Static Magnetic Field

The static C-field is calibrated by observing a particular K^{39} pi transition. Different settings of the static C-field correspond to different potassium resonance frequencies. The hyperfine separation of K^{39} ($I = 3/2$, $^2S_{1/2}$) is known to high accuracy, and the resonance frequency in megacycles versus magnetic field in gauss, or $\mu_0 H/h$ in Mc, has been tabulated. The other transitions in this hfs system with their respective transition probabilities are discussed in a previous thesis.[30]

Metallic potassium is loaded in a metal cylinder with a circular aperture on the side. This screws into a rod which contains an electric heating element inside. The potassium oven is thus heated by conduction. This oven is lowered in front of the radioactive-source oven whenever a field calibration is desired. At the detector end of the machine, a hot tungsten strip ionizes the incident K beam. The intensity of the beam as a function of applied radio frequency is displayed by an electrometer which measures the ion current. The tungsten strip is inserted in the beam path by means of a micrometer arrangement.

The values of the electronic and nuclear constants used in the calibration tables are:

for K^{39}, $g_J = -2.00228$

$\Delta\nu = 461.71971$ Mc (for $I = 3/2$, $^2S_{1/2}$)

$\mu_0/h = 1.399677$ Mc/gauss-sec.

D. The Radioactive-beam Detection System

The detector end plate is mounted with a rotating arrangement (Fig. 5) which alternately positions three small detector holders. A platinum foil (1-mil thick and 0.495 in. in diameter) is slipped into the detector holder and held in place by a circular spring. While one foil is in position for exposure to the beam, the second detector holder may be removed and its platinum foil replaced. Then the holder, which is provided with an "O-ring", is screwed back into the machine, and the small air space is evacuated before the new detector is rotated into the machine vacuum and the path of the beam. There is also an observation port which is rotated into place so that the oven slit may be aligned with respect to the collimators. The light from the filament in the oven loader is sometimes sufficient to allow alignment of the oven aperture. When this is not possible, the oven is heated up until a clear image of the slit is seen through a telescope.

After exposure to the atomic beam, the platinum foils are placed in suitable beta counters. At a particular setting of the static C-field, the number of counts per minute of radioactivity deposited on the collecting foils is plotted as a function of the applied radio frequency. A frequency range is spanned by discrete frequency points until the entire resonance curve is traced out. For the frequencies where the C field is found to have drifted away from resonance, the exposure is repeated.

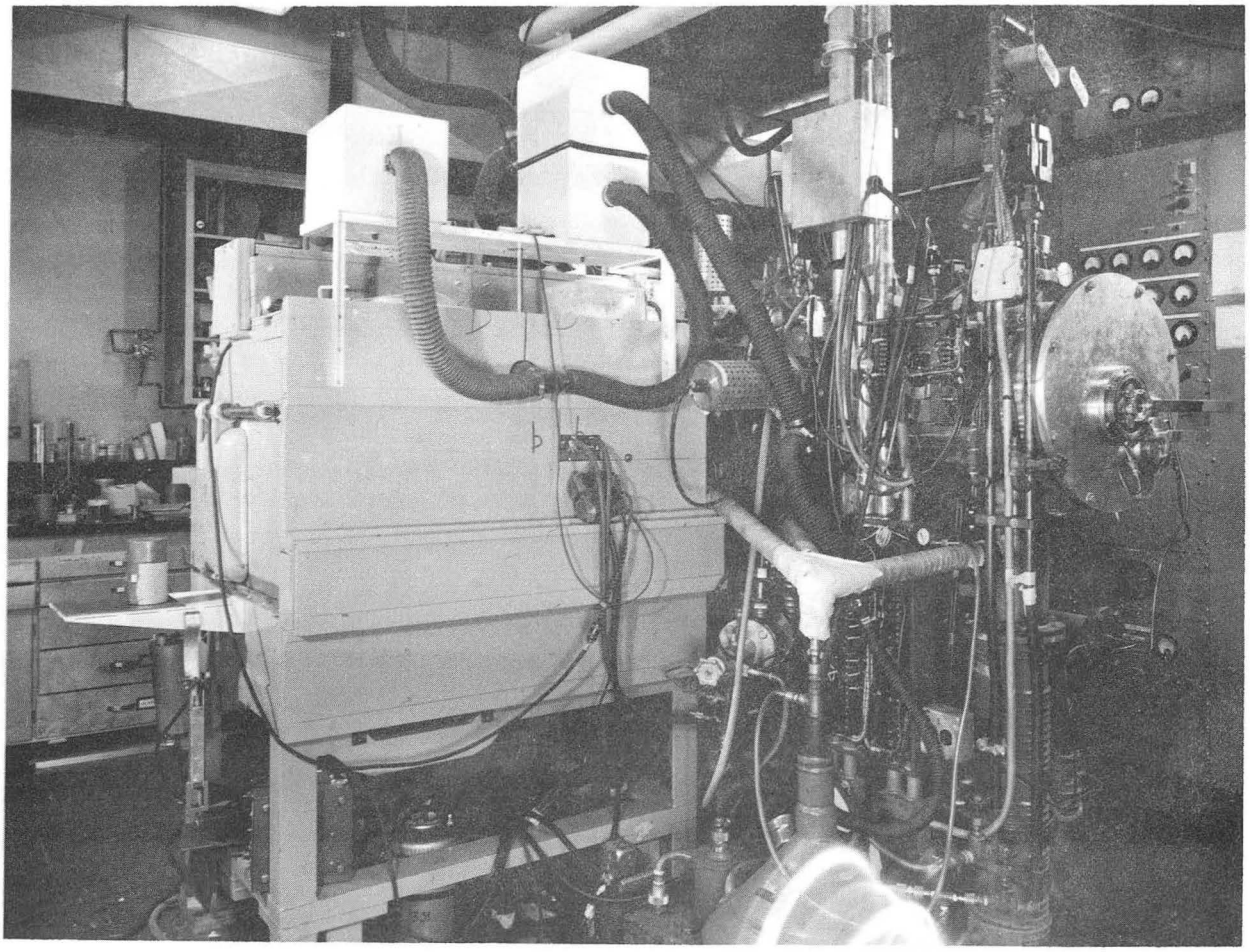

ZN-2591

Fig. 5. The atomic-beam apparatus. On the right is the detector end of the apparatus. Note the rotating mechanism with the port hole for beam alignment. Also note the three detector holders. On the left is the back end of the "cave".

IV. HYPERFINE-STRUCTURE MEASUREMENTS ON PRASEODYMIUM-142

The nuclear ground-state spin has been reported previously (I=2) and is in agreement with the result from beta-decay studies.[31] Grace et al. have determined the magnetic dipole moment by the method of nuclear alignment, and their result is lower than the value obtained here.[32] An attempt to reconcile these two calculations is made in a later section.

For the early members of the rare earth series, the nuclear shape is assumed to be spherical, in contrast to the main part of this region, where the equilibrium nuclear shape is strongly deformed. Therefore the nuclear spin and moments are discussed on the basis of the single-particle shell model.[33, 34]

A. Experimental Observations

Transitions of the type $\Delta F=0$, $\Delta m = \pm 1$ yield information on the hfs separations as soon as the resonance frequencies include energy contributions that are nonlinear in H. Figures 6, 7, and 8 are a set of representative resonances of the type observed. The hfs separations are calculated from Eq. (9) to be:

$$\begin{aligned} \Delta\nu\ (13/2, 11/2) &= 13/2\ a + 13/24\ b \\ \Delta\nu\ (11/2,\ 9/2) &= 11/2\ a \\ \Delta\nu\ (9/2,\ 7/2) &= 9/2\ a - 5/16\ b \\ \Delta\nu\ (7/2,\ 5/2) &= 7/2\ a - 7/16\ b \end{aligned} \tag{34}$$

Initial values of a and b are calculated from the resonance frequencies. The b/a ratio indicates that the ordering of the F states is normal (i.e. the lowest value of F lies lowest in energy, assuming a positive μ_I). The experimental data is fed to an IBM-704 program which diagonalizes the energy matrix and calculates the energy eigenvalues.[35] The observed resonance frequencies are compared with the theoretical frequencies, and the differences are summed to give a "goodness of fit" parameter. The final iterated values of a and b, together with g_J are then printed out. The results for this isotope are:

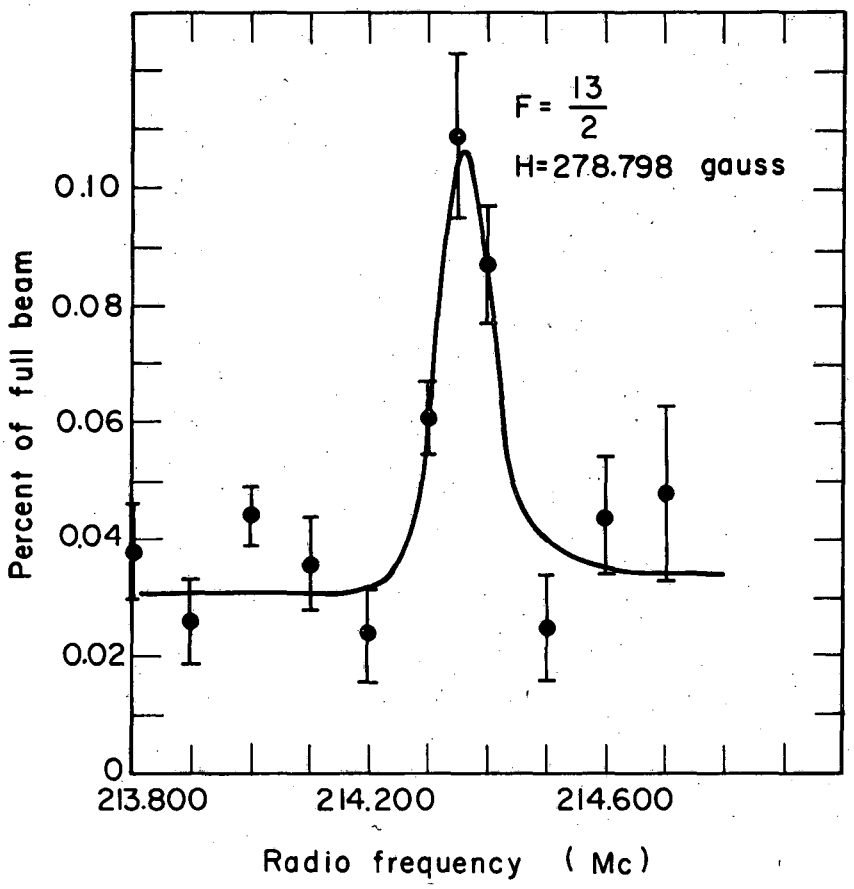

Fig. 6. Alpha resonance in Pr^{142} at 278.798 gauss.

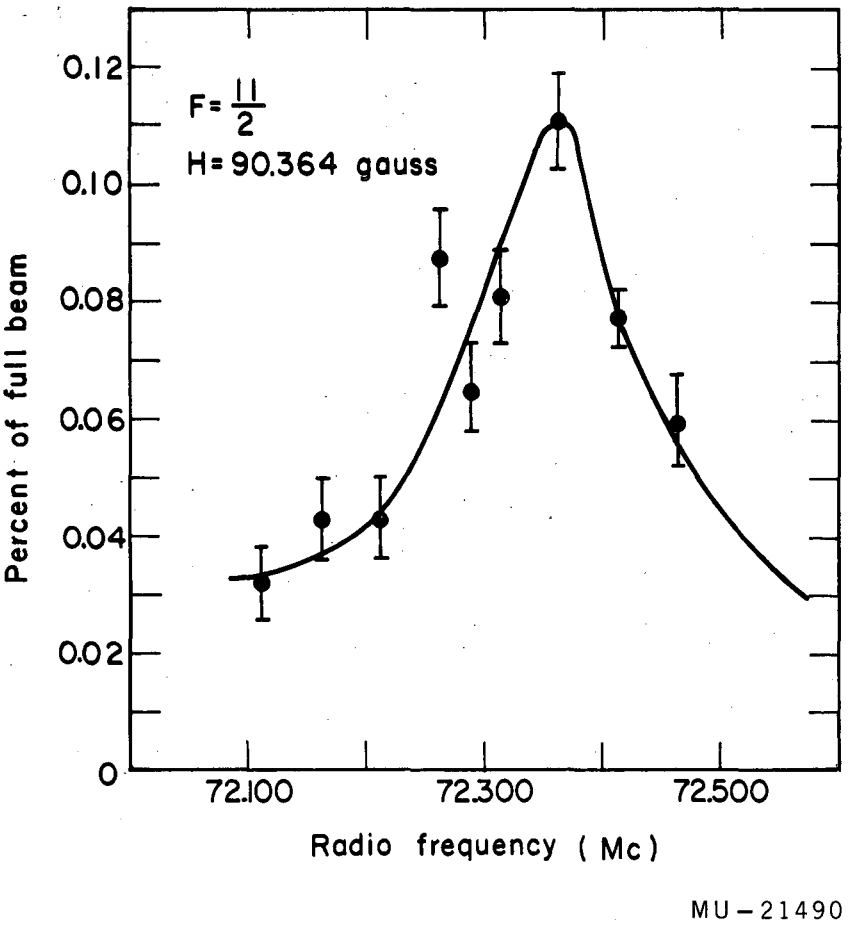

Fig. 7. Beta resonance in Pr^{142} at 90.364 gauss.

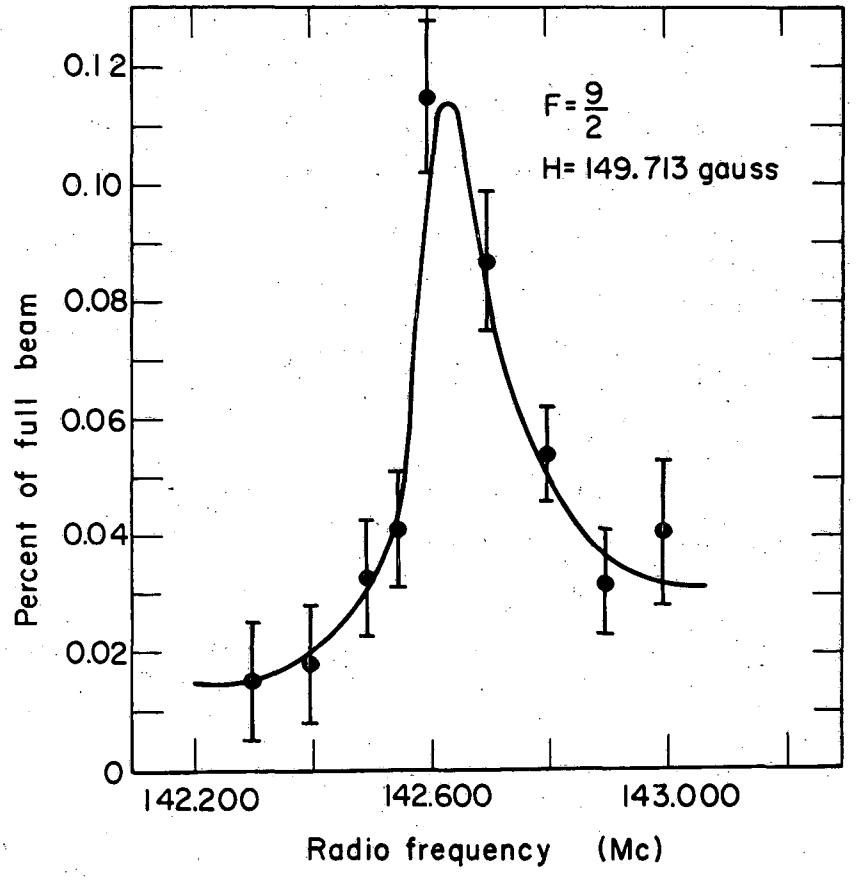

Fig. 8. Gamma resonance in Pr^{142} at 149.713 gauss.

$$\begin{aligned} |a| &= 67.5(5) \quad \text{Mc} \\ |b| &= 7(2) \quad\;\; \text{Mc} \\ g_J &= -0.7311(3) \text{ compared with } g_J(\text{RS}) = -0.7273. \end{aligned} \tag{35}$$

A graph of observed frequencies divided by H versus H is shown in Fig. 9 to illustrate the agreement of experiment with theory. Figure 10 is a schematic diagram of the hfs levels in a magnetic field. A summary of the experimental observations is given in Table II.

B. Nuclear Magnetic-Dipole Moment

The close agreement of the measured g value with the RS value implies that Russell-Saunders coupling is a good approximation. Therefore, for the evaluation of the nuclear moments, we make the initial assumption that the ground level is pure $^4I_{9/2}$. In a later section, we analyze the effect of the admixture of excited levels with the ground level. The hfs constant a is related to the nuclear dipole moment by Eq. (14). This is evaluated for $^4I_{9/2}$ to be

$$a(^4I_{9/2}\ 9/2) = \frac{2\mu_0\mu_I}{I}\left\langle \frac{1}{r^3} \right\rangle \frac{476}{363} . \tag{36}$$

The average value $\left\langle \frac{1}{r^3} \right\rangle$ has been calculated using a modified hydrogenic wave function with two parameters.[2, 36] One of these is determined from comparison with self-consistent-field calculated wave functions and the other from an interpolated value of the spin-orbit coupling constant. The result is[37]

$$\left\langle \frac{1}{r^3} \right\rangle = \frac{3.63}{a_0^3} , \tag{37}$$

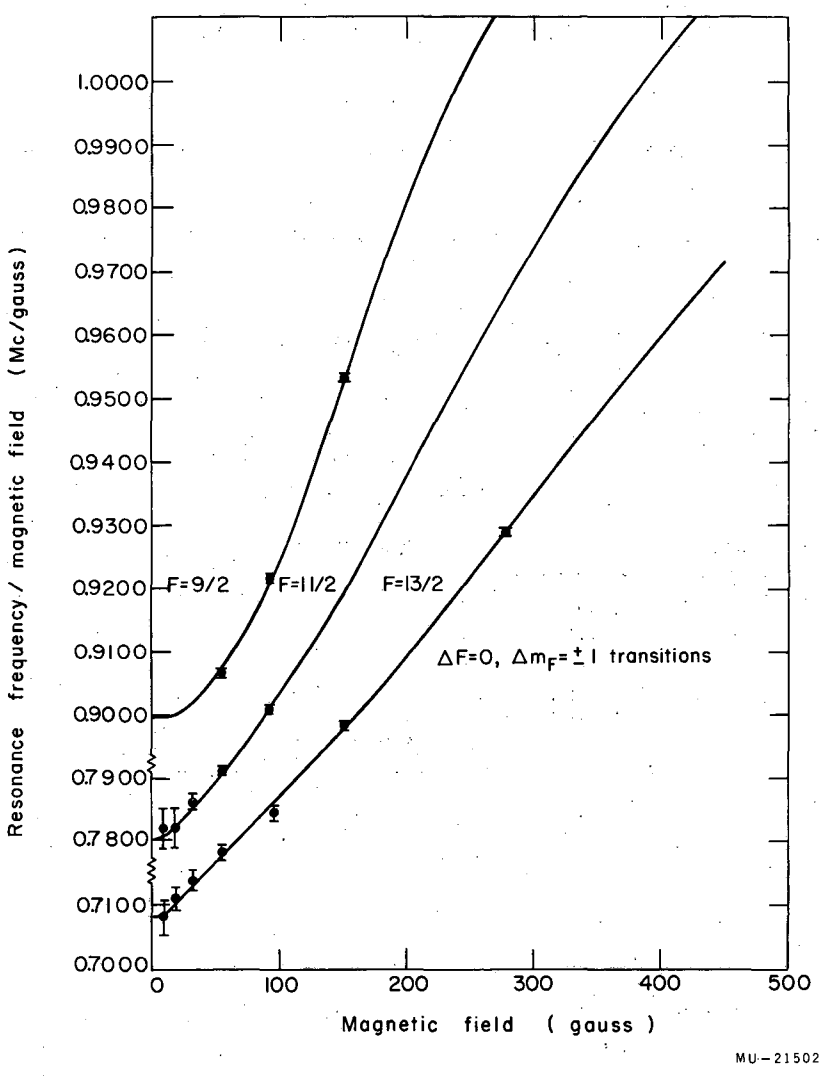

Fig. 9. Plot of magnetic field vs resonance frequency divided by magnetic field. The experimental points compared with theoretical curves, which are calculated with the final values of a, b, and g_J.

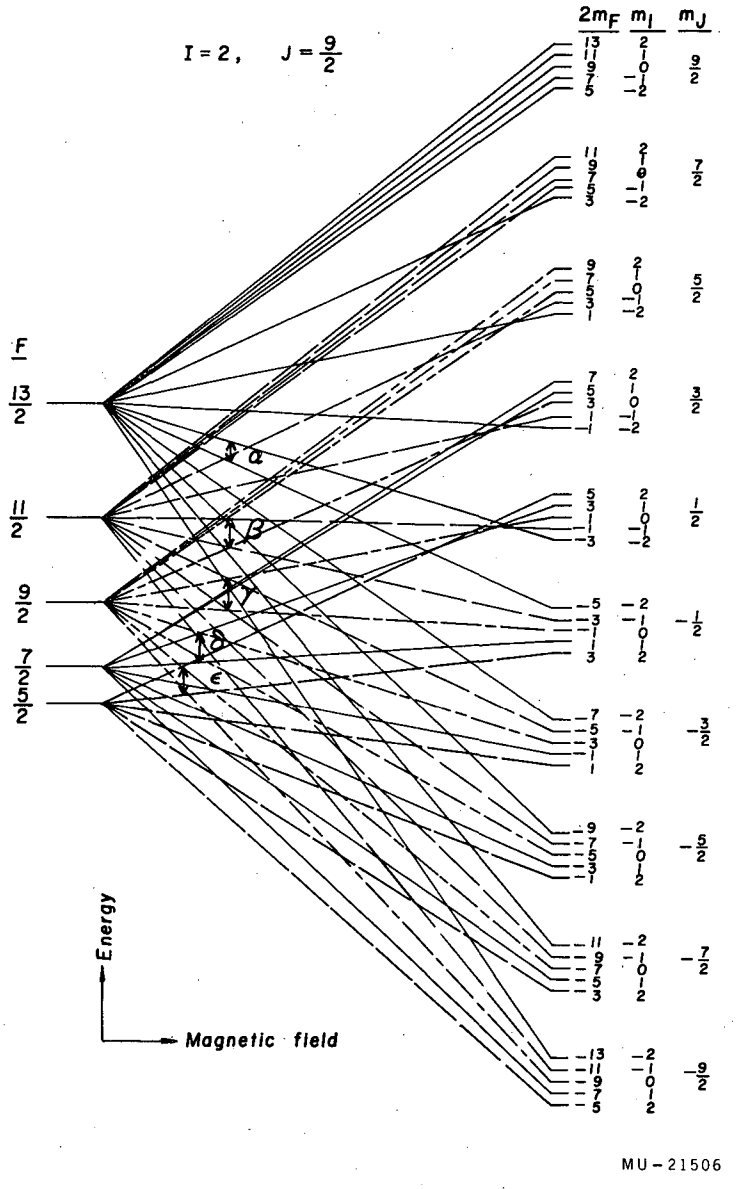

Fig. 10. Schematic diagram of the hfs energy levels of Pr^{142} in an external magnetic field.

Table II. Summary of observations in Pr^{142}

Data No.	H (gauss)	Observed frequency (Mc)	Obs. freq. -calc. freq. (Mc)	Transition[a]
1	8.248(66)	5.837(25)	-0.018	α
2	8.248(66)	6.450(25)	+0.005	β
3	15.920(62)	11.320(30)	-0.002	α
4	15.920(62)	12.450(50)	-0.012	β
5	29.836(54)	21.300(50)	+0.006	α
6	29.836(54)	23.460(30)	+0.025	β
7	53.423(44)	38.375(50)	+0.016	α
8	53.423(44)	42.260(25)	+0.020	β
9	53.423(44)	48.412(30)	-0.052	γ
10	90.364(34)	65.475(50)	-0.063	α
11	90.364(34)	72.360(50)	+0.035	β
12	149.713(50)	110.525(50)	+0.040	α
13	149.713(50)	142.630(50)	-0.003	γ
14	279.798(29)	214.360(20)	-0.001	α
15	90.364(34)	83.240(60)	+0.004	γ

[a] α: $(F = 13/2, m = -3/2) \leftrightarrow (F = 13/2, m = -5/2)$
β: $(F = 11/2, m = -1/2) \leftrightarrow (F = 11/2, m = -3/2)$
γ: $(F = 9/2, m = 1/2) \longleftrightarrow (F = 9/2, m = -1/2)$

where a_0 is the first Bohr radius. The uncertainty is estimated to be less than 5%.

Using Eqs. (36) and (37) and the experimental value of a, we get

$$\left|\mu_I^{142}\right| = 0.297(15) \text{ n.m.} \tag{38}$$

The assigned uncertainty is due mainly to the uncertainty in the value of $\left\langle \frac{1}{r^3} \right\rangle$. The magnitude of the moment is too small to allow a determination of the sign.

C. Nuclear Electric-Quadrupole Moment

The quadrupole moment is related to b by

$$b(^4I_{9/2}\ 9/2) = -e^2 Q \left\langle \frac{1}{r^3} \right\rangle (f^3\ ^4I_{9/2}\ 9/2 \left| \sum_i 3\cos^2\theta_i - 1 \right| f^3\ ^4I_{9/2}\ 9/2), \tag{39}$$

where the electronic matrix element of the angular part has been evaluated by using Eq. (15). The result is $-28/121 = -0.2314$. This agrees with the value given by Hin Lew.[38] Relativistic effects are discarded here. Using Eqs. (39) and (15) with the experimental value of b, we obtain

$$\left|Q^{142}\right| = 0.035(15) \text{ barns.} \tag{40}$$

The uncertainty does not include polarization effects arising from the distortion of the electron core by the quadrupole moment and the subsequent change in the electric-field gradient.[39] Here again, the sign of the moment is undetermined.

The atomic beam work of Hin Lew on Pr^{141} yielded nuclear moments which were calculated by using hydrogenic wave functions. With a screening constant ($\sigma = 35.5$) and the fine-structure constant from Nd I, one gets $\left\langle a_0^3/r^3 \right\rangle = 4.83$. This value is 25% larger than that

obtained with the modified-hydrogenic wave function mentioned above. With the latter value, we obtain

$$\mu_I^{141} = 5.1(3) \text{ n m}$$

and

$$Q^{141} = - 0.070(4) \text{ barns}$$

compared with 3.8(4) nm and -0.054(5) barns given by Hin Lew.

D. Theoretical Estimates of the Nuclear Moments

The nuclear spin of the odd-odd nucleus of Pr^{142} is consistent with the single-particle shell model. On the basis of this model, the fifty-ninth proton and eighty-third neutron are assigned to the orbitals 4 d 5/2 and 5 f 7/2 respectively. The measured spin value is then consistent with Nordheim's weak rule.

If g_p and g_n are the g values of the odd proton and odd neutron with spins j_p and j_n, then the nuclear magnetic moment is[40]

$$\mu_I = 1/2 \left\{ (g_p + g_n) I + (g_p - g_n) \frac{j_p(j_p+1) - j_n(j_n + 1)}{2 I + 1} \right\}. \qquad (41)$$

Values of g_p and g_n are obtained from the experimental dipole moments of two odd-A isotopes.[31,41] From Pr^{141} ($I = 5/2$), $\mu_I = + 5.1(3)$ nm gives $g_p = + 2.04$; from Ce^{141} ($I = 7/2$), $\mu_I = \pm 0.89$ nm gives $g_n = \pm 0.25$. We find that the negative sign of the neutron moment results in a theoretical moment of - 0.88 for Pr^{142}, which is three times larger than our estimated value. With a positive sign we get the theoretical value $\mu_I^{theor} = + 0.20(14)$ nm, compared with the experimental result $\mu_I^{exp't} = \pm 0.30(2)$ nm. It follows from this that a positive sign of the magnetic moment is most probable.

For the quadrupole moment of an odd-odd nucleus, the following formula has been derived from the single-particle shell model:[40]

$$Q = \frac{(2I+1)!}{2j_p!} \left\{ \frac{(2j_p-2)!\ (2j_p+3)!}{(2I-2)!\ (2I+3)!} \right\}^{1/2} W(j_p I\ j_p I; j_n 2)$$

$$(-1)^{j_n - j_p - I} Q_{j_p}, \qquad (42)$$

where Q_{j_p} is the quadrupole moment of the odd proton. In this case the value of the Racah coefficient is

$$W(5/2\ 2\ 5/2\ 2;\ 7/2\ 2) = W(5/2\ 5/2\ 2\ 2;\ 2\ 7/2) = -\ 17/35(24)^{1/2}. \qquad (43)$$

With the experimental value of Q_{j_p} from Pr^{141}, we obtain

$$Q^{theor} = 0.034(2) \text{ barns},$$

compared with the experimental value

$$\left| Q^{exp't} \right| = 0.035(15) \text{ barns}.$$

E. Ground-State Electronic Wave Function with Admixtures via the Spin-Orbit Effect

The term ^2H occurs twice in the configuration f^3. In order to differentiate between the two, the irreducible representations of R_7 and G_2 are used in the state assignments. For convenience, let us sometimes refer to the groups (210)(21) as A and (210)(11) as B. It has been found that these are the two lowest energy levels that can perturb $^4I_{9/2}$ via the spin-orbit interaction. From Judd and Lindgren,[37] the term that actually occurs in nature is a linear combination of the two, so that the eigenfunction is

$$0.9217\ |f^3\ A\ ^2H) - 0.3878\,|f^3\ B\ ^2H) \tag{44}$$

with the energy eigenvalue $32.9\times F_2$, where F_2 is a radial integral defined by Condon and Shortley. The ground term ^4I is taken as the zero of energy. Now the ground level wave function is

$$|GJ = 9/2\ J_z) = \alpha\,|f^3\ ^4I_{9/2}J_z) + \beta\big[0.9217\,|f^3\ A^2H_{9/2}J_z) - 0.3878\,|f^3\ B\ ^2H_{9/2}J_z)\big], \tag{45}$$

where the remaining quantum numbers in the first ket are denoted by G.

The admixture is calculated from first-order perturbation theory to be

$$\beta = \frac{0.9217\ (^4I_{9/2}\,|\mathbb{A}|\ A^2H_{9/2}) - 0.3878\ (^4I_{9/2}\,|\mathbb{A}|\ B^2H_{9/2})}{\Delta E(^4I,\ ^2H)}\ , \tag{46}$$

where the spin-orbit operator is

$$\mathbb{A} = \zeta \sum_i \vec{s}_i \cdot \vec{\ell}_i\ ,$$

with the fine-structure energy constant $\zeta = 619\ cm^{-1}$.

The energy separation ΔE is $-32.9\,F_2$ with $F_2 = 298\ cm^{-1}$. These numbers are results obtained by Judd and Lindgren.[37]

The complete spin-orbit matrix for $J = 9/2$ in the configuration f^3 has been published.[42] The part of this matrix which is of interest here is

	$B\ ^2H$	$A\ ^2H$	^4I
$B\ ^2H$	0	0	$-(13/22)^{1/2}$
$A\ ^2H$	0	$-(81/25)^{1/2}$	$(70/11)^{1/2}$
^4I	$-(13/22)^{1/2}$	$(70/11)^{1/2}$	$-(25/9)^{1/2}$

$\zeta.$

By using Eqs. (45) and (46), the coefficients are evaluated as $\beta = -0.165$ and $\alpha = (1 - \beta^2)^{1/2} = 0.986$.

Therefore the electronic wave function for the ground level is

$$|G\ 9/2\ 9/2) = 0.986\,|f^3\ (111)\ (20)\ ^4I_{9/2}\ 9/2) - 0.152\,|f^3\ (210)(21)^2H_{9/2}9/2)$$

$$+ 0.064\,|f^3(210)(11)^2H_{9/2}9/2). \qquad (47)$$

The states have been specified for $J_z = J = 9/2$ since this particular ket will be used in subsequent calculations.

A paramagnetic-resonance experiment on Pr^{142} by Grace et al.[32] was performed in order to investigate the polarization of beta emitters by the low-temperature method. This work was stimulated by the theoretical predictions of Lee and Yang that parity may not be conserved in beta decay.[43] This was subsequently confirmed by Wu et al.[44]

A crystal of cerium magnesium nitrate together with some Pr^{142} was grown from solution. The crystal was then cooled by adiabatic demagnetization and the gamma-ray anisotropy was measured as a function of temperature at zero field. The nuclear magnetic moment is determined from the gamma-ray anisotropy in the magnetic field.

They obtain two values of μ_I from the two possible changes in angular momentum (i_β) accompanying the beta transition:

i_β	μ_I (n m)
0	0.11(1)
1	0.17(2) .

F. Effect of Admixtures on the Magnetic Field due to Electrons

In the following calculations we attempt to reconcile our value of μ_I with the lower value estimated by Grace et al. The modified electronic wave function of Eq. (47) is used, and off-diagonal matrix elements connecting the ground level with excited levels are calculated, using the methods outlined in Chapter II-B.2.

The matrix elements of the orbital part of the magnetic field operator are

$$(f^3(111)(21)\,{}^4I_{9/2} \,\|\, \Sigma_i \ell_i \,\|\, f^3(111)(20)\,{}^4I_{9/2})$$

$$= 260/3(21)^{1/2}\,\delta(S,S')\begin{Bmatrix} 6 & 9/2 & 3/2 \\ 9/2 & 6 & 1 \end{Bmatrix}\left[2\begin{Bmatrix} 3 & 6 & 3 \\ 6 & 3 & 1 \end{Bmatrix} + 7\begin{Bmatrix} 3 & 6 & 5 \\ 6 & 3 & 1 \end{Bmatrix}\right]$$

$$= 21\,(10/11)^{1/2}$$

$$(f^3(111)(20)\,{}^4I_{9/2} \,\|\, \Sigma \ell_i \,\|\, f^3(210)(21)\,{}^2H_{9/2}) = 0$$

and

$$(f^3(111)(20)\,{}^4I_{9/2} \,\|\, \Sigma \ell_i \,\|\, f^3(210)(11)\,{}^2H_{9/2}) = 0$$

The following coefficients of fractional parentage for f^3 are extracted from the complete table given by Judd:[45]

ψ	$\bar{\Psi}$	
	^3F	^3H
(210)(11) H	$-(1/2)^{1/2}$	0
(210)(21) H	0	$-(1/2)^{1/2}$
(111)(20) I	$-(2/9)^{1/2}$	$(7/9)^{1/2}$

(48)

Where $\bar{\Psi}$ and ψ are the parent and daughter states respectively. These coefficients occur in all the evaluations of the matrix elements in the three states considered.

The contribution from the orbit, when combined with the spin part, gives the following

$$(I) \equiv (f^3(111)(20)\ ^4I_{9/2} \left|\left| \underset{\sim}{N} \right|\right| f^3(111)(20)\ ^4I_{9/2})$$

$$= 21\ (10/11)^{1/2} + 3640\ (5)^{1/2} \begin{pmatrix} 3 & 2 & 3 \\ 0 & 0 & 0 \end{pmatrix} \begin{Bmatrix} 1/2 & 3/2 & 1/2 \\ 3/2 & 1/2 & 1 \end{Bmatrix}$$

$$\begin{Bmatrix} 3/2 & 3/2 & 1 \\ 6 & 6 & 2 \\ 9/2 & 9/2 & 1 \end{Bmatrix} \left[2 \begin{Bmatrix} 3 & 6 & 3 \\ 6 & 3 & 2 \end{Bmatrix} + 7 \begin{Bmatrix} 3 & 6 & 5 \\ 6 & 3 & 2 \end{Bmatrix} \right]$$

$$= 238/11\ (10/11)^{1/2}\ . \tag{49}$$

The off-diagonal contributions from the higher terms are

$$(II) \equiv (f^3(210)(21)\ ^2H_{9/2} \left|\left| \underset{\sim}{N} \right|\right| f^3(111)\ (20)\ ^4I_{9/2})$$

$$= -\ 420\ (5005)^{1/2} \begin{pmatrix} 3 & 2 & 3 \\ 0 & 0 & 0 \end{pmatrix} \begin{Bmatrix} 1/2 & 3/2 & 1 \\ 1/2 & 1/2 & 1 \end{Bmatrix} \begin{Bmatrix} 3 & 6 & 5 \\ 5 & 3 & 2 \end{Bmatrix} \begin{Bmatrix} 3/2 & 1/2 & 1 \\ 6 & 5 & 2 \\ 9/2 & 9/2 & 1 \end{Bmatrix}$$

$$= -\ 34/55\ (7)^{1/2} \tag{50}$$

and

$$(\mathrm{III}) \equiv (f^3(210)(11)\ {}^2H_{9/2} \| \underset{\sim}{N} \| f^3(111)(20)\ {}^4I_{9/2})$$

$$= 420\ (1430)^{1/2} \begin{pmatrix} 3 & 2 & 3 \\ 0 & 0 & 0 \end{pmatrix} \begin{Bmatrix} 1/2 & 3/2 & 1 \\ 1/2 & 1/2 & 1 \end{Bmatrix} \begin{Bmatrix} 3 & 6 & 3 \\ 5 & 3 & 2 \end{Bmatrix} \begin{Bmatrix} 3/2 & 1/2 & 1 \\ 6 & 5 & 2 \\ 9/2 & 9/2 & 1 \end{Bmatrix}$$

$$= 7/11\ (13/5)^{1/2}\ . \tag{51}$$

The total electronic matrix element is related to the above reduced matrix elements by

$$(G\ \ JJ \left| \underset{\sim}{N} \right| G\ \ JJ) = (-1)^{J-J} \begin{pmatrix} J & 1 & J \\ -J & 0 & J \end{pmatrix} (G\ \ JJ \| \underset{\sim}{N} \| G\ \ JJ)\ . \tag{52}$$

The interaction constant $a(J)$ measured in the ground level J, is given in terms of Eq. (52) and the nuclear dipole moment by

$$a(9/2) = \frac{\mu_I \mu_0}{9/2} \left\langle \frac{1}{r^3} \right\rangle\ (G\ 9/2\ \ 9/2 \| \underset{\sim}{N} \| G\ 9/2\ \ 9/2)\ . \tag{53}$$

and

$$\frac{2}{9}\ (G\ 9/2\ \ 9/2 \left| \underset{\sim}{N} \right| G\ 9/2\ \ 9/2) = \begin{pmatrix} 9/2 & 1 & 9/2 \\ -9/2 & 0 & 9/2 \end{pmatrix}$$

$$\times \left\{ c_1^2\ (\mathrm{I}) + 2\, c_1\, c_2\ (\mathrm{II}) + 2\, c_1\, c_3\ (\mathrm{III}) \right.$$

$$\left. + 2\, c_2\, c_3\ (\mathrm{IV}) + c_2^2\ (\mathrm{V}) + c_3^2\ (\mathrm{VI}) \right\} \tag{54}$$

$$= 1.3143\ .$$

The coefficients c_i are the amplitudes of the ground-level eigenfunction (47). The last three terms in Eq. (54) are neglected in view of the smallness of the factors multiplying the matrix elements (IV), (V), and (VI). The matrix elements (I), (II), and (III) have been defined previously. These other elements are

$$(IV) = (A\ ^2H_{9/2}\ 9/2 \| \underset{\sim}{N} \| B^2H_{9/2}\ 9/2)\ ,$$

$$(V) = (A\ ^2H_{9/2}\ 9/2 \| \underset{\sim}{N} \| A^2H_{9/2}\ 9/2)\ ,$$

and

$$(VI) = (B\ ^2H_{9/2}\ 9/2 \| \underset{\sim}{N} \| B^2H_{9/2}\ 9/2)\ .$$

Combining the result of Eq. (54) with Eq. (53), we get

$$\left| \mu_I{}^{142} \right| = 0.296(15)\ \text{n m}\ , \tag{55}$$

It is seen that the considered admixtures only lower the value of the dipole moment by about 0.3%. Excited levels higher in the configuration would certainly give even more negligible effects. Thus it does not seem possible to reconcile our value with that obtained by Grace et al.[32]

V. EXPERIMENTAL OBSERVATIONS AND RESULTS ON NUCLEAR GROUND-STATE SPINS AND ELECTRONIC GROUND LEVELS; THEORETICAL SPECULATIONS ON ELECTRONIC STRUCTURE

The transition energy between hyperfine states W_1 and W_2 is

$$\nu = W_1/h - W_2/h \, . \tag{56}$$

For pi transitions ($\Delta F = 0$, $\Delta m = \pm 1$), the resonance frequency is independent of the energy difference, which depends on the interaction constants a, b, and so on. This is easily seen to be so from Eq. (9), since F is unchanged for these transitions. If the external magnetic-field perturbation is weak enough so that second- and higher-order terms in H may be neglected in the energy levels, the transition frequency is given by the single term

$$\nu = g_J \frac{F(F+1) + J(J+1) - I(I+1)}{2F(F+1)} \frac{\mu_0 H}{h} \tag{57}$$

where μ_0 is the Bohr magneton and H is the value of the external magnetic field.

If the ground levels and corresponding g values are known, then Eq. (57) is used to determine the nuclear spin. This is called a "spin search", where a single frequency exposure is obtained for each spin possible. If the atomic beam is reasonably steady, then the nuclear spin may essentially be measured within ten frequency exposures.

Until recently, the ground levels and g values of some of the lanthanides studied were not known. Also the nuclear spins were unknown for the isotopes investigated. In these cases, the procedure is as follows. The frequency spectrum of resonances is covered at a low magnetic field (about 0.5 gauss). In many instances, the resonances observed at this low field are superpositions of several resonances. Later on, resolution is obtained by repeating the frequency sweep at a higher value of the magnetic field. Then the resonances are fitted to transitions between

(F, m) states belonging to hfs systems denoted by I, J_1, I, J_2, etc., where $J_1, J_2, \cdots$ are the levels assumed to be present in the atomic beam. For those elements with measured fine-structure separations, it is possible to estimate which J levels are sufficiently populated at beam temperature. A measured g value is assigned to each level, and comparison is made with theoretical values based on a coupling scheme for the electrons. In most cases, the Russell-Saunders approximation is found to be valid, and the small deviations are attributed to spin-orbit and relativistic effects.

A. Samarium-153

As early as 1935, optical spectroscopic measurements on samarium had established the ground-state electronic configuration to be $4f^6 6s^2$, resulting in the ground term ^7F.[46] The fine-structure separations were used to estimate the relative population per J level at 1,000 ^0K (Fig. 11). This is approximately the effusion temperature of the samarium atomic beam. Tantalum ovens with inner liners were used for most of the lanthanides investigated (Fig. 12). The first four low-lying levels are J = 0, 1, 2, and 3. No resonances were observed in J = 0 because the electronic moment is zero for this level.

With a nuclear spin of 3/2, three resonances were observed in J = 1 and 2. The resonances are multiple-quantum transitions between the following hfs states. For I = 3/2, and J = 1, $(F_1, m_1) \leftrightarrow (F_2, m_2)$, we have

$$(F = 5/2, m = 5/2) \leftrightarrow (F = 5/2, m = -5/2)$$
$$(F = 5/2, m = 3/2) \leftrightarrow (F = 5/2, m = -5/2)$$
$$(F = 5/2, m = 1/2) \leftrightarrow (F = 5/2, m = -5/2)$$
$$(F = 5/2, m = -1/2) \leftrightarrow (F = 5/2, m = -5/2).$$

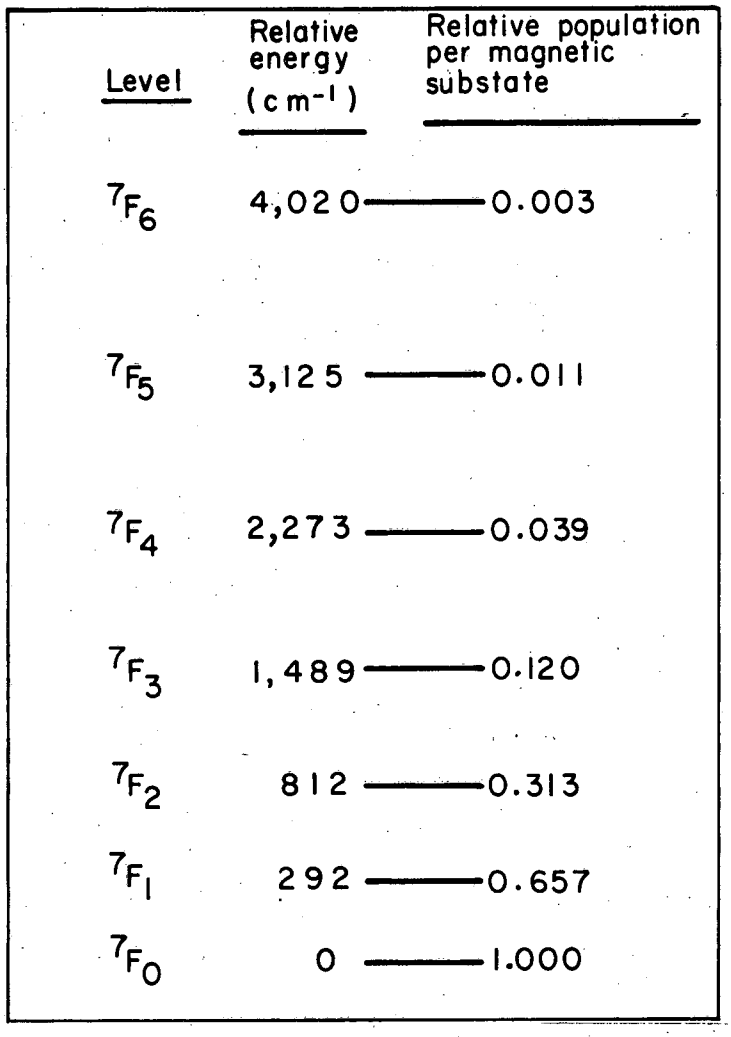

MU-21493

Fig. 11. Schematic diagram of the fine structure of samarium in the ground term ^7F.

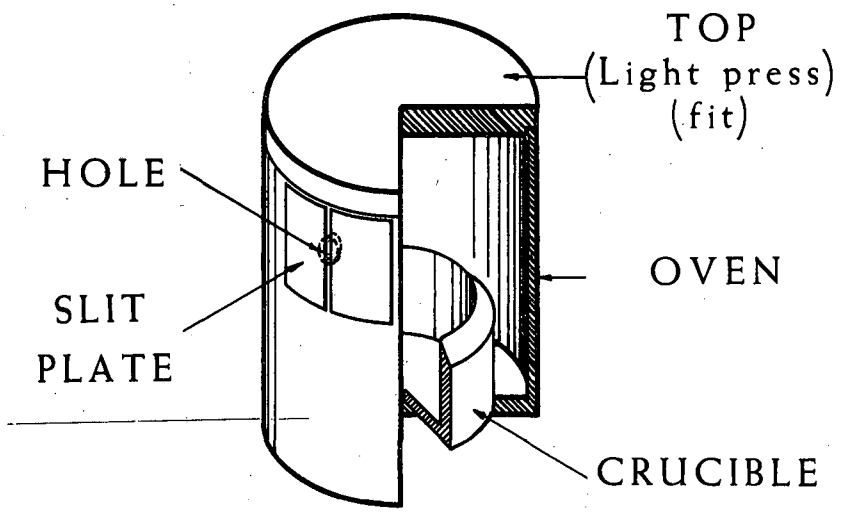

Fig. 12. Tantalum oven with inner liner used for most of the rare-earth investigations.

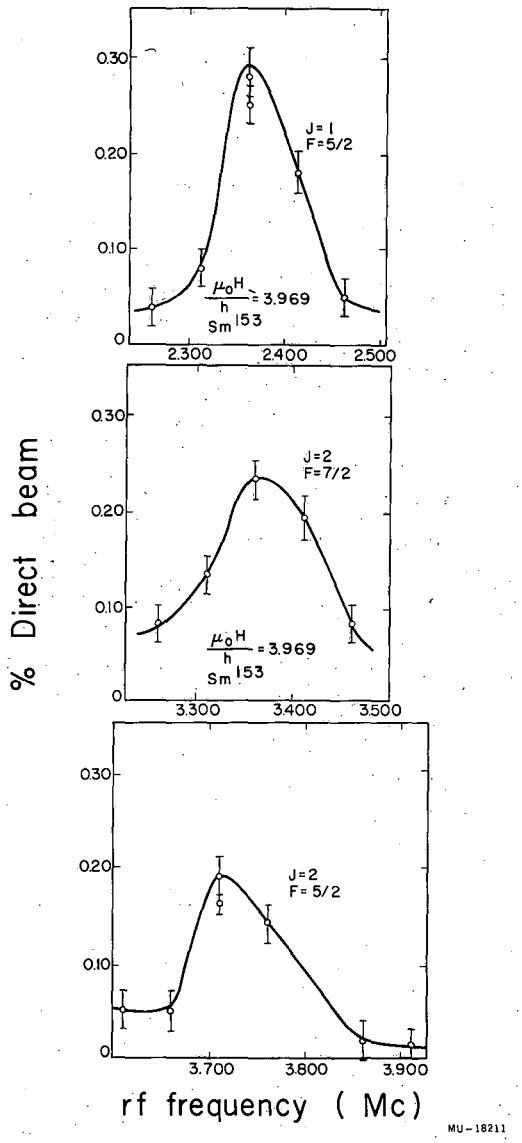

Fig. 13. Samarium-153 resonances in the levels J = 1 and J = 2.

For $I = 3/2$, and $J = 2$, the multiple quantum transitions are

$$(F = 7/2, m = 7/2) \leftrightarrow (F = 7/2, m = -7/2)$$
$$(F = 7/2, m = 5/2) \leftrightarrow (F = 7/2, m = -7/2)$$
$$(F = 7/2, m = 3/2) \leftrightarrow (F = 7/2, m = -7/2)$$
$$(F = 7/2, m = 1/2) \leftrightarrow (F = 7/2, m = -7/2)$$
$$(F = 7/2, m = -1/2) \leftrightarrow (F = 7/2, m = -5/2).$$

With $I = 3/2$, and $J = 2$, the transitions in $F = 5/2$ are

$$(F = 5/2, m = 5/2) \leftrightarrow (F = 5/2, m = -3/2)$$
$$(F = 5/2, m = 3/2) \leftrightarrow (F = 5/2, m = -3/2)$$
$$(F = 5/2, m = 1/2) \leftrightarrow (F = 5/2, m = -3/2)$$

In the Zeeman region, all the transitions in each F state occur at the same frequency and contribute to the resonance frequency.

Each of the three transitions were observed at three settings of the magnetic field. One set of resonance curves are shown in Fig. 13. Table III compares the predicted g_F with the mean g_F obtained. These results indicate that the g values are

$\frac{J}{1}$	$\frac{g_J(\text{exp't})}{-1.495(15)}$	$\frac{g_J(\text{RS})}{-1.5000}$
2	$-1.497(15)$	-1.5000 .

Note that since $L = S$ for ^7F, the theoretical g values for all the levels are equal to $3/2$ in RS coupling.

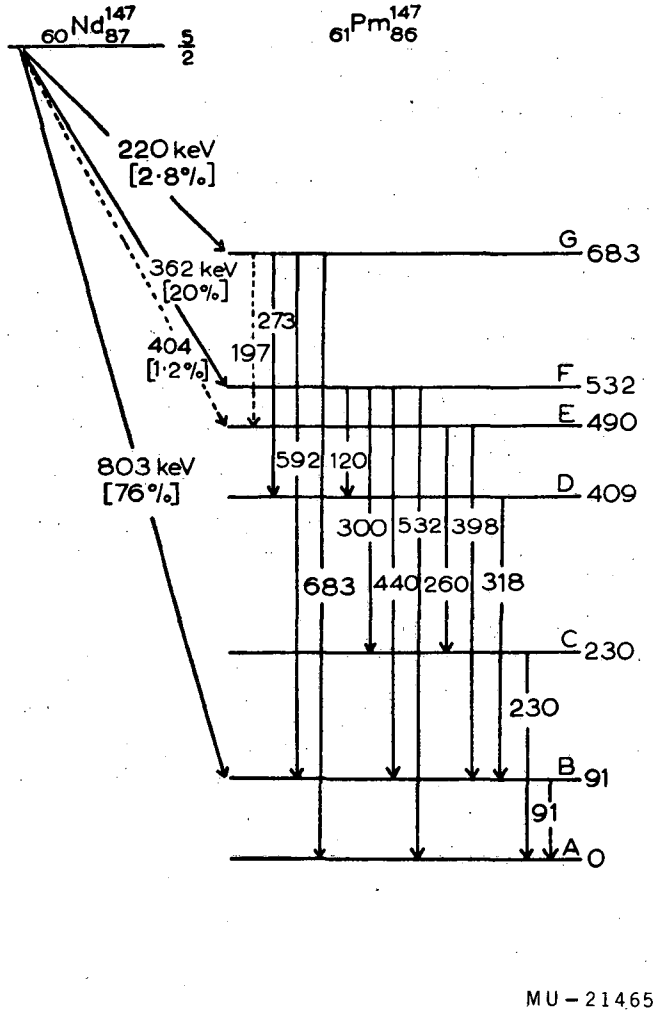

Fig. 14. Proposed nuclear decay scheme for Nd^{147}.

Table III. All observed g_F values in samarium-153

$\frac{\mu_0 H}{h}$ (Mc)	J=1, F=5/2	J=2, F=7/2	J=2, F=5/2
1.000	0.61(5)	0.95(5)	1.01(5)
1.985	0.60(3)	0.86(2)	0.94(2)
3.945	0.598(10)	0.855(11)	0.941(13)
Mean g_F	0.598(10)	0.856(11)	0.941(10)
Predicted g_F	0.6000	0.857	0.943

B. Neodymium-147 and Promethium-147

The purpose of our investigations on these isobars was two-fold. The first was to add understanding to the decay picture of Nd^{147} which decays by beta emission to Pm^{147} (Fig. 14). The second objective was to infer the ground electronic configuration of promethium. It is noted that this element is the only rare earth that does not have a stable isotope. Several investigations of the beta decay of Nd^{147} have failed to reveal a direct beta transition to the ground state.[47] The most intense beta line decays to the first excited state which then decays to the ground state with an M1 gamma-ray transition. The spin of Nd^{147} has been measured to be 5/2 by paramagnetic resonance,[41] and the probable ground-state spin of Pm^{147} is 5/2 or 7/2, based on the single-particle shell model.[48]

Neodymium-147 was produced by neutron irradiation of Nd metal at the reactor in Arco, Idaho. The decay rate of a detector exposed to the beam at resonance determines the identity of the isotope. (Fig. 15). Promethium-147 may be obtained in curie amounts from the

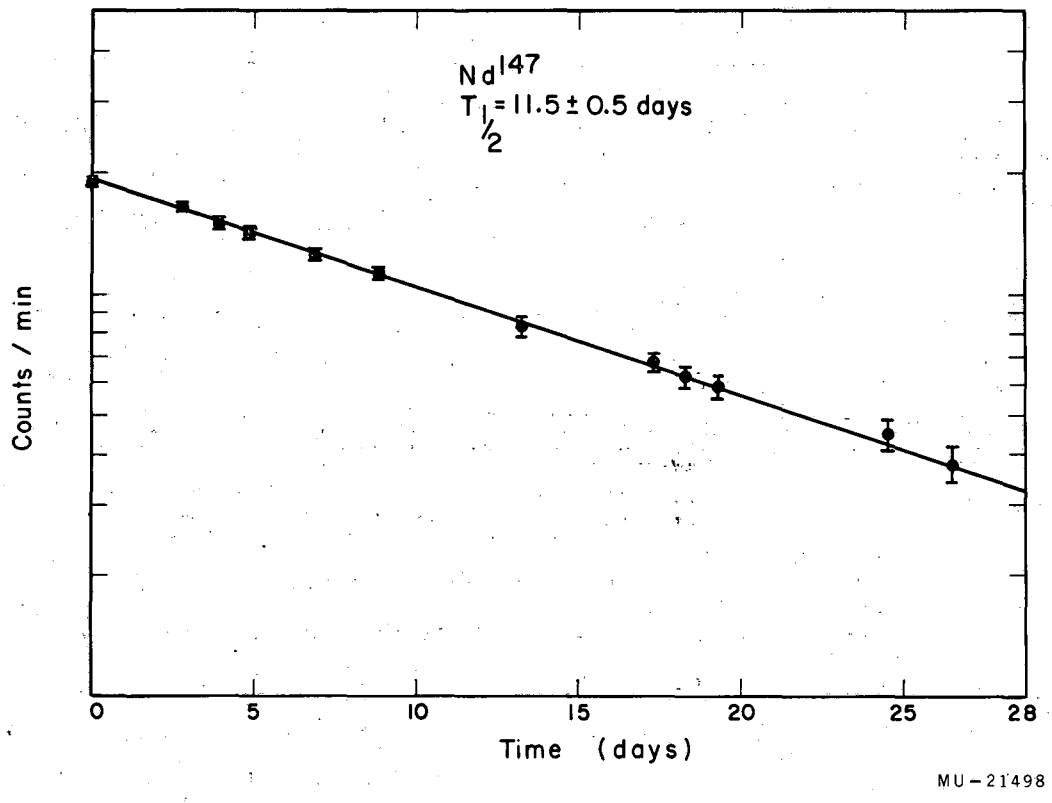

Fig. 15. Radioactive decay of Nd^{147}.

Oak Ridge National Laboratory. It comes in a weak HCl solution. This is converted to the nitrate by adding an excess of nitric acid to the solution. The nitrate salt is then mixed with an excess of lanthanum metal in the source oven. This is then transferred to the oven loader and inserted into the machine. The oven is then heated up slowly by electron bombardment. It is believed that the nitrate is first converted to the oxide which then reacts with the lanthanum to set free the promethium atoms.

Stable atomic beams of neodymium have been investigated,[49] and the ground level is characterized by $^5I_4$ with $g_J = -0.603$. We have confirmed the spin of Nd^{147} to be 5/2, and this couples with J = 4 in Zeeman region. The resonance frequencies of the pi transitions are given by

$$\nu_F = g_F \frac{\mu_0 H}{h} = 0.603 \quad \frac{F(F+1) + 55/4}{2F(F+1)} \frac{\mu_0 H}{h} . \qquad (58)$$

Transitions in the three highest F states 13/2, 11/2, and 9/2 have been observed at two values of the magnetic field (Fig. 16). The observed g_F values are compared with the predicted values using Eq. (58). The small discrepancies in some of the g_F values are due to quadratic and higher-order shifts arising from a small hyperfine structure.

A systematic search for resonances was conducted at a low magnetic field to cover the reasonable range of possible g values. This gave the first information on the electronic ground levels of promethium. Three resonances were observed, each of which were followed up in field to a maximum of 38.2 gauss. The g_F values corresponding to the observed resonances are given in Table IV. Figure 17 shows the single Pm^{147} resonance in the Zeeman region for J = 7/2.

The most probable configuration for Pm, which has 61 protons seems to be $4f^5$. The configurations of $_{60}Nd$ and $_{62}Sm$ are known to be $4f^4$ and $4f^6$, respectively.[46, 50] The Hund's rule term is expected to be ^6H, with the levels J = 5/2, 7/2, and 9/2 sufficiently populated at

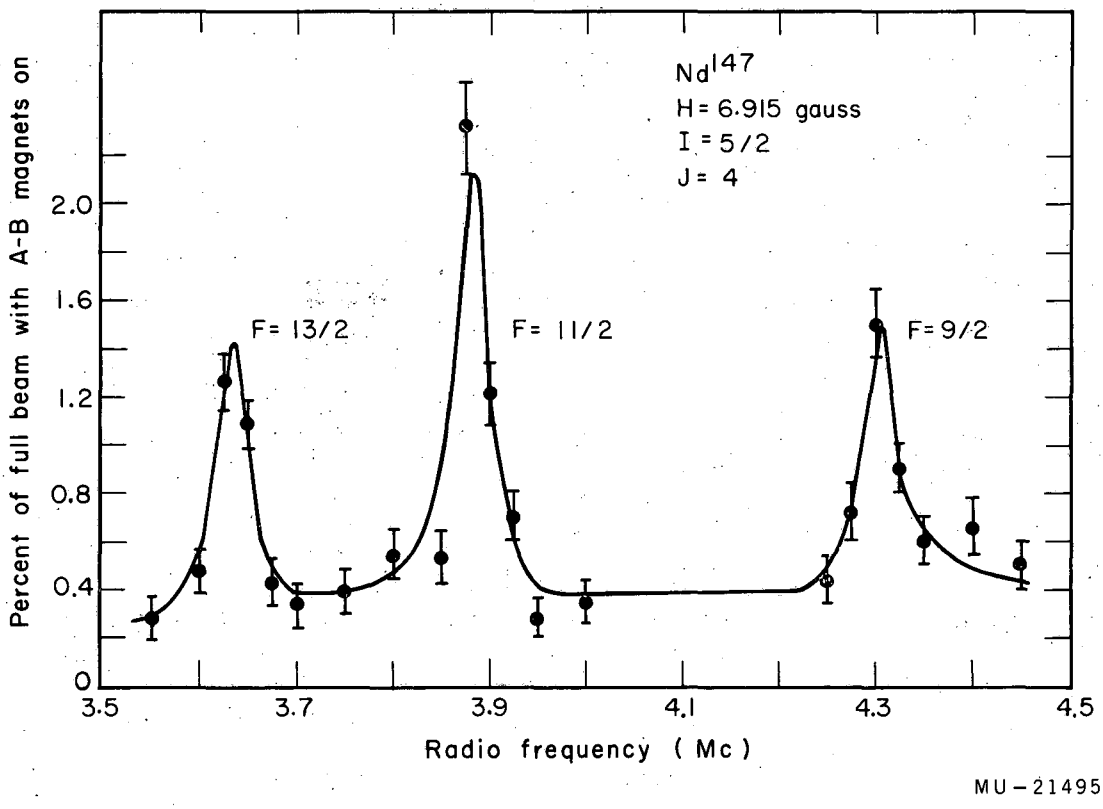

Fig. 16. Neodymium-147 resonances in the three highest F states.

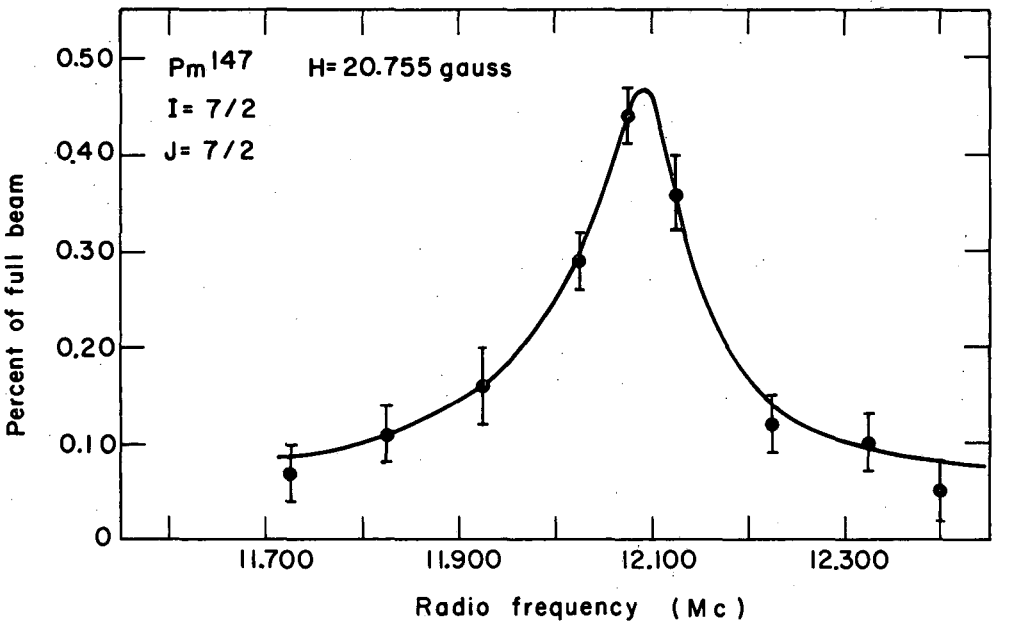

Fig. 17. Promethium-147 resonance curve at 20.755 gauss.

beam temperature in order to be observed in the experiment. The fine-structure separations have been estimated, and these three low-lying levels are assumed to be present. The resonances observed indicate that the nuclear spin of Pm^{147} is 7/2, coupling to the following levels:

$$^6H_{7/2}, \quad g_J(\text{expt}) = -0.831(5) \text{ compared with } g_J(\text{RS}) = -0.8254$$

$$^6H_{9/2}, \quad g_J(\text{expt}) = -1.068(4) \text{ compared with } g_J(\text{RS}) = -1.0707.$$

The $J = 5/2$ level was not observed, and we believe that this is because its g value, 0.286, is too low to be refocused by the magnetic fields of the apparatus. The theoretical and experimental g_F values for the observed transitions in Pm^{147} are given in Table V.

The only other possible configuration is $4f^4\ 5d^1$, in analogy to the transuranic homologue, neptunium, with $5f^4\ 6d^1$. A calculation of the electrostatic energies for f^4d has been performed by Judd for this configuration,[51] and it is shown that the Hund's-rule term should lie lowest in energy. The levels arising from this term would also be half-integral. Possible J values are between 11/2 and 21/2.

The observed transitions were fitted in a g_J-independent way; that is, the ratios of three observed frequencies were taken and compared with ratios of the cosine factors given by $\left[F(F+1) + J(J+1) - I(I+1)\right] / 2F(F+1)$. These were computed with all possible combinations of I and J. All I between 3/2 and 13/2 with all J between 3/2 and 21/2 were tried. No consistent set of I and J was obtained which would explain the observed frequencies, except for the set assigned above. Therefore we conclude that the ground nuclear spin of Pm^{147} is 7/2 and that the ground term of promethium is ^6H arising from the ground electronic configuration $4f^5\ 6s^2$.

The shell-model energy-level assignment for the sixty-first proton in promethium is 4d 5/2. Since this does not agree with the measured spin, the nearest proton level is 5g 7/2, which then has to

Table IV. Observed resonances in neodymium-147. The calculated g_F's are based on the previously measured g_J's.[49]

$\mu_0 H/h$ (Mc)	Pi transitions I=5/2, J = 4 F = 13/2	I= 5/2, J = 4 F = 11/2	I =5/2, J = 4 F = 9/2
5.880	0.371(18)	0.394(20)	0.438(21)
9.679	0.3755(21)	0.4008(26)	0.4452(25)
Mean experimental g_F	0.3755(21)	0.4008(26)	0.4452(25)
Calculated g_F	0.3710	0.3943	0.4385

Table V. Observed resonances in promethium-147. The calculated g_F's are based on the assumption of pure RS coupling among the electrons of the configuration f^5 to the Hund's-rule term ^6H.

$\mu_0 H/h$ (Mc)	Pi transitions I=7/2, J=7/2 All F	I=7/2, J=9/2 F = 8	I=7/2, J=9/2 F = 7
15.208	0.416(2)	0.600(3)	0.620(3)
29.050		0.602(2)	0.623(2)
53.528	0.4164(10)	0.6044(15)	0.6230(15)
Mean experimental g_F	0.4164(10)	0.6037(15)	0.6230(15)
Calculated g_F	0.4127	0.6023	0.6214

be placed above 4d 5/2 in order to give an interpretation of this spin on the basis of this model. However, the measured spins of $_{59}Pr^{141}$ and $_{63}Eu^{151,153}$ are all 5/2 so that for these nuclei, the converse is true.[52,53]

In view of the measured spins of Nd^{147} and Pm^{147} together with the observed beta-decay picture, the failure to observe the beta ray between the ground states of these isobars lead us to two possible conclusions: (a) the decay scheme is so unusual that the ordinary selection rules are inadequate for the explanation of the beta decay, or (b) the resolution is insufficient to allow one to determine whether the beta ray in question decays to the first excited level or to the ground level.

C. Gadolinium-159

The second half of this transition series starts with gadolinium, which has atomic number Z = 64. The ground-state electronic configuration has been inferred to be $4f^7\ 5d^1$ from optical-spectroscopic results.[54] It is interesting to note that in this first element of the second half, the d electron is undoubtedly present. This is in complete analogy with the first element of the first half, lanthanum.

The ground term of Gd is believed to be ^9D, with J = 2 lying lowest in energy. The fine-structure separations between the levels are

Level	Separation (cm^{-1})	% atomic beam
$^9D_6$	1719.06	8
$^9D_5$	999.11	15
$^9D_4$	532.13	21
$^9D_3$	215.13	26
$^9D_2$	0.00	30

The numbers on the right are estimates of the percent of atomic beam at 2000°K in a given level. These are calculated from the fs separations.

In an atomic-beam experiment on stable even-even Gd^{158}, five g values have been measured.[55] These are now to be compared with two sets of theoretical values using two types of coupling for the seven f electrons and the single d electron. The ground electronic state may be written as

$$(3^+2^+1^+0^+ -1^+-2^+-3^+)\,(2^+)\,,$$

with all the intrinsic electronic spins "up" (+1/2) as indicated.

In the first type of coupling, all the electrons including the d electron are RS-coupled. This gives rise to $^9D_{2,3,4,5,6}$. The theoretical g values are computed from

$$-g_J = g_S \frac{J(J+1) + S(S+1) - L(L+1)}{2\,J(J+1)} + g_L \frac{J(J+1) + L(L+1) - S(S+1)}{2\,J(J+1)}\,, \tag{59}$$

with $g_S = 2.0000$ and $g_L = 1.0000$. Table VI shows that these values agree very well with the experimental results.

An alternative coupling scheme may be considered. Russell-Saunders coupling among the seven f electrons results in $^8S_{7/2}$. The single d electron gives the Hund's rule ground level $^2D_{3/2}$. Now the two levels are coupled to give rise to the levels denoted by $(^8S_{7/2}, {}^2D_{3/2})_{2,3,4,5}$. This is often called j-j coupling. Note that this scheme allows only four possible J's for the ground term. It may be argued that the fifth level observed arises from the coupling $(^8S_{7/2}, {}^2D_{5/2})$. The g values are calculated from

$$g_J = g_{J_1} \frac{J(J+1) + J_1(J_1+1) - J_2(J_2+1)}{2\,J(J+1)} + g_{J_2} \frac{J(J+1) + J_2(J_2+1) - J_1(J_1+1)}{2\,J(J+1)}\,, \tag{60}$$

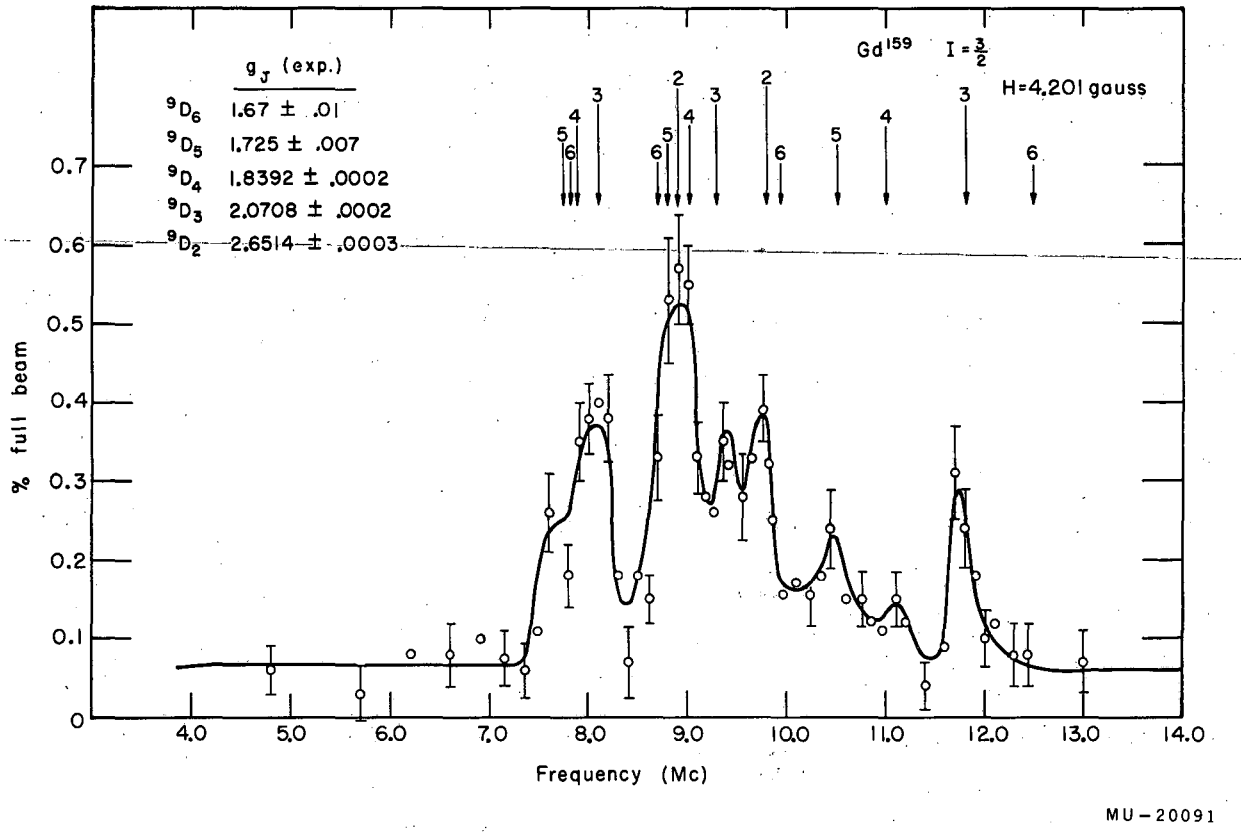

Fig. 18. Spectrum of resonances observed in Gd^{159} at 4,201 gauss. The arrows above indicate the positions of the predicted Pi transitions for each J with I = 3/2.

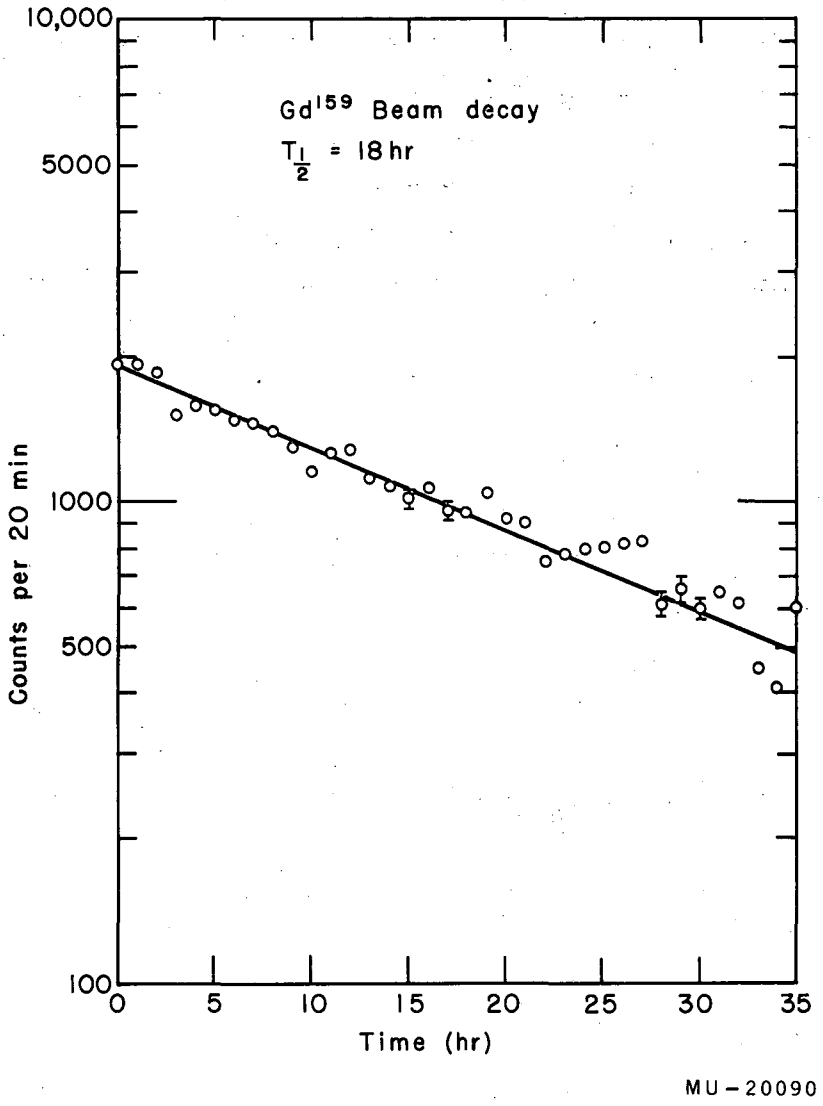

Fig. 19. Radioactive decay of Gd^{159}.

where $J_1 = 7/2$ with g_{J_1} (RS) = - 2.0000 and $J_2 = 3/2$ with g_{J_2} (RS) = - 0.8000. These theoretical values from Eq. (60) are calculated for all four levels and are compared with the experimental results in Table VI. The agreement is seen to be poor.

The $4f^8$ configuration with no d electron gives rise to $^7F_{6,5,\ldots}$. All the theoretical g values are -1.5000 since L = S. Thus this possibility is completely excluded.

It is seen from the table that straight RS coupling among all the electrons seems to give g values which agree very well with the measured g's.

We measure the nuclear spin

$$I = 3/2$$

for Gd^{159} and together with J = 2, 3, 4 and 5, a satisfactory analysis of the observed resonance spectrum is made. Note that only J = 6 is not observed in the Zeeman resonances (Fig. 18). Gadolinium-159 is identified by observing its radioactive decay (Fig. 19).

D. Terbium-160

The second element of the second half of the rare earths is terbium. This also has a d electron in the ground state. Note the similarity with cerium, the second element of the first half of the series.

The atomic-beam group at Heidelberg has investigated stable Tb^{159}. They measure $I = 3/2$ and determine four J levels with the corresponding g values.[55]

Our theoretical speculations on the electronic configuration are as follows. We feel certain that $^6H_{15/2}$ from $4f^9\ 6s^2$ belongs to the measured g value, -1.3225. The next lower level, $^6H_{13/2}$ has g_J(RS) = - 1.2827 and this finds no agreement with any of the remaining g values measured. Therefore we are forced to hypothesize that together with $4f^9$, terbium has $4f^8\ 5d^1$ giving rise to the observed low-lying electronic levels. Note that there are two $J = 15/2$ levels observed.

Table VI. Gadolinium, $4f^7\ 5d^1\ 6s^2$: Comparison of experimental with theoretical g values using two types of coupling schemes

J	$-g_J$(expt)[a]	$-g_J$(RS)	$-g_J$(j-j)
2	2.6514(3)	2.6667	2.6000
3	2.0708(2)	2.1083	2.0000
4	1.8392(2)	1.8500	1.7600
5	1.725(7)	1.7333	1.6400
6	1.67(1)	1.6667	----

[a] From Smith and Spalding, reference 49.

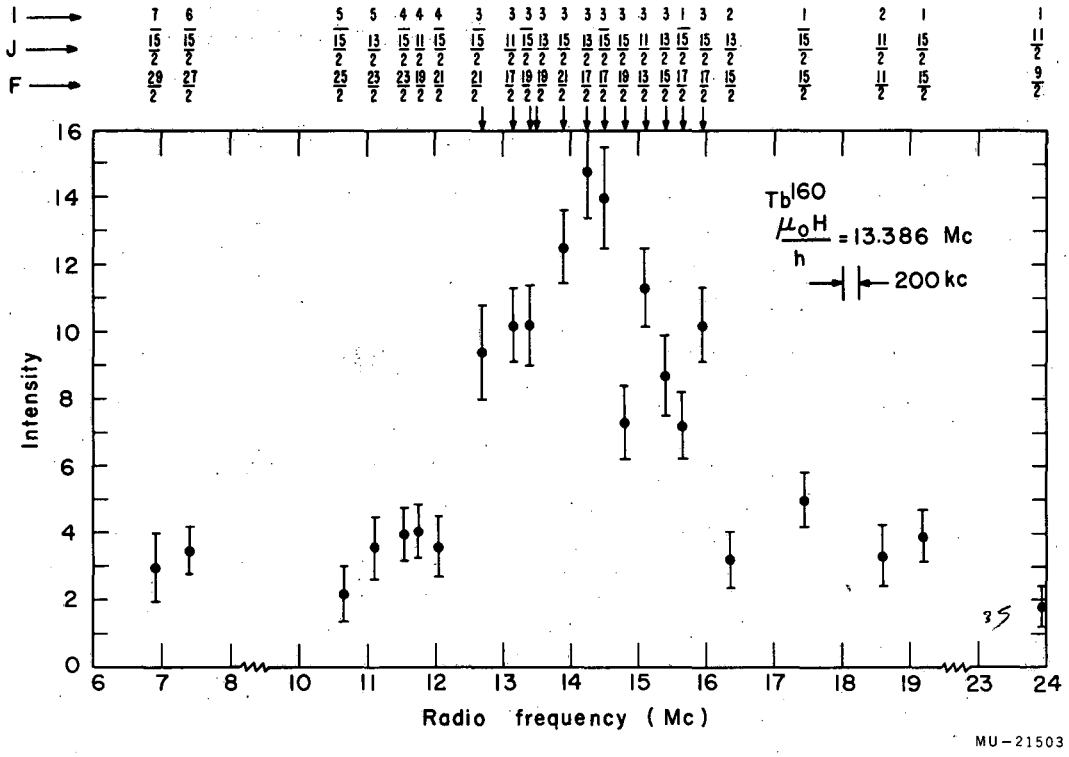

Fig. 20. Terbium-160 resonances. Note the I-, J-, and F-state assignments for each pi transition.

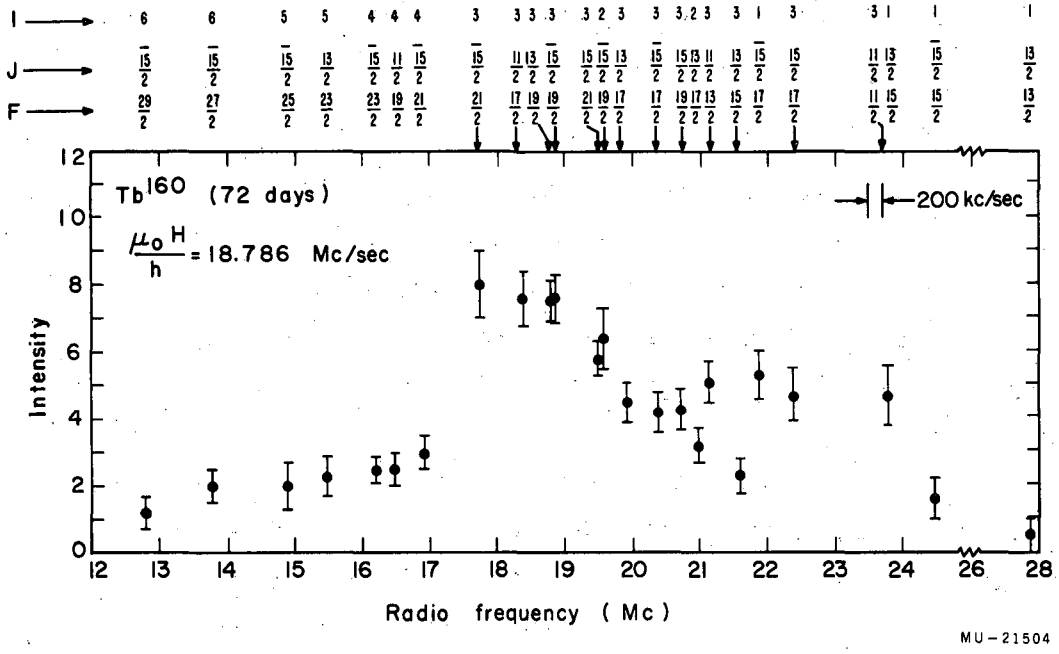

Fig. 21. Terbium-160 resonances. These indicate that the transition frequencies are still linear in magnetic field. The I-, J-, and F-state assignments for the pi transitions are indicated.

(refer to Table VII). From the latter configuration, we assume j-j coupling between $^7F_6$, $4f^8$ and $^2D_{3/2}$, $5d^1$. This gives rise to three levels whose values and g_J's may account for the other three measured J's and g_J's. The theoretical g values are computed using Eq. (60).

Straight RS-coupling in $4f^8\ 5d^1$ is not possible, since this gives rise to the term ^8H with a ground level of 17/2. This level was not observed in the Heidelberg experiment.

After taking frequency exposures for each possible spin coupling to each J in the Zeeman region, we conclude that

$$I = 3 \text{ for } Tb^{160} .$$

We have observed a total of twelve resonances at each setting of the magnetic field. Using the measured g values, we observed three pi transitions in each of the four levels. The F states are labeled in Fig. 20 and 21. Each resonance was taken at two values of the static magnetic field corresponding to $\mu_0 H.h$ equal to 13.386 Mc and 18.786 Mc.

This 72-day terbium isotope was produced by neutron bombardment of 100% abundant Tb^{159}. The large number of energetic beta and gamma rays resulting from the excited nuclear levels presented a severe radioactive hazard.[56] This necessitated the construction of some heavier lead shielding around the apparatus. After completion of the experiment, the oven loader was discarded in order to reduce the background activity.

Table VII. Terbium: Comparison between measured g values and theoretical g values calculated from possible electronic ground-state configurations

J	Heidelberg results[55] (experimental)	f^9 in RS coupling, $^6H_{\overline{15}/2, a}13/2, 11/2$	f^8d in j-j coupling $(^7F_6, ^2D_{3/2})_{15/2,13/2}$	f^8 d in RS coupling $^8H_{17/2, 15/2, 13/2}$
17/2	not observed	none	none	1.4117
$\overline{15}/2$[a]	1.3225	<u>1.3341</u>	1.3600[b]	1.3882
15/2	1.4563	1.3341	<u>1.3600</u>[b]	1.3882
13/2	1.4633	1.2827	<u>1.4245</u>[b]	1.3538
11/2	1.5165	1.2028	<u>1.5245</u>[b]	1.3007

[a]The bar over 15/2 is used to differentiate between the two levels which have the same value. This distinction is also made in Figs. 20 and 21.

[b]Calculated using Eq. 60 with $g_J(RS) = -1.5000$ for $^7F_6$, and $g_J(RS) = -0.8000$ for $^2D_{3/2}$. The underlined g values are noted as the assignments favored here.

E. Dysprosium-166 and 140-min Dysprosium-165

These isotopes are produced by irradiating stable dysprosium metal with thermal neutrons. The decay scheme of 140-min Dy^{165} includes an isomeric transition from 1.25 min Dy^{165} (see Fig. 22 from reference 57). Part of the 1.25 min-Dy^{165} yield from the irradiation decays to 140-min Dy^{165} by means of the isomeric transition (IT). These isomers eventually go by beta decay to the ground state, Ho^{165}. Dysprosium-166 is produced by a double neutron-capture process. The series of reactions proceeds as

$$Dy^{164}(n, \gamma)\ 1.25\text{-min } Dy^{165} \xrightarrow{IT} 140\text{-min } Dy^{165}$$

together with

$$Dy^{164}(n, \gamma)\ 140\text{-min } Dy^{165}\ ,$$

then,

$$140\text{-min } Dy^{165}(n, \gamma)\ Dy^{166}\ .$$

These isotopes were identified by noting their half lives (Fig. 23 and 24).

Since Dy^{166} has an even-even nucleus, its ground-state nuclear spin is $I = 0$. Then by referring to Eq. (32) for the resonance frequency of a pi-transition at low external fields, one obtains

$$\nu = g_J \frac{F(F+1) + J(J+1)}{2F(F+1)} \frac{\mu_0 H}{h} \qquad (61)$$

$$= g_J \mu_0 H/h\ ,$$

since we have $F = J$. This means that the experiment on Dy^{166} could only yield information on the g values (Fig. 25). This was fortunate, because it allowed a clear-cut measurement of this important atomic property.

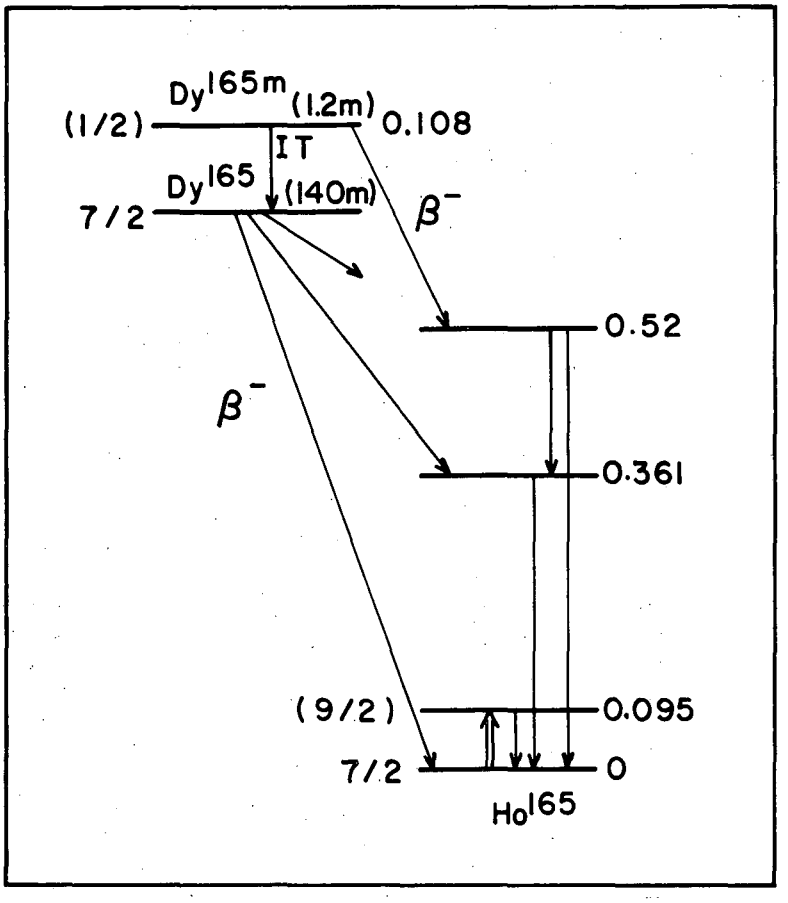

MU-21485

Fig. 22. Nuclear decay scheme for the isomers of Dy^{165}.

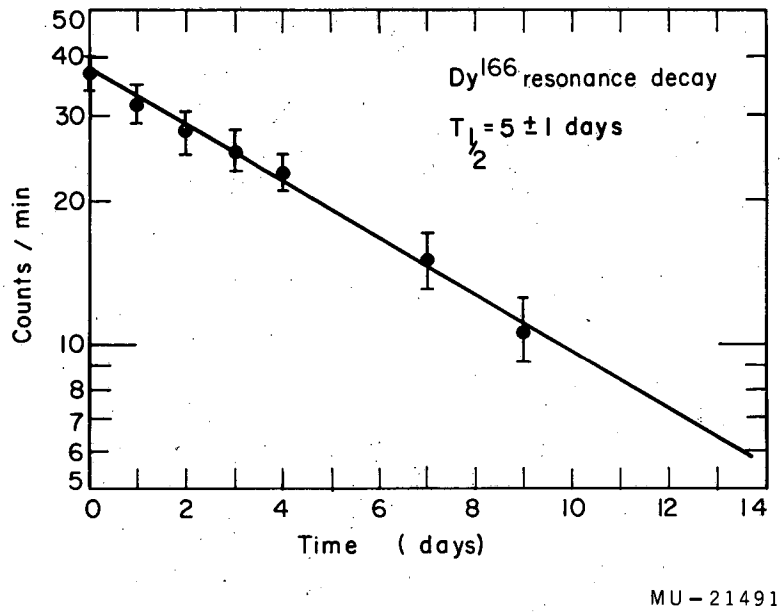

Fig. 23. Radioactive decay of Dy^{166}.

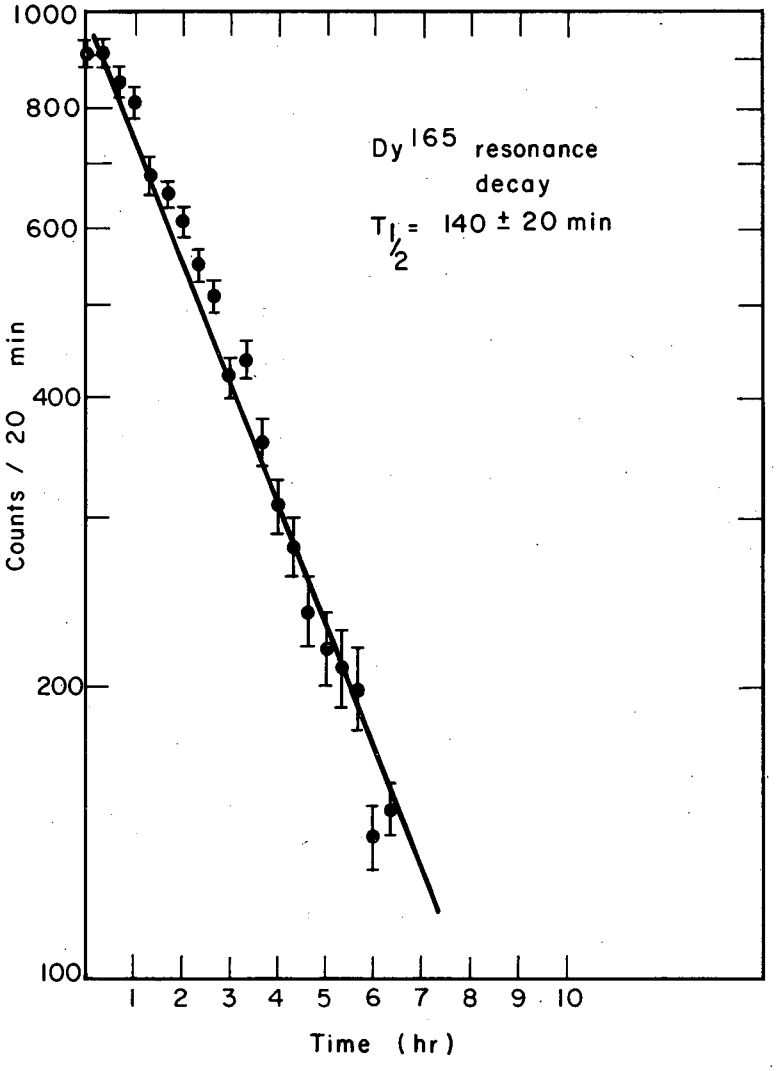

Fig. 24. Radioactive decay of Dy^{165}.

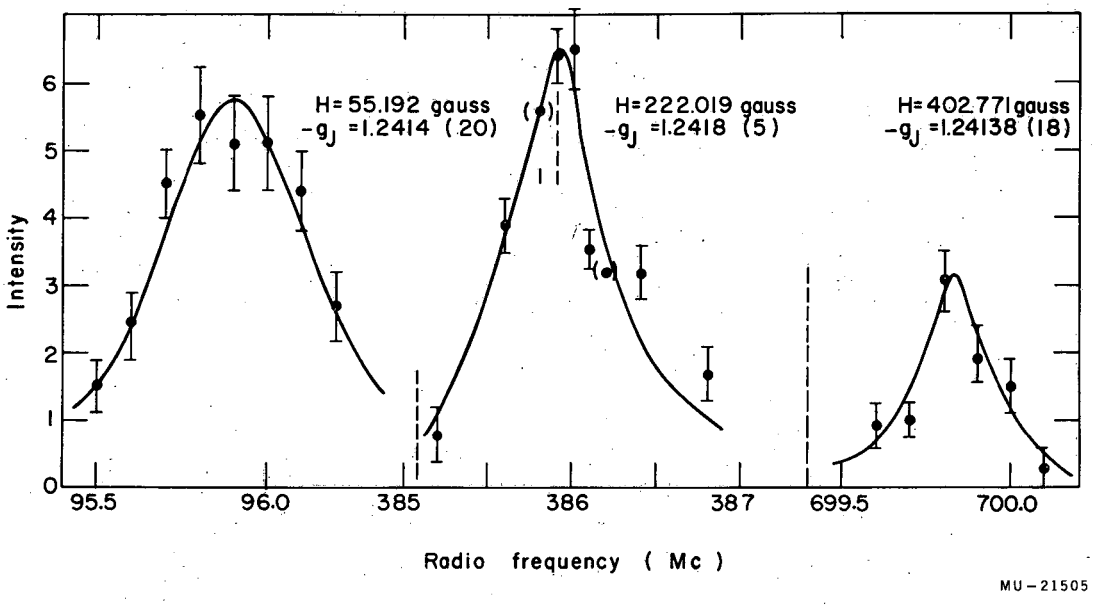

Fig. 25. Dysprosium-166 resonance followed up in magnetic field in order to obtain an accurate measurement of g_J for $^5I_8$.

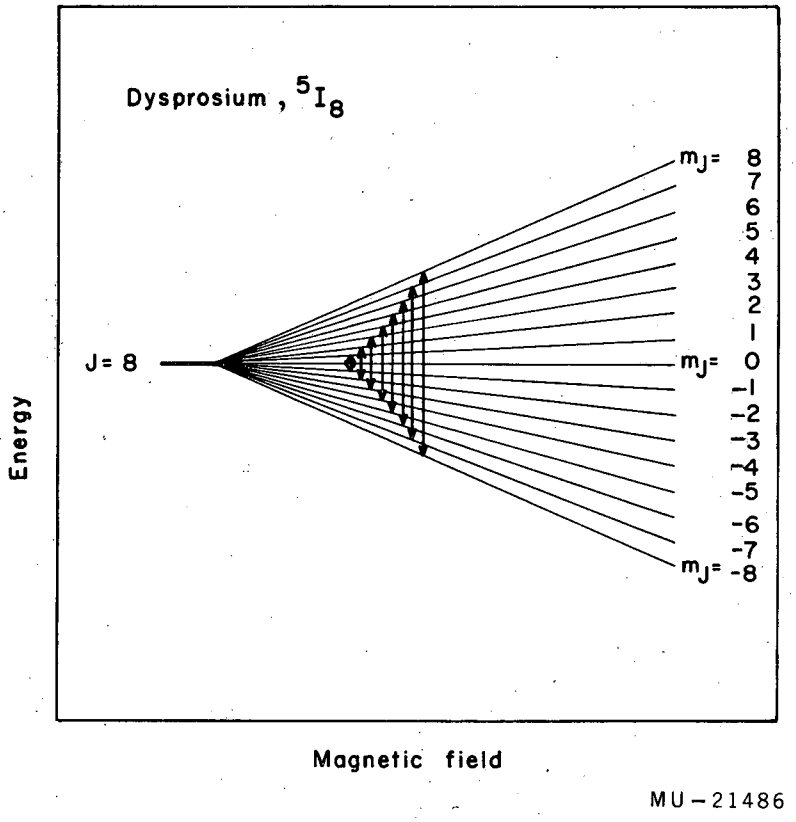

Fig. 26. Energy levels of $^5I_8$ of Dy^{166}(I=0) in an external magnetic field.

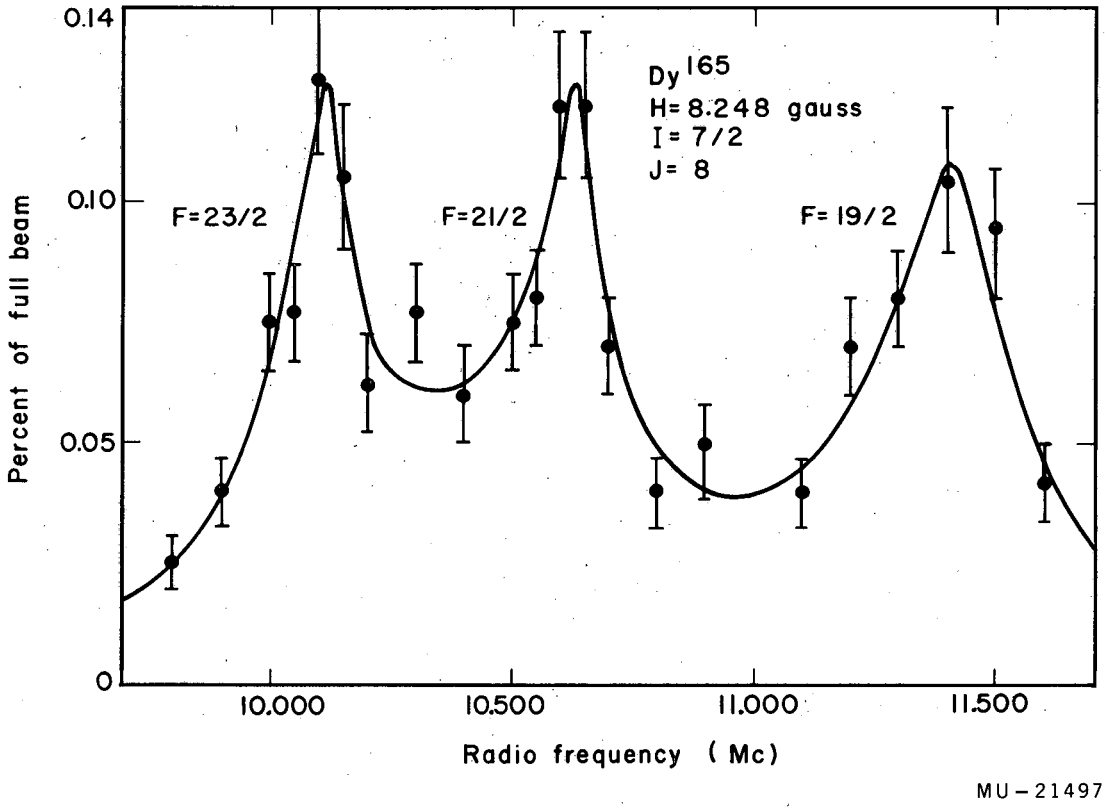

Fig. 27. Dysprosium-165 resonances in the three highest F states at 8.248 gauss.

To identify the ground levels, we had to perform the experiment on a dysprosium isotope with a nonzero nuclear spin. Beta-spectroscopy studies[57] on the Dy^{165} isomers indicated nuclear spins of (7/2+) for 140-min Dy^{165} and (1/2 -) for 1.25-min Dy^{165}. The signs on the spin predictions are parity assignments.

Dysprosium-166 was investigated first, and the measurements indicate that only one J-level is sufficiently populated at beam temperature to permit observation. The other levels are then believed to be several thousand wave numbers above the ground level. The g value obtained is

$$g_J(\text{expt}) = -1.2414(3) .$$

The number in parentheses is the uncertainty in the last figure. This average value is taken over resonances observed at five settings of the magnetic field, with the last measurement taken at 402.771 gauss (see Table VIII). All five resonances were carefully traced out so that estimates on the uncertainty of each measurement were possible. The energy levels of this atom in an external magnetic field are schematically plotted in Fig. 26.

A nuclear spin of 7/2 for 140-min Dy^{165}, together with J = 8, is favored in the assignments of the states in the three observed pi transitions (Fig. 27). The multiple-quantum transitions (see Table IX) are believed to belong to the states, F = 23/2, 21/2, and 19/2. The resonances in the remaining F states were too weak to be observed because of the large number of m states. This number is

$$(2I+1)(2J+1) = 136$$

for this hfs system, compared to, say only 8 m states for potassium-39. This means that the Dy^{165} resonance intensities are lower than the K^{39} resonance intensities by about a factor of 8/136.

Table VIII. Observed resonance frequencies in dysprosium-166 and 140-min dysprosium-165

I	J	F	H (gauss)	ν_{obs}(Mc)	ν_{calc}(Mc)
Dysprosium-166					
0	8	8	0.709	1.250(50)	1.241
0	8	8	4.201	7.325(75)	7.299
0	8	8	55.192	95.900(150)	95.899
0	8	8	222.019	385.900(150)	385.774
0	8	8	402.771	699.830(80)	699.843
140-min dysprosium-165					
7/2	8	23/2	8.248	10.120(60)	9.968
7/2	8	21/2	8.248	10.630(40)	10.502
7/2	8	19/2	8.248	11.400(100)	11.205

Table IX. Multiple-quantum pi transitions between $(F, m_1) \leftrightarrow (F, m_2)$ in 140-min dysprosium-165, with I = 7/2, J = 8

F = 23/2		F = 21/2		F = 19/2	
m_1	m_2	m_1	m_2	m_1	m_2
-5/2	-9/2	-3/2	-7/2	-1/2	-5/2
-3/2	-11/2	-1/2	-9/2	1/2	-7/2
-1/2	-13/2	1/2	-11/2	3/2	-9/2
1/2	-15/2	3/2	-13/2	5/2	-11/2
3/2	-17/2	5/2	-15/2	7/2	-13/2
5/2	-19/2	7/2	-17/2	9/2	
7/2	-21/2	9/2		11/2	
9/2		11/2		13/2	-15/2
11/2		13/2		15/2	
13/2		15/2	-19/2	17/2	
15/2	-23/2	17/2		19/2	
17/2		19/2			
19/2		21/2			
21/2					
23/2					

Dysprosium has 10 electrons in the valence shell and the most likely ground electronic configuration is either $4f^{10}$ or $4f^9\,5d^1$. If we assume that these electrons are RS coupled, the configuration $4f^{10}$ gives rise to the ground-state term ^5I. The theoretical g values of the first two levels are

$$g_J(RS) = -1.2500$$

for $J = 8$ and

$$g_J(RS) = -1.1786$$

for $J = 7$. If we also assume RS coupling among the 10 electrons for the other possible configuration, $4f^9\,5d^1$, the ground term is ^7K. In this limit, the g values for the first two low-lying levels are

$$g_J(RS) = -1.3000$$

for $J = 10$ and

$$g_J(RS) = -1.2555$$

for $J = 9$.

In conclusion, the following atomic properties were determined:

Dy^{166}: $I = 0$, $J = 8$, $g_J = -1.2414(3)$

140-min Dy^{165}: $I = 7/2$, $J = 8$.

These results lead us to believe that the ground electronic configuration of dysprosium is $4f^{10}$, resulting in the ground level $^5I_8$. The close agreement of the theoretical value of g_J with the experimental result implies that the RS approximation is adequate for the description of the electronic coupling.

F. Twenty-four-Hour Holmium-166

Neutron irradiation of holmium metal for about a day is sufficient to produce a workable source of 24-hr Ho^{166}. The other Ho^{166} isotope is not produced in detectable amounts because of the long half life ($T_{1/2} > 30$ yr). The 24-hr component is easily identified from the relatively short decay rate of the radioactivity (Fig. 28).

Only one resonance has been observed in our experiments on this isotope with an odd-odd nucleus. The observed resonance frequencies are linear in magnetic field. The nuclear spin is assumed to be zero, and the resonances are assigned to transitions of the type

$$(J, m_J) \leftrightarrow (J, -m_J) .$$

Figure 29 shows the careful search undertaken at $H = 0.709$ gauss in order to ascertain that there is only one resonance in the frequency spectrum. The possibility of a superposition of resonances at this field is eliminated by a partial repetition of the search at a sufficiently high magnetic field, $H = 5.567$ gauss (Fig. 30). The single resonance has been traced out at two higher values of H in order to get more accurate measurements of the g value (Fig. 31). The observed resonance frequencies are given in Table X. Our average value is

$$g_J(\text{expt}) = -1.196(1).$$

Experiments on this isotope were performed independently by our group and by Goodman and Childs at the Argonne National Laboratory using the same method.[10] They also assume a nuclear spin of zero for Ho^{166} and obtain

$$g_J(\text{expt}) = -1.19516(10) .$$

This agrees with our measured value.

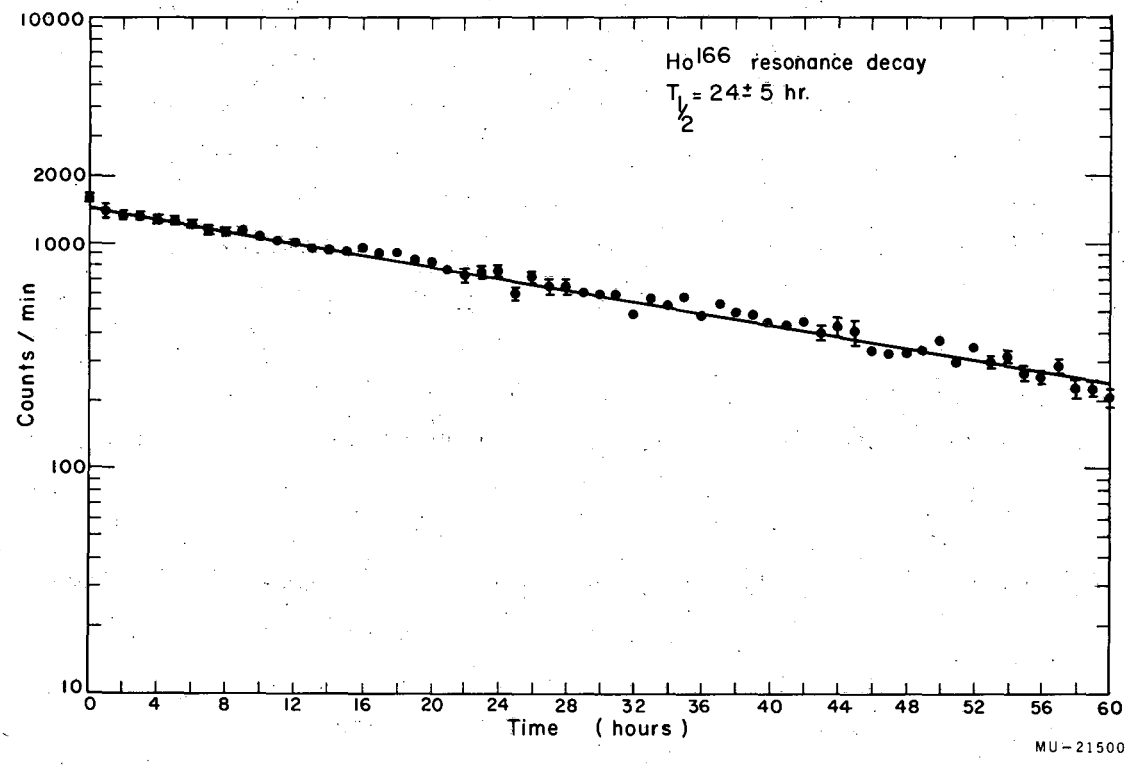

Fig. 28. Radioactive decay of a resonance exposure.

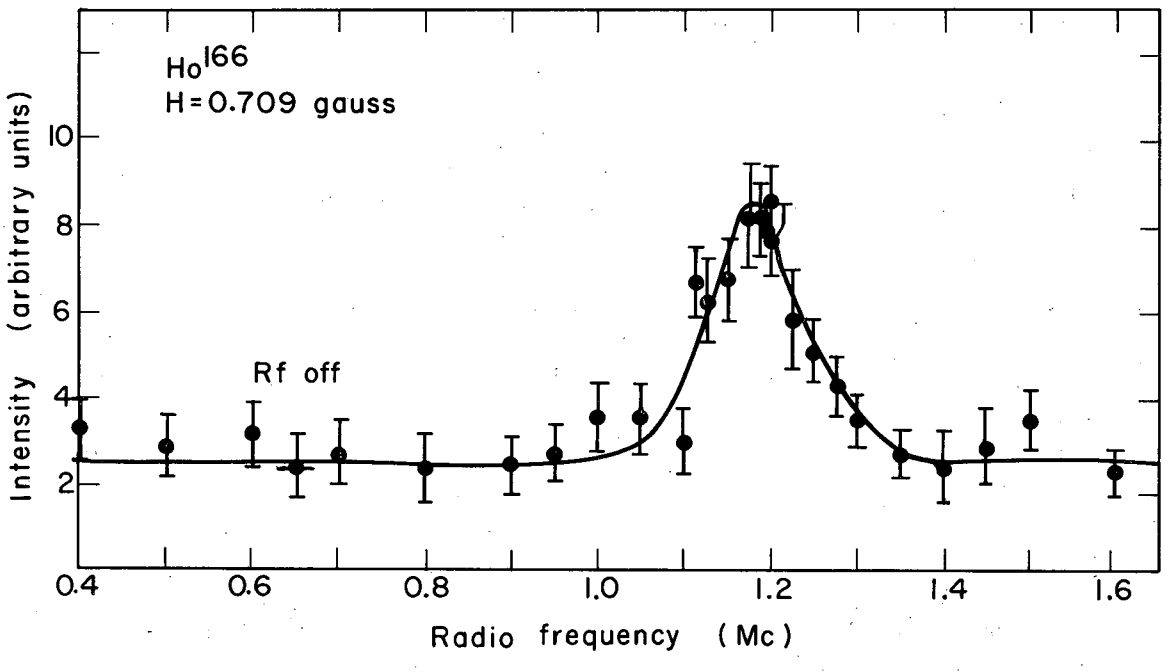

Fig. 29. Resonance curve for Ho^{166}. The absence of any resonances in the spectrum except for that at 1.2 Mc indicates that none of the other levels in the holmium beam are appreciably populated at beam temperature.

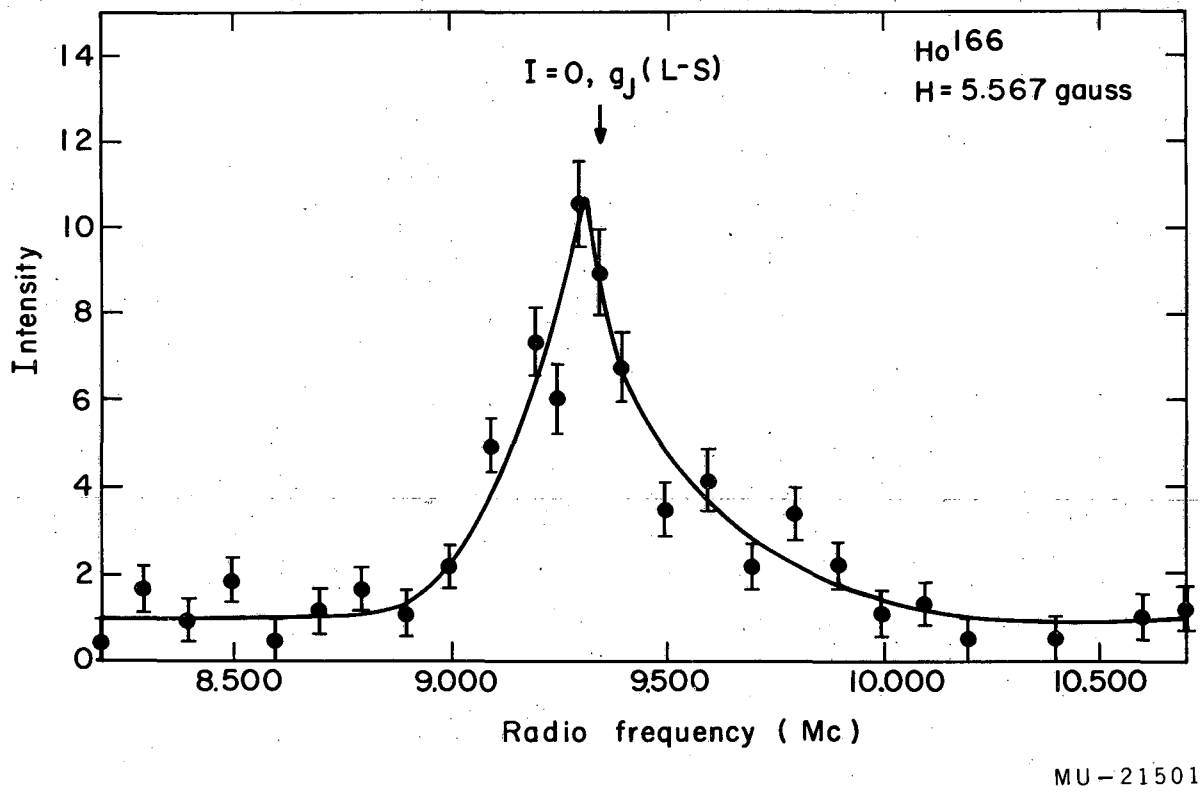

Fig. 30. Resonance curve for Ho^{166}. The single resonance was carefully traced out again at this higher value of the magnetic field in order to exclude the possibility of a superposition of resonances at the lower value.

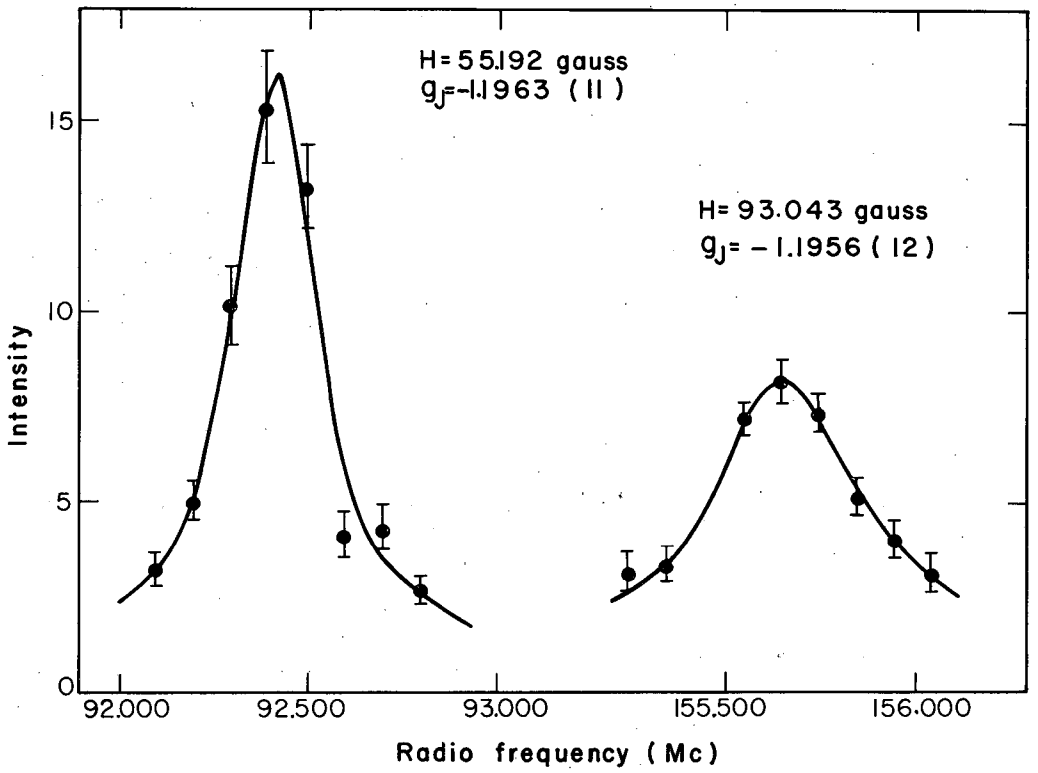

Fig. 31. Resonance curves for Ho^{166}. The resonance was observed at two higher magnetic fields in order to improve on the measurement of g_J.

The assignment I = 0 is subject to the assumption that the resonances observed were in the Zeeman region. The other possibility, although quite remote, is that the transitions were actually observed in the Paschen-Bach region because of a very small hyperfine structure. It is clear that the transition energies in this region are also linear in magnetic field. This is easily seen from Eq. (30).

Holmium (Z = 67) has eleven electrons outside of closed shells. Barium (Z = 56) marks the last closed-electronic-shell structure before the beginning of the lanthanide series. A probable ground electronic configuration for holmium is $4f^{11}$. If Russell-Saunders coupling is a valid approximation, then the ground state in the representation $(\ell_1{}^{s1}, \ell_2{}^{s2} \ldots \ell_{11}{}^{s11})$ is

$$(3^+2^+1^+0^+ - 1^+ -2^+ -3^+ 3^- 2^- 1^- 0^-) .$$

This leads to the Hund's rule ground term ^4I. The levels and corresponding g values are:

$$^4I_{15/2}, \quad g_J(RS) = -1.2000$$

$$^4I_{13/2}, \quad g_J(RS) = -1.1077$$

$$^4I_{11/2}, \quad g_J(RS) = -0.9651$$

$$^4I_{9/2}, \quad g_J(RS) = -0.7273$$

We favor the assignment J = 15/2 for the single level observed, since its theoretical g value comes closest to the measured g_J. The difference is less than 1%, and this is easily attributed to relativistic and diamagnetic effects. Note that there is no other J = 15/2 in this configuration so that this eliminates any possible spin-orbit perturbations from other terms with the same J value. The deviations of all the measured g_J's in this report are quantitatively explained by Judd and Lindgren.[37]

Table X. Summary of observations in 24-hr holmium-166, with I = 0. [a]

Data no.	H (gauss)	Calculated frequency (Mc)	Observed frequency (Mc)	$-g_J$(expt)
1	0.709	1.196	1.175(60)	1.175(60)
2	5.567	9.315	9.350(100)	1.199(20)
3	55.192	92.361	92.420(100)	1.1963(10)
4	93.043	155.704	155.700(150)	1.1956(10)
Mean				1.196(1)

[a] With the proviso that if $I \neq 0$, then the hfs is estimated to be unusually small (a < 100 kc)

The other competing configuration is $4f^{10}\ 5d^1$. The electronic ground state is then

$$(3^+2^+1^+0^+\ -1^+-2^+-3^+3^-2^-1^-)\ (2^+)\ .$$

Russell-Saunders coupling among the 10 f electrons together with the d electron results in the ground term ^6L. The possible low-lying J and g values are:

$$^6L_{21/2}\ ,\ g_J(RS) = -\ 1.2381$$

$$^6L_{19/2}\ ,\ g_J(RS) = -\ 1.1829$$

$$^6L_{17/2}\ ,\ g_J(RS) = -\ 1.1083.$$

The next possible set of excited levels are:

$$^6K_{19/2}\ ,\ g_J(RS) = -\ 1.2631$$

$$^6K_{17/2}\ ,\ g_J(RS) = -\ 1.2074.$$

In order to explain the measured g value of -1.196(1) using this configuration, there are two principal speculations: (a) The ground level is J = 21/2, although the 4% difference in the g values is rather large to be completely caused by relativistic and diamagnetic effects alone. Note that there is also only one level with this value in this configuration. This prevents the possibility of a spin-orbit effect for the reduction of the theoretical g value. (b) The observed level is $^6L_{19/2}$, which is perturbed by $^6K_{19/2}$ by means of the spin-orbit effect, which may in turn explain the g value. The problem here is that it is hard to understand why $^6L_{19/2}$ and not $^6L_{21/2}$ would be the ground level.

The question may be raised as to why we should insist on Russell-Saunders coupling among the electrons in both possible configurations. A j-j coupling between shells with RS coupling within shells is certainly a possibility. This type of coupling has been considered and the results are not much more promising. It is tempting to work with the precedent that, since gadolinium exhibits a coupling that is close to RS among all the f and d electrons, this type of a coupling scheme would also apply for the other rare earths that may have a d electron. Otherwise, if all the valence electrons are assigned to the f shell, the Russell-Saunders coupling scheme seems to be the rule for the electrons in this series. A d electron is known to be present in both gadolinium and terbium, which were treated earlier.

It is clear that a measurement of a nonzero nuclear spin for some other holmium isotope would allow an unambiguous determination of J. Experiments on neutron-deficient Ho^{161} are in progress at the laboratory. This isotope is produced by cyclotron bombardment of erbium metal and the only problem so far is insufficient source activity.

Therefore, subject to the above considerations, our tentative assignment for the electronic ground configuration of holmium is $4f^{11}$ leading to the ground level $^4I_{15/2}$ with $g_J(\text{expt}) = -1.196(1)$.

G. Erbium-169, Erbium-171 and Thulium-171

These isotopes are produced by bombarding ordinary erbium metal with thermal neutrons. Depending on the duration of the irradiation period, we are able to select dominant activities of 7.5-hr Er^{171}, 9.4-day Er^{169} or 1.9-yr Tm^{171}.

Observations were made at sufficiently low values of the magnetic field so as to limit the induced transitions in the Zeeman region (see Table XI). The hfs levels in a magnetic field are shown in Figs. 32 and 33. We obtain the following sets of atomic properties for these three isotopes:

$$\left.\begin{array}{l} Er^{169}\ I = 1/2 \\ Er^{171}\ I = 5/2 \end{array}\right\} \qquad J = 6,\ g_J = -1.164(5)$$

$$Tm^{171}\ I = 1/2 \qquad J = 7/2,\ g_J = -1.1412(2)\ .$$

The two possible pi transitions in both Er^{169} and Tm^{171} were traced out at several values of the magnetic field (Figs. 34 and 35). The resonances in the three highest F states of Er^{171} were also traced out at two values of H (Fig. 36). Identification of each isotope was achieved by observing their decay rates (Figs. 37 and 38). Figure 39 is an interesting multiple-quantum resonance observed in Er^{169} at an intermediate value of the magnetic field.

The g value for $^2F_{7/2}$ in thulium has been measured very accurately in the hfs investigations of Tm^{170}. These results are discussed in a later section.

We find that only one level is sufficiently populated in the erbium atomic beam at operating temperature and conclude that the observed level has the value J = 6. Together with the measured g_J, the evidence indicates that the ground electronic configuration is $4f^{12}\,6s^2$ leading to the ground term ^3H. The ground level $^3H_6$ has $g_J(RS) = -1.1667$ which is in excellent agreement with the measured value.

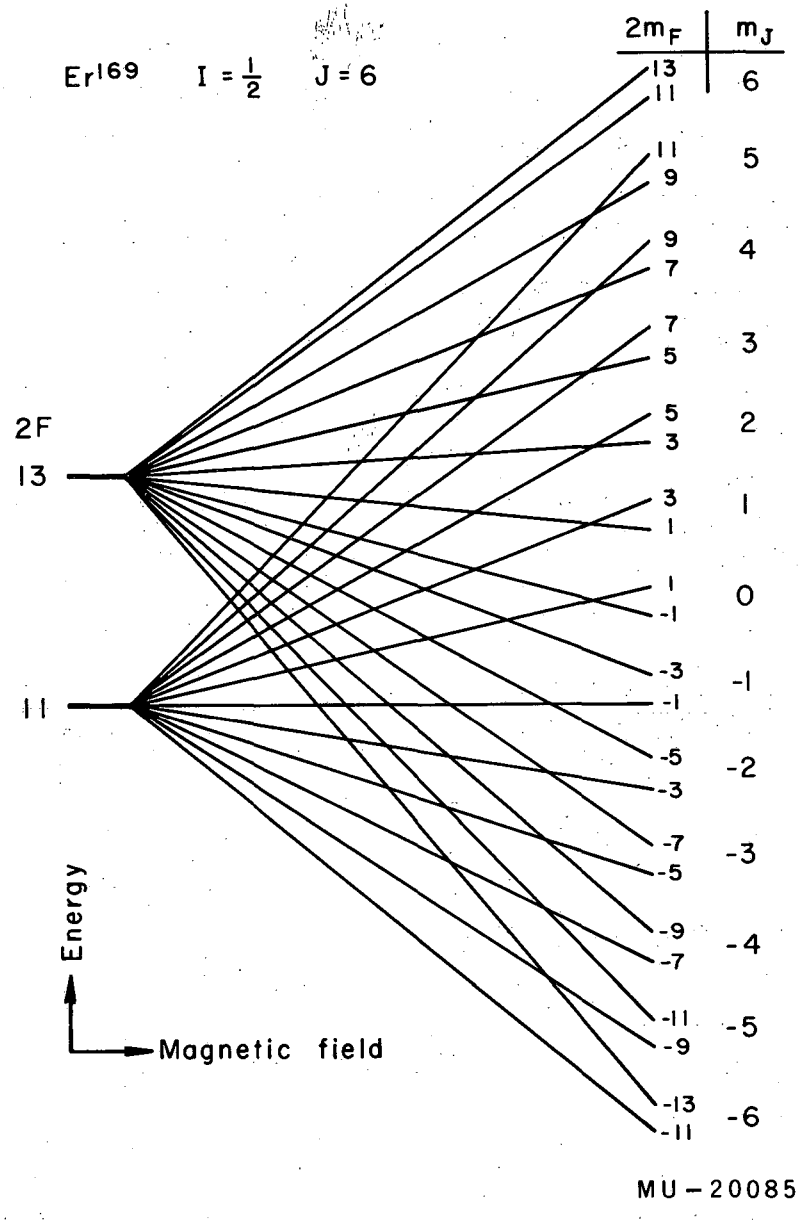

Fig. 32. Schematic diagram of the energy levels in a magnetic field of the hfs system I = 1/2, J = 6 of Er^{169}.

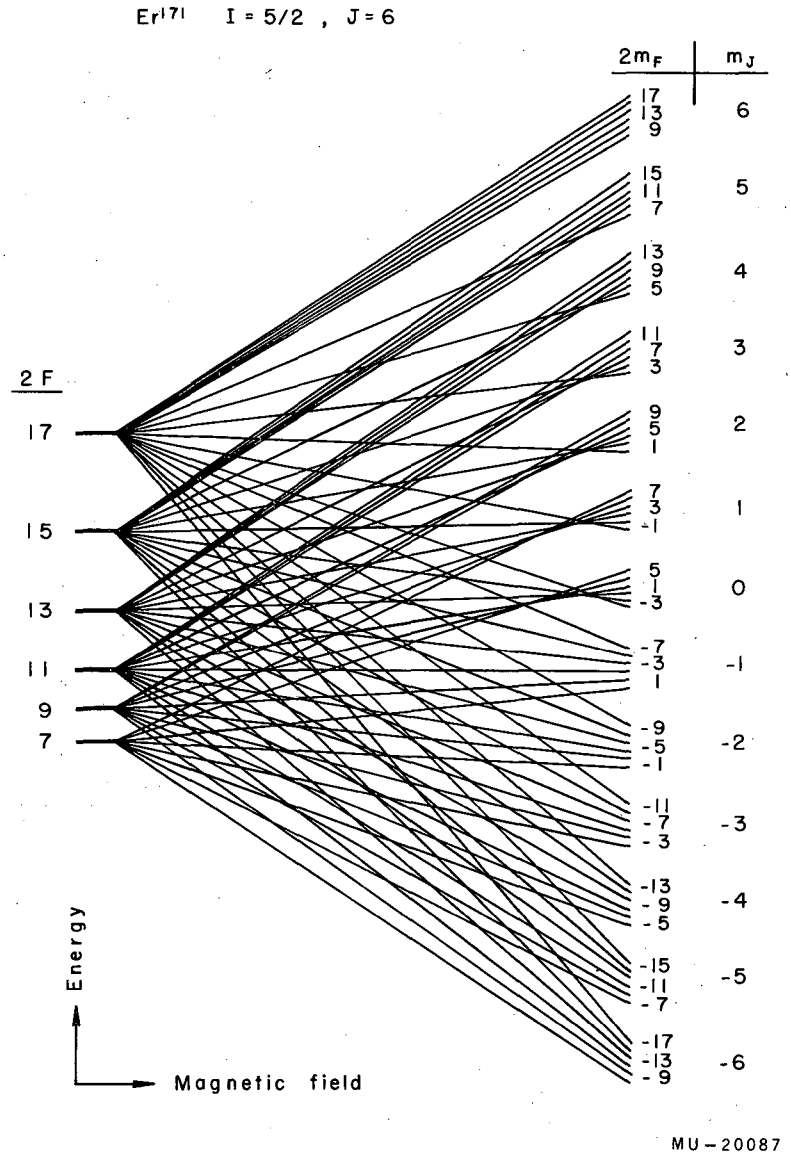

Fig. 33. Schematic diagram of the energy levels in a magnetic field of the hfs system I= 5/2, J = 6 of Er^{171}.

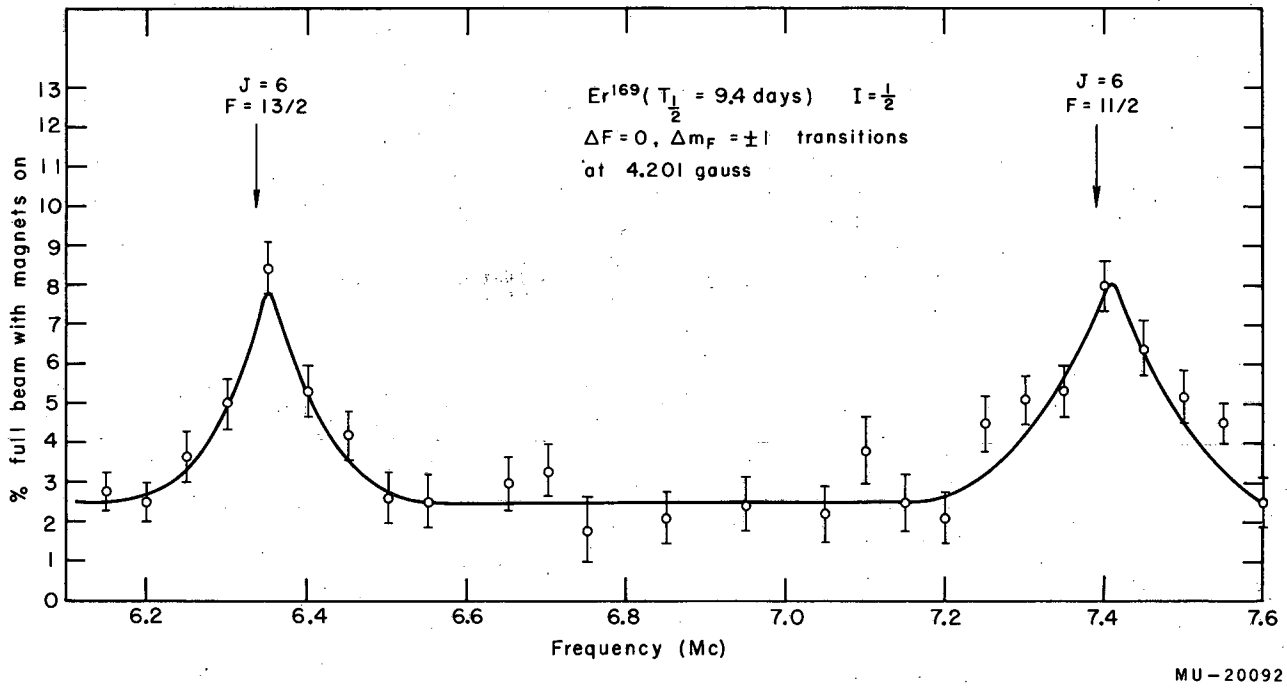

Fig. 34. Resonances observed in Er^{169}.

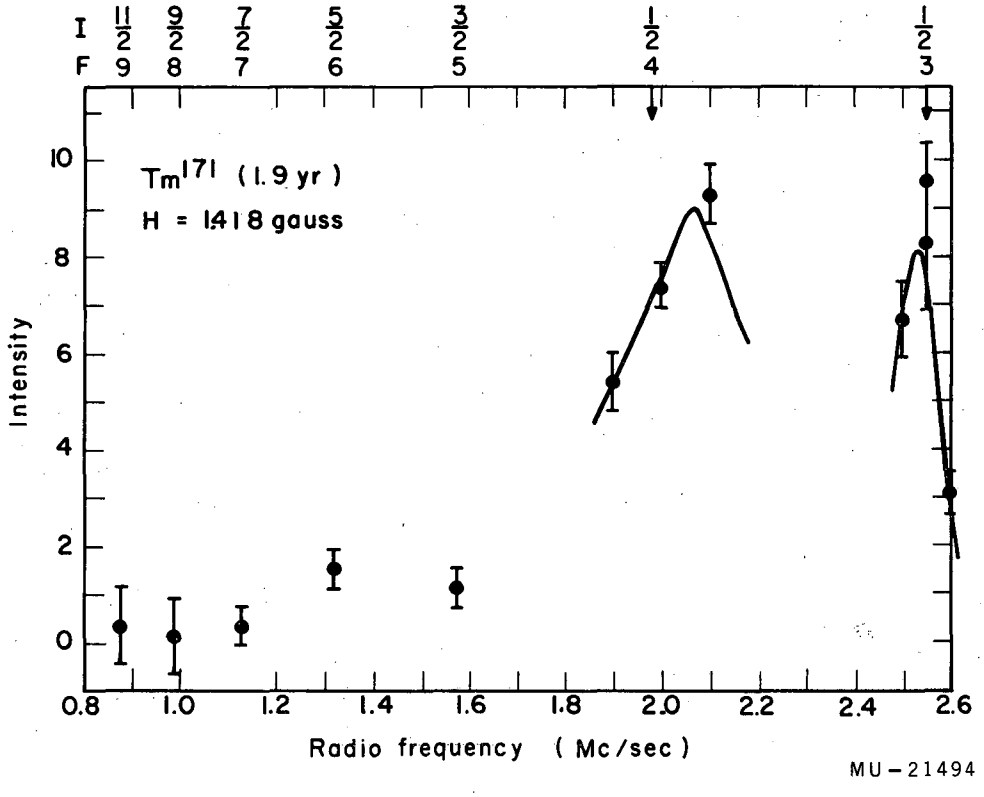

Fig. 35. Identification of the nuclear spin of Tm^{171}.

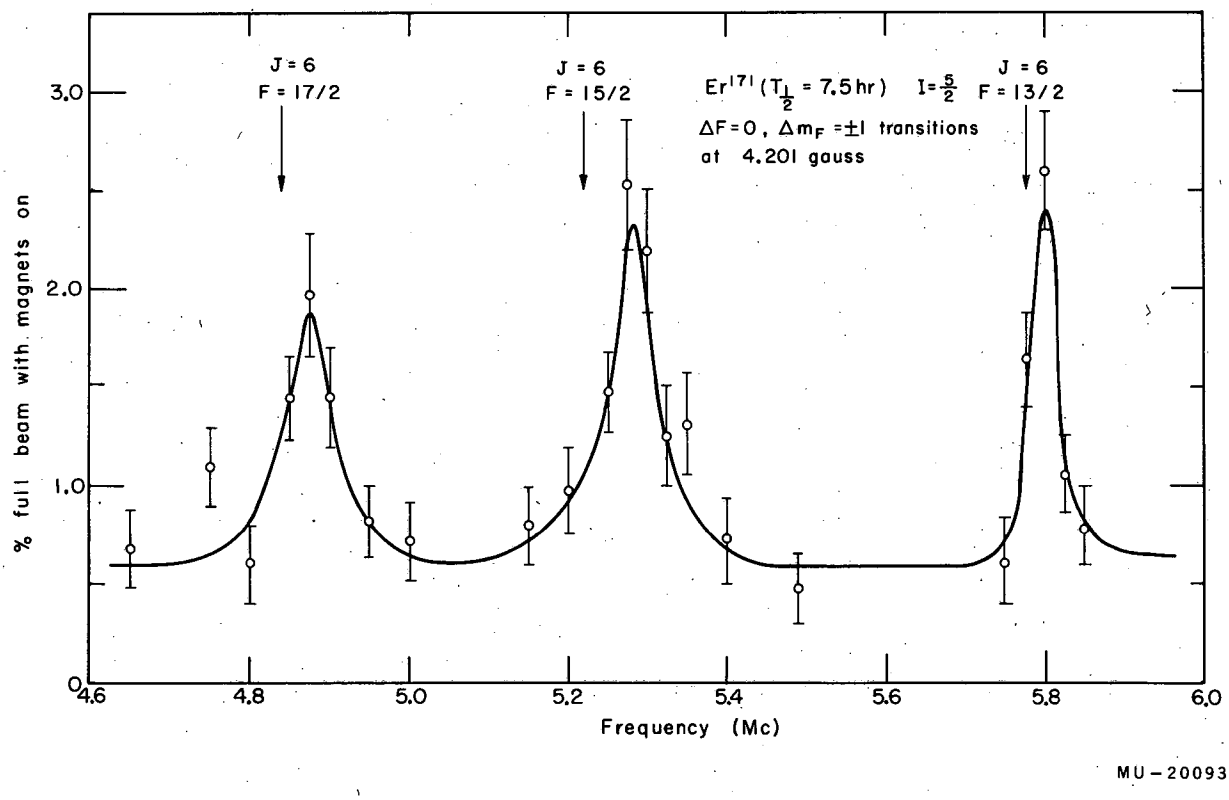

Fig. 36. Resonances in the three highest F states of Er^{171}.

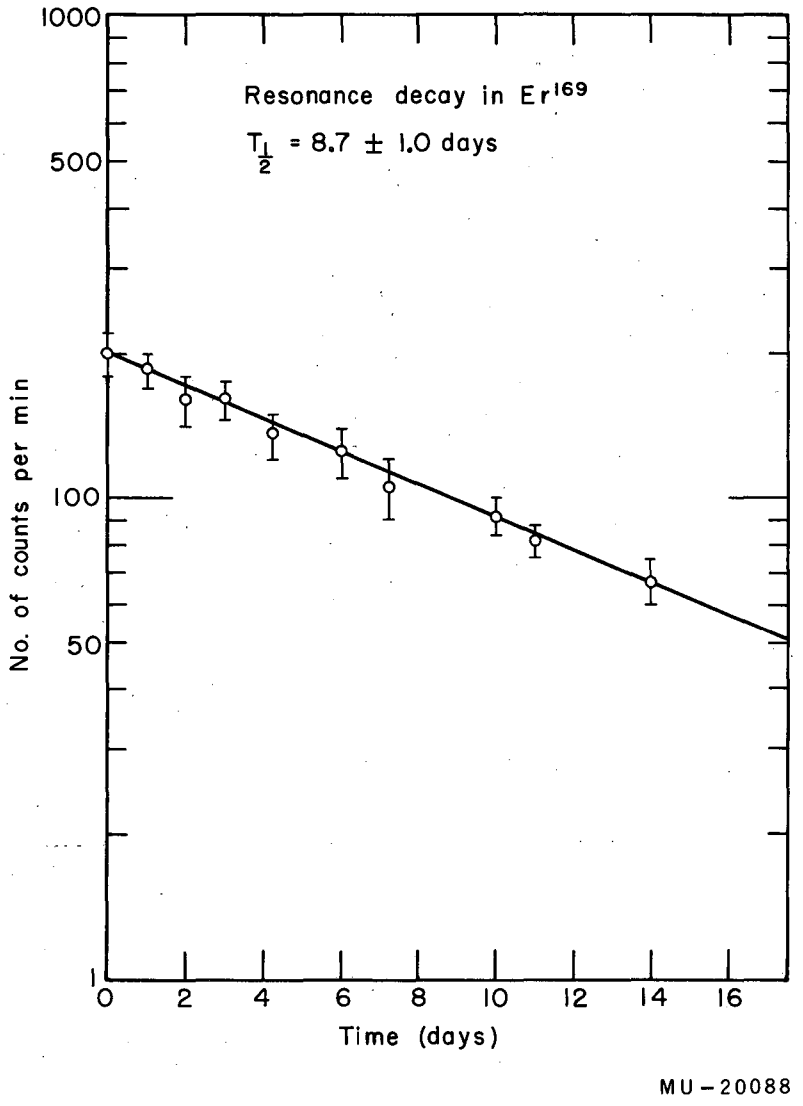

Fig. 37. Radioactive decay of Er^{169}.

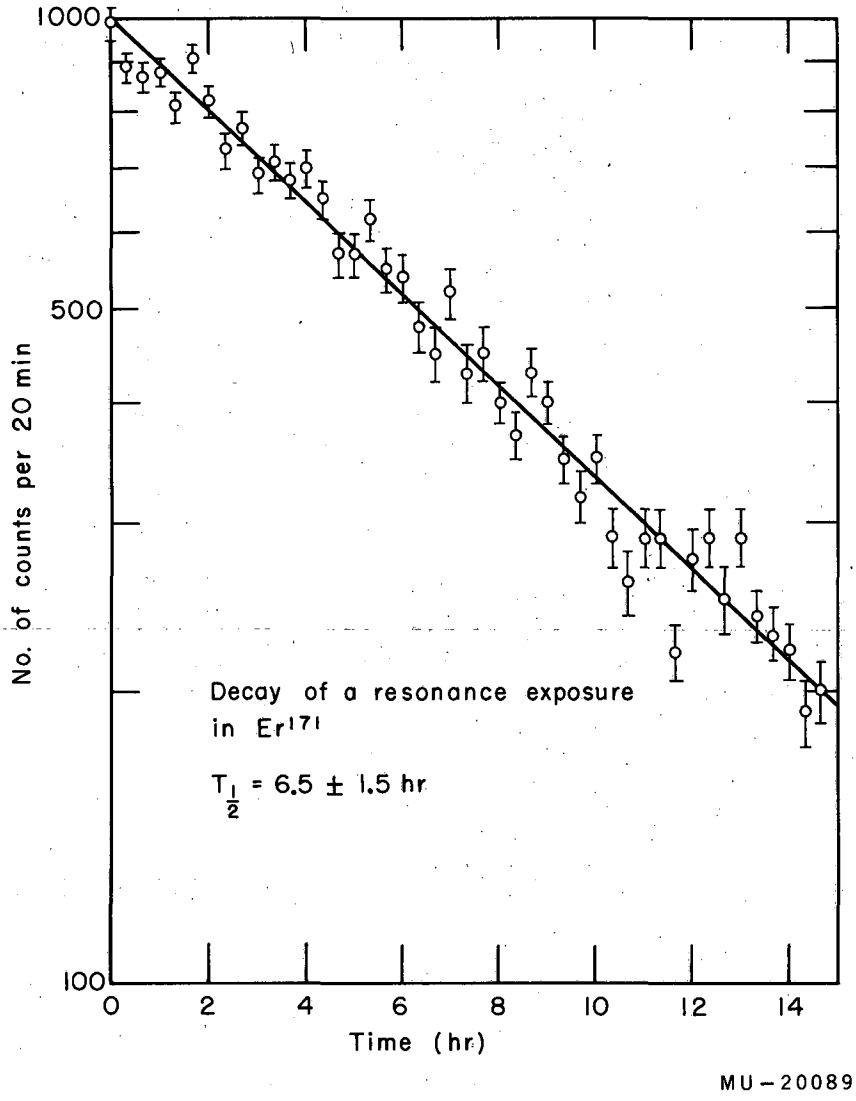

Fig. 38. Radioactive decay of Er^{171}.

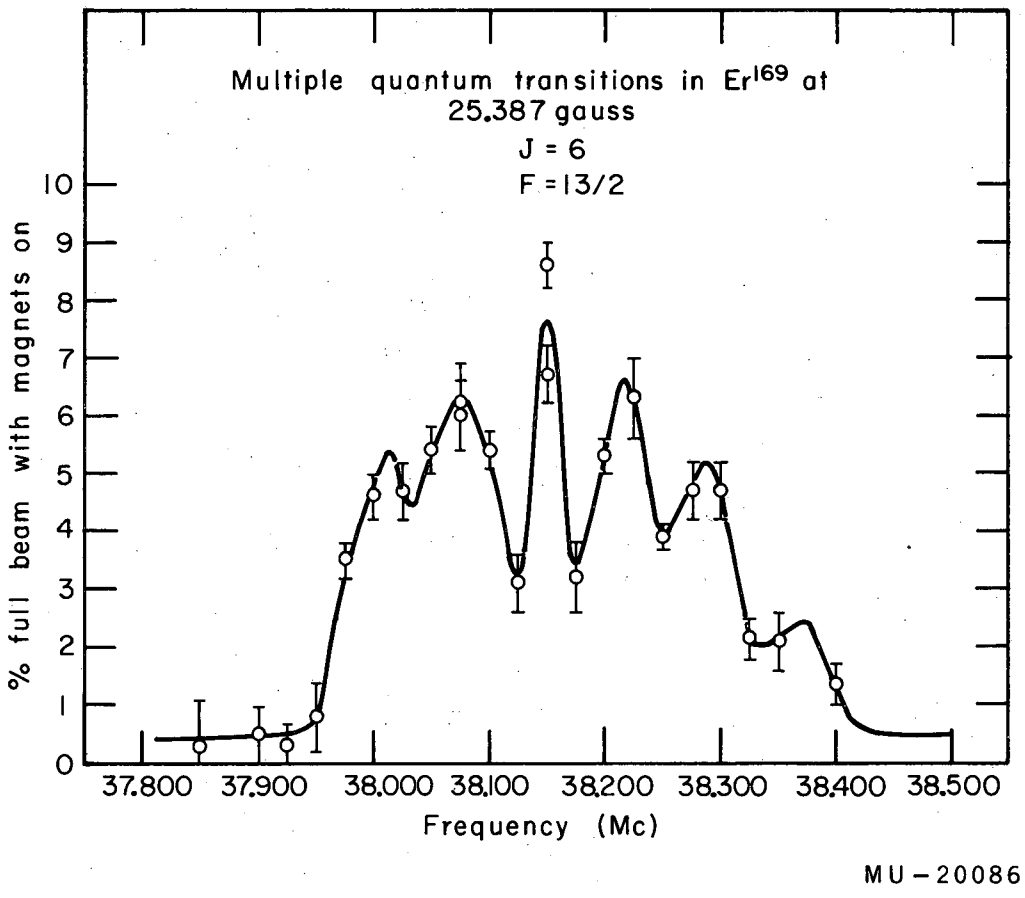

Fig. 39. Multiple quantum transition in Er^{169} at the intermediate magnetic field.

Table XI. Summary of observations

Isotope, nuclear spin and ground level	F	H(gauss)	Observed frequency (Mc)	Predicted frequency (Mc)
Erbium-169	13/2	0.709	1.070(50)	1.074
I = 1/2		1.418	2.150(50)	2.133
$^3H_6$		4.201	6.375(75)	6.317
		8.248	12.450(50)	12.403
		15.920	23.960(50)	23.940
		25.387	38.150(150)	38.177
	11/2	0.709	1.250(50)	1.253
		1.418	2.475(50)	2.488
		4.201	7.400(50)	7.370
		8.248	14.600(50)	14.470
		15.920	27.900(100)	27.931
Erbium-171	17/2	4.201	4.875(50)	4.830
I = 5/2	17/2	8.248	9.560(40)	9.483
$^3H_6$	15/2	4.201	5.280(30)	5.206
	15/2	8.248	10.325(40)	10.221
	13/2	4.201	5.800(20)	5.756
Thulium-171	4	4.201	5.950(50)	5.872
I = 1/2	4	1.418	2.000(100)	1.982
$^2F_{7/2}$	3	8.248	14.700(50)	14.823
	3	1.418	2.550(50)	2.549

H. Cerium

Cerium (Z = 58) has two electrons outside of closed electronic shells. The most probable ground-state configurations are $4f^2$, 4f 5d, and $5d^2$. Note that the configurations of the neighboring elements La and Pr are 5d and $4f^3$, respectively.

The configuration $5d^2$ can be ruled out immediately for cerium because the resulting levels cannot possibly account for three g values measured recently in an atomic-beam experiment on stable even-even cerium isotopes.[49] These results are:

$$g_1 = -0.7651(1)$$

$$g_2 = -0.9454(1)$$

$$g_3 = -1.0772(2) .$$

Since the nuclear spins of these isotopes are zero, the corresponding levels J_1, J_2, and J_3 are not determined. The g values in RS coupling for all three possible configurations are given in Table XII.

If the true configuration were f^2, one would not expect too large a breakdown of RS coupling, since most of the lanthanides with $4f^n$ exhibit electronic coupling that is very close to the RS limit. The Hund's-rule ground term for f^2 is ^3H, with J = 4 lying lowest in energy. Judd and Lindgren have performed a calculation for the corrections to the g values of this triplet.[37] They consider the Schwinger, spin-orbit, relativistic, and diamagnetic corrections and obtain:

Level	Theoretical g_J
$^3H_4$	-0.8054
$^3H_5$	-1.0325
$^3H_6$	-1.1659 .

Table XII. Possible configurations for cerium, and g (RS) for the given levels

Configuration	Term	J=6	J=5	J=4	J=3	J=2	J=1
$4f^2\ 6s^2$	^3H	1.167	1.033	0.800			
	^3F			1.250	1.083	0.667	
	^3P					1.500	1.500
	^1I	1.000					
	^1G			1.000			
	^1D					1.000	
	^1S						
$4f^1 5d^1 6s^2$	^3H	1.167	1.033	0.800			
	^3G		1.200	1.050	0.750		
	^3F			1.250	1.083	0.667	
	^3D				1.333	1.167	0.500
	^3P					1.500	1.500
	^1H		1.000				
	^1G			1.000			
	^1F				1.000		
	^1D					1.000	
	^1P						1.000
$5d^2\ 6s^2$	^3F			1.250	1.083	0.667	
	^3P					1.500	1.500
	^1G			1.000			
	^1D					1.000	

These g_J's are far from the measured values. Therefore we have ruled out $4f^2$ for the ground configuration of cerium.

The most likely assignment is now 4f 5d. The clearest way of testing this possibility is to diagonalize the appropriate total energy matrix, $\mathcal{H}$. Then the diagonal matrix, W, contains the energy of each level. (For fd the dimension of this symmetric matrix is 20 by 20.) The transformation matrix T ($T\mathcal{H}T^{-1} = W$) gives the amplitudes of each ket $|SLJJ_z)$. This energy matrix is the combined electrostatic plus spin-orbit energy matrix. The electrostatic energies $(SL|E\text{-}S|SL)$ of the atomic terms in fd have been evaluated in terms of the radial integrals F_0, F_2, F_4, G_1, G_3, and G_5 by Condon and Shortley.[58] The spin-orbit matrix for fd has been calculated by Racah in his analysis of the optical spectrum of ThIII.[59] The spin-orbit matrix elements depend on the fine-structure constants ζ_{5d} and ζ_{4f}.

To perform some numerical evaluations of the matrices, we have approximated the radial integrals F_k and G_k by using the values obtained by H. N. Russell in an analysis of the optical spectrum of LaII. Accurate 4f and 5d radial wave functions are not available. It is easy to get $\zeta_{5d} = 420\ cm^{-1}$ from the fs splitting of ^2D in LaI.[60] We calculate $\zeta_{4f} = 482\ cm^{-1}$ using a four-parameter formula which fits the known fs constants of NdI, SmI, and TmI.[37] An IBM-704 computer program which diagonalizes matrices and also calculates the g values in intermediate coupling[61] $\left[g(int) = T\ g\ (RS)\ T^{-1}\right]$ has been used in the calculations, and the results are not satisfactory. The three lowest-lying levels are noted, and the calculated g's are compared with the measured values. Although the agreement is not convincing enough to allow us to quote the results, it is felt that a better set of estimates for the radial integrals F_k and G_k would give the correct g_J's in intermediate coupling and the corresponding ground levels of cerium.

All attempts to produce a stable atomic beam of Ce^{141} and Ce^{143} have been unsuccessful so far. The source ovens are heated up to about 2500°K before a beam of cerium is obtained. Then the beam goes down monotonically after half an hour or less. It appears that cerium interacts chemically with all the metals that we have used for ovens. We have tried tantalum, tungsten, titanium diboride, molybdenum, and carbon.

It is clear that a steady atomic beam of a cerium isotope with a nonzero ground-state nuclear spin would allow us to determine the ground levels corresponding to the measured g values. Experiments on cerium are still in progress.

VI. HYPERFINE STRUCTURE OF THULIUM-170

The electronic ground state of this element as determined by optical spectroscopy is $4f^{13}\ 6s^2,\ ^2F_{7/2}$.[62] This agrees with our expermental observations. Our measurement of the g value in this level differs considerably from the classical RS value. Since this is essentially a one-electron problem, the admixture from other levels is small. Thus relativistic and diamagnetic effects are the major contributions in this case. It is shown later that together with the anomalous electron moment, these effects account very well for the observed deviation of the measured g value from the RS value.

The nuclear spin, the interaction constants a and b, and the g value have been measured in the ground level J = 7/2. The nuclear moments μ_I and Q have been calculated from the interaction constants with a modified hydrogenic radial wave function. A pulse-height analysis was performed with this isotope ($T_{1/2} \cong 2.9$ yr) for identification purposes (Fig. 40).

A. Experimental Observations and Results

The hfs energy levels in a magnetic field are shown schematically in Fig. 41 for Tm^{170} (I = 1). In this figure, the possible $\Delta F = 0$, (α, β, γ) and $\Delta F = \pm 1$, (δ, ϵ) transitions are indicated. These are:

α : (F = 9/2, m = 1/2) $\leftrightarrow$ (F = 9/2, m = -1/2)
β : (F = 7/2, m = -1/2) $\leftrightarrow$ (F = 7/2, m = -3/2)
γ : (F = 5/2, m = 3/2) $\leftrightarrow$ (F = 5/2, m = 1/2)
δ : (F = 7/2, m = -1/2) $\leftrightarrow$ (F = 9/2, m = -1/2)
ϵ : (F = 7/2, m = -1/2) $\leftrightarrow$ (F = 5/2, m = 1/2).

From Eq. (9) the hfs separations are given by:

$$\Delta\nu_1\ (9/2,\ 7/2) = 9/2\ a + 27/28\ b.$$
$$\Delta\nu_2\ (7/2,\ 5/2) = 7/2\ a - 5/4\ b. \qquad (62)$$

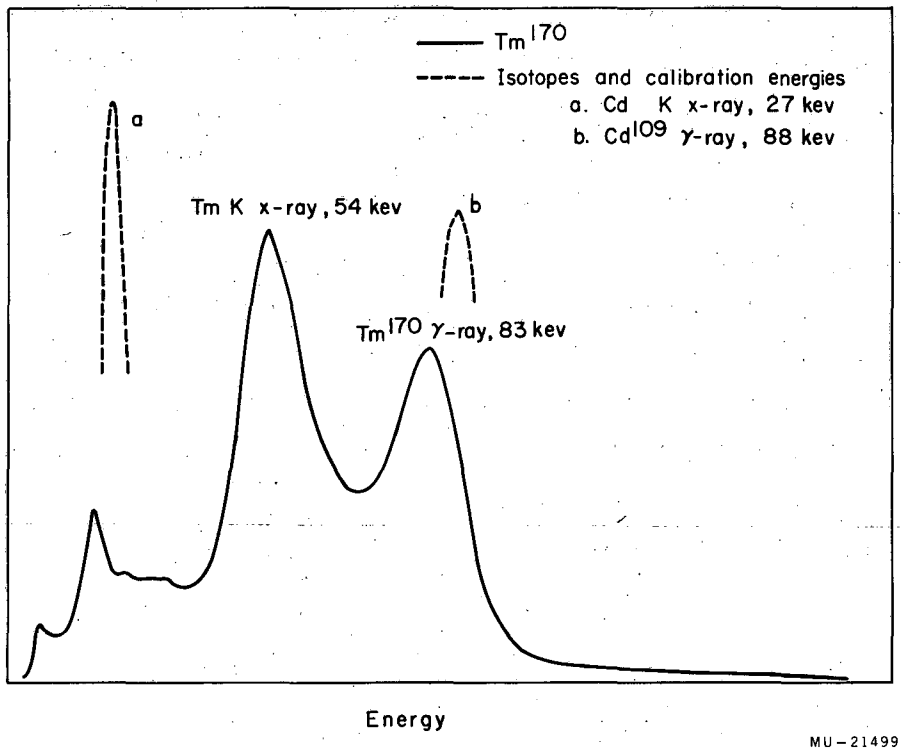

Fig. 40. Pulse-height analysis of Tm^{170}. This also includes a measurement of the energy of the thulium K X-ray.

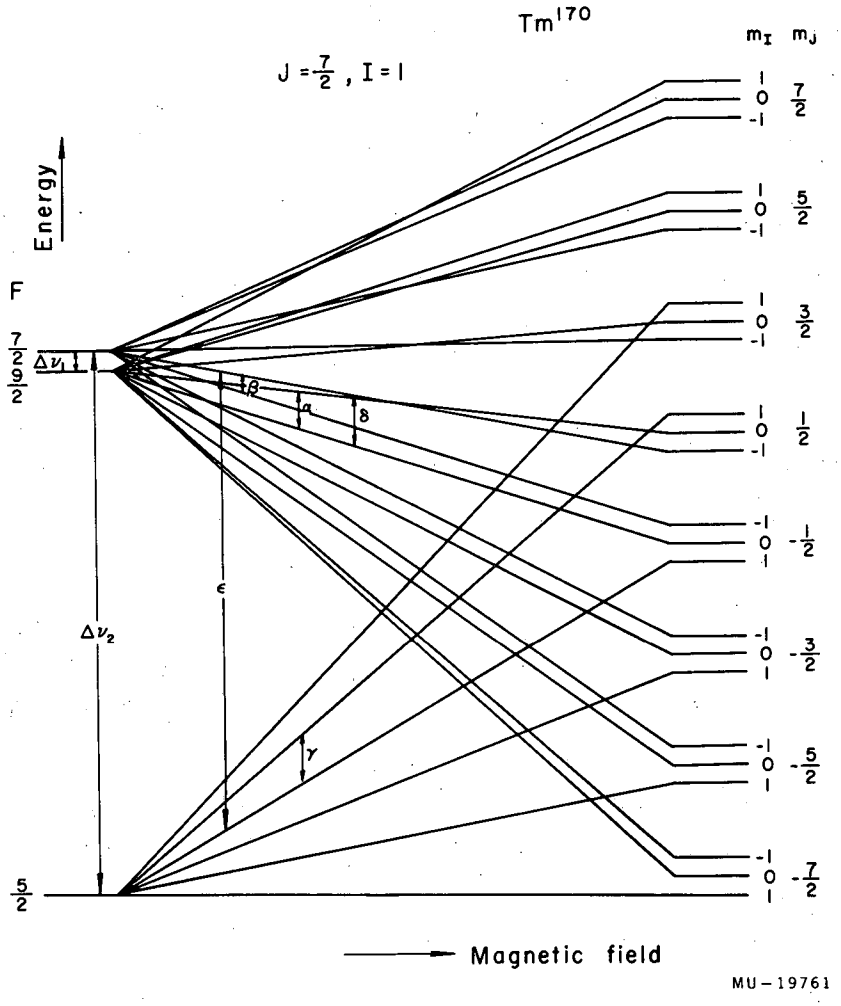

Fig. 41. Schematic Breit-Rabi diagram for the system I = 1, J = 7/2 of Tm^{170}.

The energy of each F_z state at zero field is plotted as a function of b/a in Fig. 42. In the region $-4.667 < b/a \leq 2.800$, the ordering of the F states is normal. It is observed that the F states 9/2 and 7/2 are inverted, and the measured b/a ratio is -5.05. Note that this value is very close to the critical ratio, so that the two hfs separations ($\Delta\nu_1$, $\Delta\nu_2$) are very different in magnitude (73 and 1960, respectively). Because of this, the three pi transitions have different behaviors in a magnetic field. A graph of $\nu/\mu_0 H/h$ vs $\mu_0 H/h$ is shown in Fig. 43. This illustrates the agreement between the experimental observations and the theoretical curves. In this diagram the curve starts at the g_F values and the slope corresponds to the second-order energy dependence in H. The alpha transition has no quadratic energy and starts with a zero slope. However, the higher-order terms become important at a relatively low field because of the small hfs separation $\Delta\nu_1$. The higher-order terms in the beta transition become predominant early and the total shift from linearity in H soon turns negative. The gamma transition is independent of $\Delta\nu_1$ and thus has a much smaller shift from the Zeeman frequency. The curves in Fig. 43 have been calculated with our best values of a, b, and g_J.

The three $\Delta F = 0$ transitions have been followed up to about 300 gauss, and one of the $\Delta F = 1$ transitions, δ, has been observed at two low fields. The other $\Delta F = 1$ transition, ϵ, has an inconveniently high frequency (approximately 1960 Mc) and has not been looked for. The resonance curves for each of the $\Delta F = 0$ transitions at the highest field are shown in Fig. 44, together with one curve for the $\Delta F = 1$ transition. The latter transition is of the type sigma ($\Delta m = 0$), and the resonance curve is therefore double-peaked. In general, the uncertainty in the resonance frequency has been taken to be about one-fourth of the half-width of the resonance curve. The observed resonance frequencies are given in Table XIII.

An IBM-704 program was used to analyze the experimental data. This program has been described elsewhere.[35] A least-square fit was

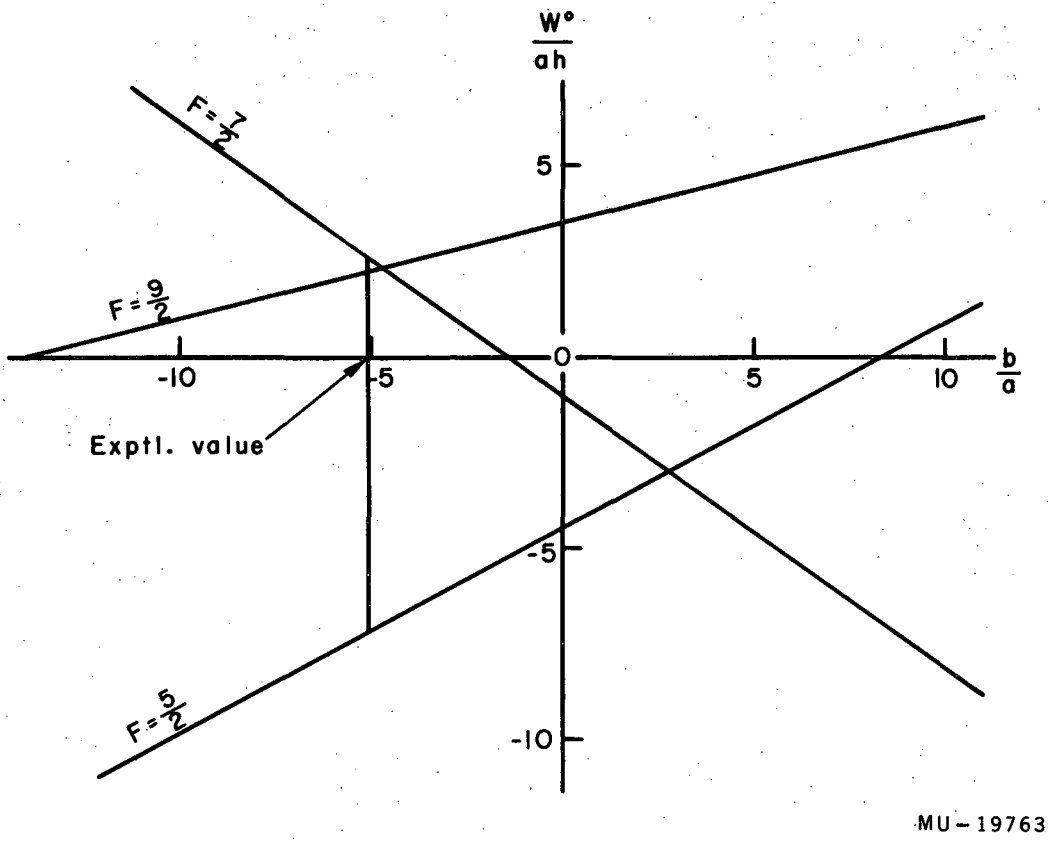

Fig. 42. Energy levels of each F state in zero magnetic field as a function of b/a.

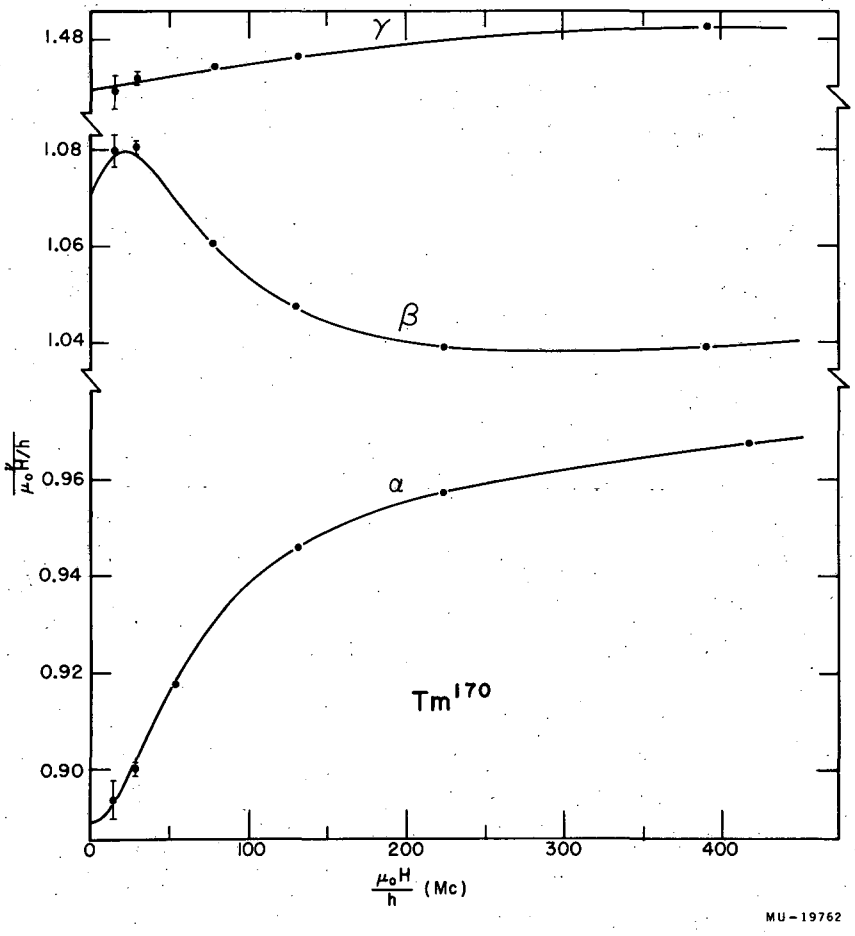

Fig. 43. Plot of magnetic field vs resonance frequency divided by magnetic field. The experimental points are compared with the theoretical curves calculated by using the final values of a, b, and g_J.

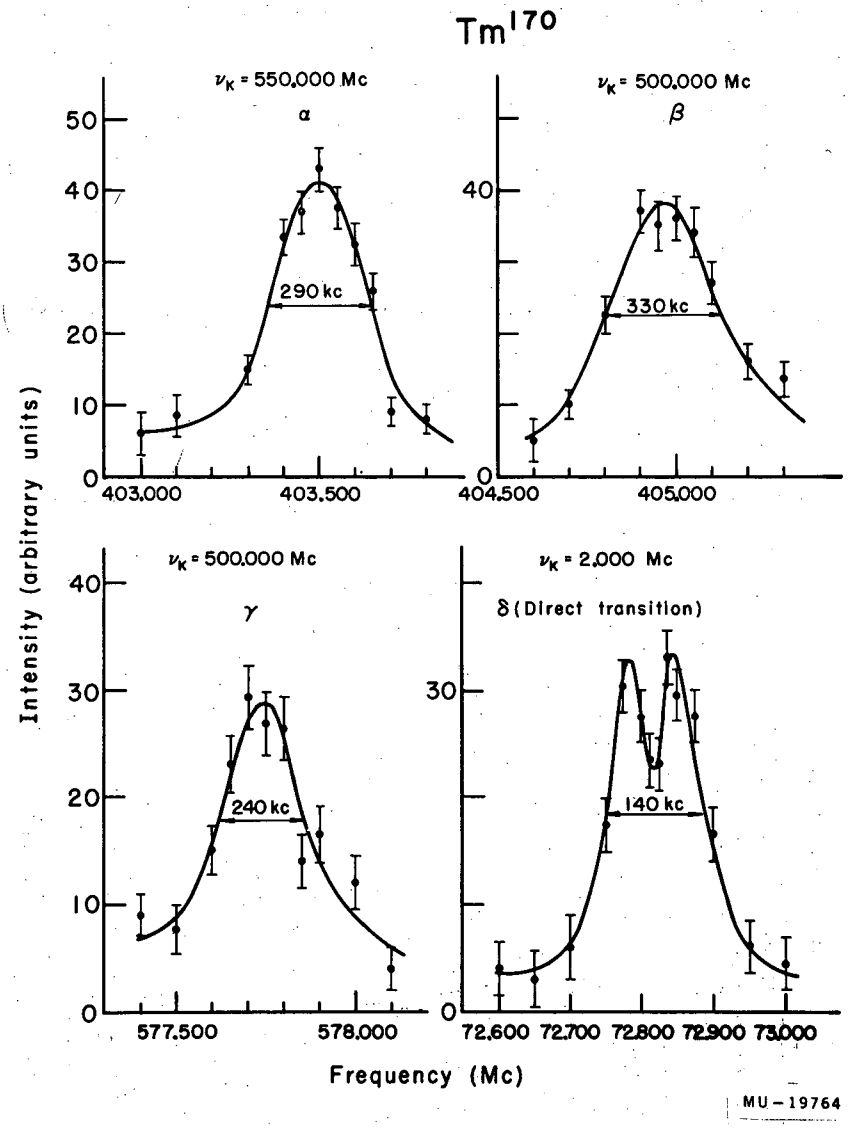

Fig. 44. Three $\Delta F = 0$ transitions observed in Tm^{170}. The double-peaked resonance is a $\Delta F = \pm 1$ transition.

Table XIII. Experimental data for Tm^{170}

Data No.	H (gauss)	$\nu_{obs.}$ (Mc)	$\nu_{obs.}-\nu_{calc.}$ (Mc)	Transition
1	0.711(71)	0.950(50)	0.066	α
2	1.418(70)	1.760(50)	-0.002	α
3	10.865(39)	13.600(70)	0.039	α
4	20.754(59)	26.100(40)	-0.055	α
5	38.243(50)	49.070(30)	-0.007	α
6	93.043(33)	123.000(50)	-0.021	α
7	0.711(71)	1.100(50)	0.035	β
8	1.418(70)	2.125(50)	0.000	β
9	10.865(39)	16.400(50)	0.020	β
10	20.754(59)	31.350(50)	0.061	β
11	55.192(43)	81.830(40)	0.048	β
12	93.043(33)	136.150(60)	-0.012	β
13	0.711(71)	1.470(50)	0.008	γ
14	10.865(39)	22.310(50)	-0.019	γ
15	20.754(59)	42.700(30)	0.024	γ
16	55.192(43)	113.745(40)	0.054	γ
17	159.545(24)	213.460(60)	-0.045	α
18	159.545(24)	231.715(75)	-0.034	β
19	278.798(20)	577.740(75)	0.030	γ
20	278.798(20)	404.970(100)	0.017	β
21	298.380(19)	403.505(80)	-0.011	α
22	0.740(41)	72.855(25)	0.002	δ
23	2.818(42)	72.815(25)	-0.003	δ
24	93.043(33)	192.010(60)	0.016	γ

made of the three parameters (a, b, and g_J), and a correction for the small contribution of g_I to the energy levels was included. The sign of the nuclear moment was determined by comparing the two fits arising from each choice of sign. It was found, however, that for this case, the moment is too small to allow a definite determination of the sign.

The final results are

$$I = 1, \quad |a| = 200(3)\ \text{Mc}, \quad |b| = 1010(15)\ \text{Mc}$$

with $b/a < 0$, and

$$J = 7/2$$

with $g_J = -1.14122(15)$. The figures in the parentheses denote the uncertainty in the last places of the numbers. We have stated larger errors than those obtained from the computer in order to include possible systematic errors.

B. Calculations of the Nuclear Moments

Since the electronic configuration of thulium consists of completely filled shells minus one electron, the relations between the hfs interaction constants and the nuclear moments are given by Eqs. (12) and (13). The relativistic correction factors $\mathcal{F}$ and $\mathcal{R}$ are for f electrons very close to unity and are discarded here.

In order to estimate $\langle r^{-3} \rangle$, one needs some approximate radial wave function. In most applications, hydrogenic wave functions have been used, but these cannot be expected to be good approximations, except for electrons moving very close to the nucleus. This is clearly demonstrated by self-consistent-field (SCF) calculations.

With the wave function discussed in Appendix E, which is a modification of the hydrogenic wave function to better agreement with SCF calculations, we get (in atomic units)

$$\langle r^{-3} \rangle = 10.6$$

for $\kappa = 0.40$, and

$$\langle r^{-3} \rangle = 10.4$$

for $\kappa = 0.44$. This shows, as one would expect, that the shape of the

wave function (parametrized by κ) is not critical when $\langle r^{-3} \rangle$ is determined from the experimental spin-orbit coupling constant. Ridley[63] gives 11.5 a.u. for Tm^{+3}, which should be slightly higher for the neutral atom, since the removal of the outer electrons pushes the other electrons a little closer to the nucleus. The crude hydrogenic formula for the spin-orbit coupling constant,

$$\zeta = hc\, R_y\, a^2\, Z_{eff} \langle r^{-3} \rangle = hc\, R_y\, a^2 \frac{Z_{eff}^4}{n^3\, \ell(\ell+1/2)(\ell+1)}, \quad (63)$$

gives $\langle r^{-3} \rangle = 13.1$ a.u. which is certainly too high.

With $\langle r^{-3} \rangle = 10.5$ a.u. we get, for the nuclear moments (uncorrected)

$$|\mu_I| = 0.26(2) \text{ nm}$$

and

$$|Q| = 0.61(5) \text{ barns}.$$

The error in the magnetic moment is large enough to include diamagnetic corrections. For the quadrupole moment, on the other hand, corrections of the Sternheimer type,[39] which have not been considered here, might make the corrected value fall outside the given limits.

The hfs of the stable isotope Tm^{169} has been investigated optically by Lindenberger,[64] and he gives for the magnetic moment

$$\mu_I^{169} = -0.20_5 \pm 0.02 \text{ nm}.$$

Although he uses hydrogenic wave functions, he gets, surprisingly enough, consistent results from the hfs constants for the 4f and 6s electrons. With our value of $\langle r^{-3} \rangle$ for the 4f electron, which we believe is more accurate, we obtain from his data

$$\mu_I^{169} = -0.25 \text{ nm},$$

which is outside the given limits of error.

C. Corrections to the g Value

Since the ground state of thulium is essentially a single-electron state, the admixture of other states is very small. Furthermore, the electrostatic interaction can only mix states with the same S, L, and J and hence has no effect on the g value. An estimate of the configuration interaction caused by the spin-orbit coupling shows that its effect is quite negligible compared with the experimental uncertainty. Therefore, all the measurable deviation from the classical Lande value must be due to (a) the anomalous magnetic moment of the electron, and (b) relativistic and diamagnetic effects. By relativistic effects we mean here the change in the interaction between the atomic moment and the external field, due to the velocity of the electron, and the change in the spin-orbit coupling, due to the external field. These corrections follow directly from the Dirac equation for a single electron, and are proportional to the kinetic energy T in the first approximation. The diamagnetic correction is caused by changes in the spin-other-orbit and orbit-orbit interactions, due to the external field. This correction depends essentially on the electron density in the core.

The relativistic correction to the magnetic moment of a single electron has been calculated by Breit[65] and Margenau[66] and can be written as

$$\delta g_1 = \alpha^2 (j+1/2)^2 \langle T \rangle / j(j+1). \qquad (64)$$

All radial integrals are expressed in atomic units here. This correction is usually referred to as the Breit-Margenau correction.

In their discussion of the Zeeman effect in atomic oxygen, Abragam and Van Vleck[67] have calculated the diamagnetic correction, assuming a spherically-symmetric electron density. From their expressions we get for the diamagnetic correction to the Zeeman energy for a single electron in the state ($n \ell\ m_s\ m_\ell$),

$$\delta Z = -\mu_0 H a^2 \left[(m_\ell + 2m_s) \langle Y \rangle - m_s \left\langle \sin^2\theta \right\rangle \langle U \rangle \right] , \qquad (65)$$

where

$$U = \frac{1}{r^3} \int_0^r r'^2 \rho(r')\, dr',$$

$$Y = (1/3) \left[U + \int_r^\infty \frac{\rho(r')}{r'} dr' \right]$$

and

$$\left\langle \sin^2\theta \right\rangle = 2 \frac{\ell(\ell+1) - 1 + m_\ell^2}{(2\ell - 1)(2\ell + 3)} .$$

Here $\rho(r')$ is the radial density of all electrons except the one electron over which the average is taken.

From Eqs. (64) and (65) we get the total correction for an f electron in the state $^2F_{7/2}$,

$$\delta g = -a^2 \left[\frac{64}{63} \langle T \rangle + \frac{8}{7} \langle Y \rangle - \frac{8}{63} \langle U \rangle \right] . \qquad (66)$$

With the wave function described in Appendix E and the electron density from the Thomas-Fermi model, (Fig. 45) we obtain the following values of the radial integrals:

$\kappa = 0.40$: $\langle T \rangle = 24.7$, $\langle U \rangle = 16.5$, $\langle Y \rangle = 13.3$ a.u.
$\kappa = 0.44$: $\langle T \rangle = 23.3$, $\langle U \rangle = 15.6$, $\langle Y \rangle = 12.5$ a.u.

It is seen that the agreement between the experimental and calculated g values is extremely good with κ around 0.4, the value obtained by comparison with SCF wave functions. (See Table XIV).

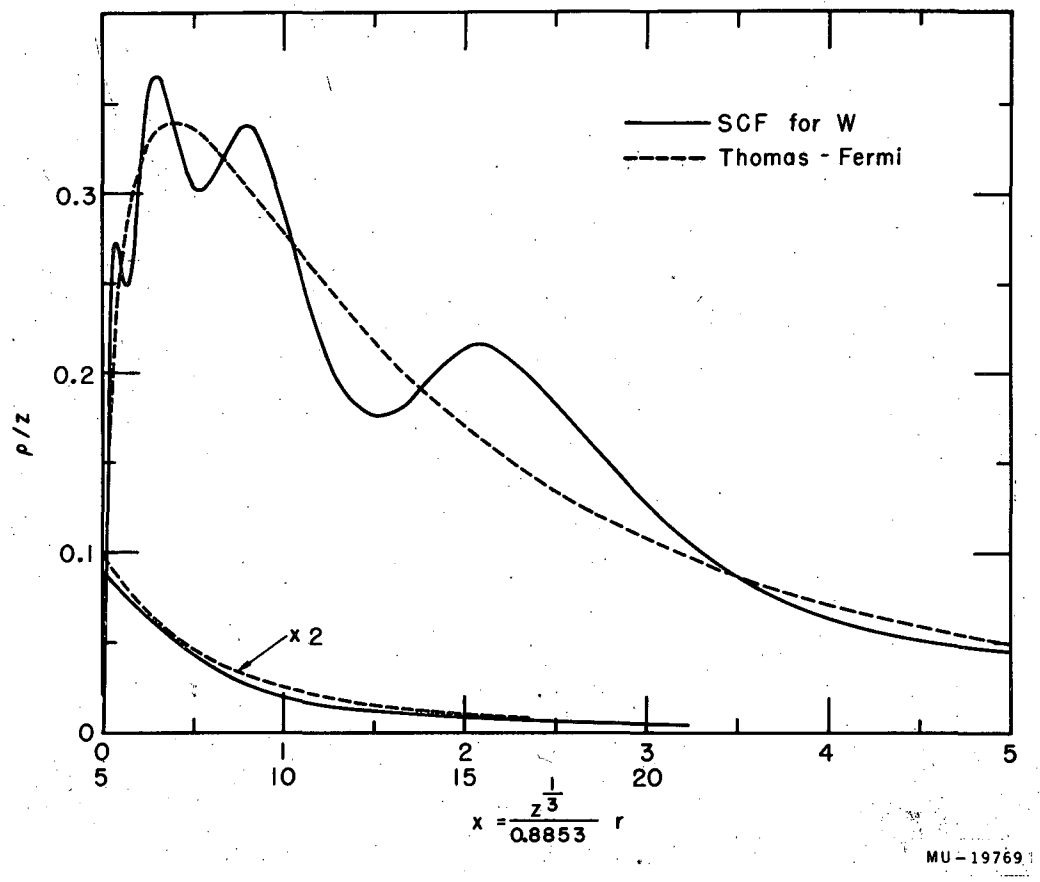

Fig. 45. Electronic charge density as a function of r.

Table XIV. Summary of all corrections. For comparison we have also given the corresponding values obtained with a hydrogenic wave function.

	Hydrogenic wave function	Modified hydrogenic wave functions	
	($\kappa = 0$)	$\kappa = 0.40$	$\kappa = 0.44$
Landé value	1.14286	1.14286	1.14286
Schwinger correction	0.00033	0.00033	0.00033
Breit-Margenau correction	-0.00166	-0.00134	-0.00126
Diamagnetic correction	-0.00084	-0.00070	-0.00066
Theoretical value	1.14069	1.14115	1.14127
Experimental value		1.14122(15)	

Since all wave functions used here are fitted to the experimental spin-orbit coupling constant with the same potential, the difference in result is entirely due to the difference in shape. The experimental deviation from the Landé value together with the spin-orbit coupling constant therefore constitutes a measure of the shape of the wave function. Although the accuracy here is not very high, it definitely shows that the hydrogenic wave function is too sharp. The hydrogenic wave function used above has been fitted to the experimental spin-orbit coupling constant by means of the Thomas-Fermi potential. If Z_{eff} is determined from Eq. (63), the agreement is even poorer.

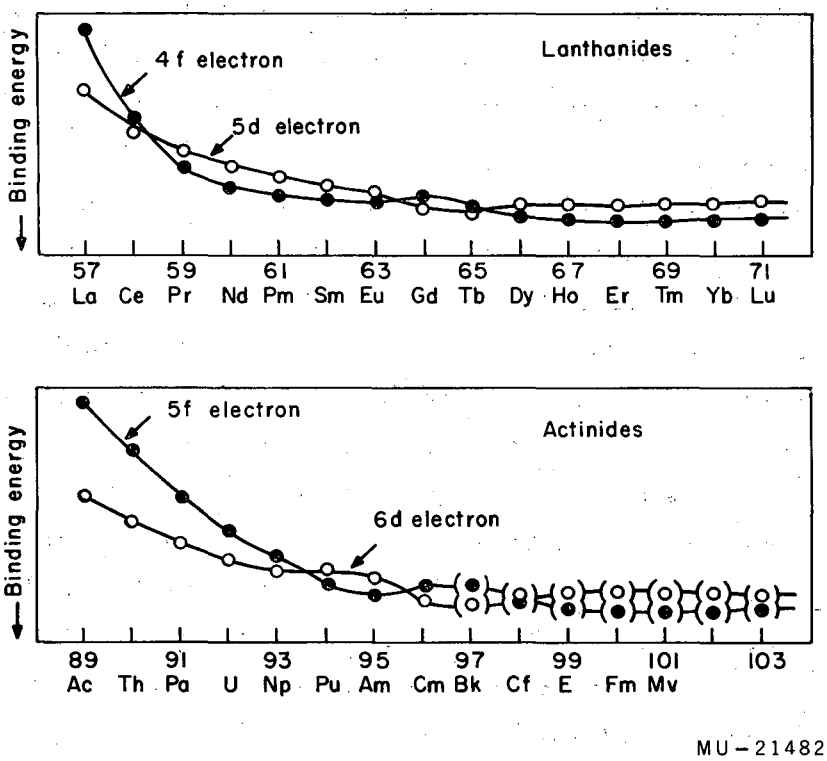

Fig. 46. Qualitative comparisons of the binding energies of the last competing electron in the lanthanides and the actinides.

VII. CONCLUDING REMARKS ON THE ELECTRONIC CONFIGURATIONS OF THE LANTHANIDES

The atomic-beam spectroscopy method has been especially powerful in treating this problem. The theory of the method allows a unique determination of the ground levels in most cases. From these electronic levels, speculations on the ground electronic configuration and resulting ground term are possible. In cases where it is not possible to positively identify the ground term, there is, however, no doubt that the complexity is brought about by a competing 5d electron in the rare earth.

It is now clear that this transition series is concerned with the filling of the 4f and not the 5d subshell. Only the first two elements of each half of the series has a 5d electron which is more tightly bound to the atomic core than the 4f electron (La and Ce in the first half, and Gd and Tb in the second half.) All the remaining rare earths have exclusively 4f electrons in the unfilled subshell.

Figure 46 is a very qualitative picture of the behavior of the binding energy of the last valence electron from one lanthanide to another. This is based on the observations on the ground levels and inferred configurations. The curves are not expected to be smooth, but the relative binding energy between the 4f and 5d electron in each element are believed to be as indicated. Note that there are three crossover points between the two curves. The first crossover point is understandable in view of the presence of the d electron in cerium but its absence in praseodymium. The second cross over is greatly influenced by the stability of half-filled closed shells so that the seventh f electron is favored over the d electron at this point. The third and last crossover point in this series is also clear in view of the inferred terbium configuration ($4f^9$ and $4f^8$ 5d).

Therefore we now have a somewhat comprehensive treatment of electronic structure which specifically points out those lanthanides

that include a 5d electron in the ground state. A summary of the ground-state electronic configurations and ground levels is given in Table XV. The measured g values for the levels observed here are given in Table XVI.

There is definitely an analogy between the actinides (this series starts with actinium, Z = 89) and the lanthanides. Here again, it is clear that it is the 5f and not the 6d subshell that is being filled up in the series. Atomic-beam experiments by the Berkeley group on Pa, U, Np, Pu, Am, and Cm have contributed much towards the understanding of electronic structure in this region.[16, 22, 30, 35] A summary of the ground-state electronic configurations and ground levels of the actinides is made in Table XVII.

Figure 46 shows an analogous picture for the behavior of the binding energy of the last electron (5f or 6d) competing in the ground state in each of the elements. It is most interesting to note that the general features of the picture are the same in both transition series. In this latter case, there are also three critical points. The main difference is that the 6d electron is more tightly bound than the 5d electron so that it appears in the first five actinides. However, the sixth actinide, plutonium, definitely has no d electron so that the first crossover point occurs just before this element. Then the stability of half-filled closed shells is again manifested so that americium is $5f^7$. The second crossover point comes after this element so that curium, like gadolinium is f^7d. Since it would be expected that to complete the analogy between the two series, the late members of the actinides should have no d electron, there must be a third crossover point in the diagram. It is likely that this occurs after berkelium or californium. In view of the terbium results, its actinide homologue, berkelium, may very well contain a d electron in the ground state. In addition, since the 6d electron seems to be more tightly bound than the 5d electron, californium may quite conceivably contain a d electron in the ground state. It is clear that future atomic-beam work on these transuranics should yield some very interesting answers to the problem.

Table XV. The ground-state electronic configurations and ground levels of the rare earths

Z	Element	Ground configuration	Ground level
57	lanthanum	$5d\ 6s^2$	$^2D_{3/2}$
58	cerium	$(4f\ 5d\ 6s^2)$	
59	praseodymium	$4f^3\ 6s^2$	$^4I_{9/2}$
60	neodymium	$4f^4\ 6s^2$	$^5I_4$
61	promethium	$4f^5\ 6s^2$	$^6H_{5/2}$
62	samarium	$4f^6\ 6s^2$	$^7F_0$
63	europium	$4f^7\ 6s^2$	$^8S_{7/2}$
64	gadolinium	$4f^7\ 5d\ 6s^2$	$^9D_2$
65	terbium	$4f^9\ 6s^2$	$^6H_{15/2}$
		and $(4f^8\ 5d\ 6s^2)$	$\left[(^7F_6,\ ^2D_{3/2})\ 15/2\right]$
66	dysprosium	$4f^{10}\ 6s^2$	$^5I_8$
67	holmium	$(4f^{11}\ 6s^2)$	$(^4I_{15/2})$
68	erbium	$4f^{12}\ 6s^2$	$^3H_6$
69	thulium	$4f^{13}\ 6s^2$	$^2F_{7/2}$
70	ytterbium	$4f^{14}\ 6s^2$	$^1S_0$
71	lutetium	$4f^{14}\ 5d\ 6s^2$	$^2D_{3/2}$

Table XVI. Summary of measured g values

Z	Element	Observed term	J	$-g_J$(RS)	$-g_J$(exp't)
59	Pr	^4I	9/2	0.7273	0.7311(2)
61	Pm	^6H	7/2	0.8254	0.831(5)
			9/2	1.0707	1.068(4)
62	Sm	^7F	1	1.5000	1.495(15)
			2	1.5000	1.497(15)
66	Dy	^5I	8	1.2500	1.2414(3)[b]
67	Ho	(^4I)[a]	$(15/2)$[a]	1.2000	1.196(1)[b]
68	Er	^3H	6	1.1667	1.164(5)[b]
69	Tm	^2F	7/2	1.1428	1.1412(2)

[a] Speculative assignment

[b] These values agree with those independently obtained from spin-zero isotopes for Dy and Er by Spalding,[49] and for Ho by Goodman and Childs.[10]

Table XVII. The ground-state electronic configurations and ground levels of the actinides[a]

Z	Element	Ground configuration	Ground level
89	actinium	$6d\ 7s^2$	$^2D_{3/2}$
90	thorium	$6d^2\ 7s^2$	$^3F_2$
91	protactinium	$5f^2\ 6d\ 7s^2$	$\left[^3H_4,\ ^2D_{3/2}\right]_{11/2}$ [b]
92	uranium	$5f^3\ 6d\ 7s^2$	$\left[^4I_{9/2},\ ^2D_{3/2}\right]_6$ [c]
93	neptunium	$5f^4\ 6d\ 7s^2$	$\left[^5I_4,\ ^2D_{3/2}\right]_{11/2}$ [d]
94	plutonium	$5f^6\ 7s^2$	$^7F_0$ [d]
95	americium	$5f^7\ 7s^2$	$^8S_{7/2}$ [b]
96	curium	$5f^7\ 6d\ 7s^2$	$\left[^8S_{7/2},\ ^2D_{3/2}\right]_2$ [d]
97	berkelium	$(5f^8\ 6d\ 7s^2)$	$\left(\left[^7F_6,\ ^2D_{3/2}\right]\right)$
98	californium	$(5f^{10}\ 7s^2$	$(^5I_8)$
99	einsteinium	$(5f^{11}\ 7s^2)$	$(^4I_{15/2})$
100	fermium	$(5f^{12}\ 7s^2)$	$(^3H_6)$
101	mendelevium	$(5f^{13}\ 7s^2)$	$(^2F_{7/2})$
102		$(5f^{14}\ 7s^2)$	$^1S_0$
103		$(5f^{14}\ 6d\ 7s^2)$	$(^2D_{3/2})$

[a] The assignments enclosed in the parentheses are speculations.

[b] Reference 16,

[c] Reference 51,

[d] Reference 30.

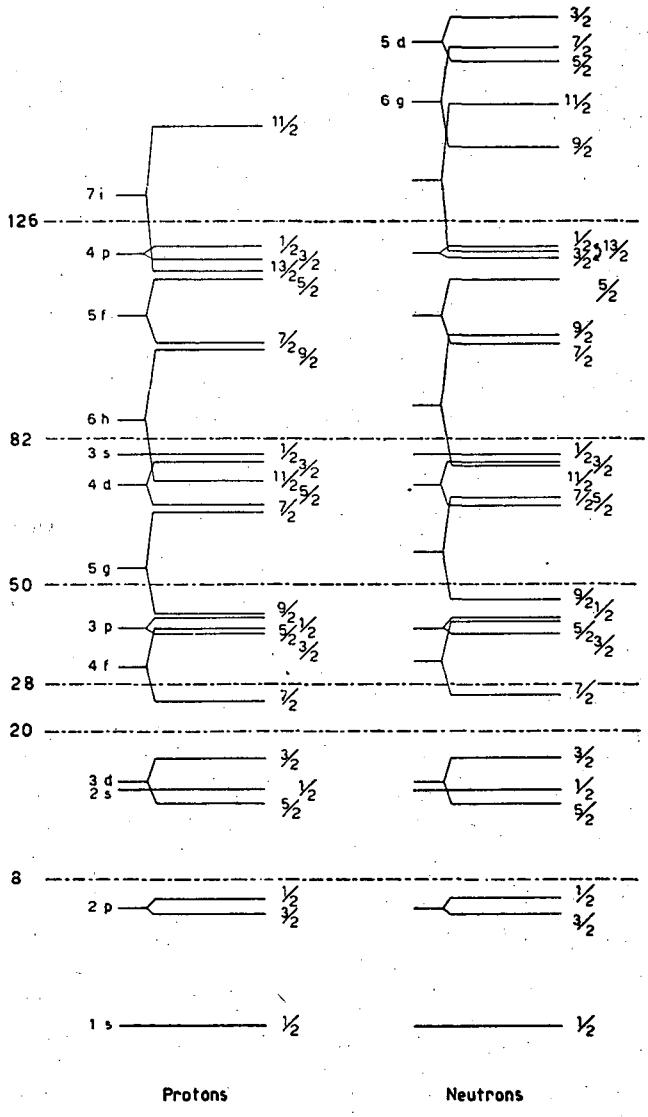

Fig. 47. Nucleon level assignments in the shell model.

VIII. INTERPRETATIONS OF THE MEASURED NUCLEAR SPINS

A. Nuclear Shell Model

The single-particle shell model theory has been successful in accounting for the behavior of nuclei with nucleon numbers near the magic numbers. These numbers, 2, 8, 20, 28, 50, 82, and 126 indicate a type of periodicity in nuclear structure which is somewhat analogous to that which exists in electronic structure. In the latter case, the "electronic magic numbers" are the atomic numbers of the noble gases, 2, 10, 18, 36, 54 and 86. Also, the theoretical Schmidt lines derived from this theory, are fairly adequate for setting limits to the magnitudes of the nuclear moments.

This model assumes that the nucleons move in a central potential which has a form somewhere between a square-well and a harmonic oscillator potential.[33] Together with this, the introduction of a spin-orbit interaction, usually written as $f(r)\,\vec{s}\cdot\vec{\ell}$ allows the determination of sequences of nucleon energy levels which have the correct characteristics in the vicinity of the nuclear closed-shell regions.

A nucleon level is designated by $(n\ell)\,j$, where n, ℓ, and j are the principal, orbital, and total-angular-momentum quantum numbers, respectively (Fig. 47.) The intrinsic spin of a nucleon (proton, neutron) is 1/2 so that $j = \ell \pm 1/2$. The degeneracy of each level is $2j + 1$.

The following nucleon coupling properties are observed: (a) An even number of protons and an even number of neutrons couple separately to give a resultant nuclear ground-state spin of zero. All even-even nuclei are observed to have zero spin. (b) For nuclei with odd n and even p or odd p and even n, the ground-state properties are determined by the odd nucleons alone. In addition, the odd number of nucleons couple in such a way that the angular momentum of the nucleus is that of the last odd nucleon. In the early part of the rare earth series, this model seems to be successful. This is supported by the investigations here on ${}_{58}Ce^{141}_{83}$, ${}_{59}Pr^{142}_{83}$, and ${}_{60}Nd^{147}_{87}$. These are tabulated in Table XVIII.

Table XVIII. Summary of measured nuclear spins

Z	E	A	Measured Spin	Nilsson state or shell-model state		Prediction of beta-decay on spin and parity
				Odd proton	Odd neutron	
59	Pr	142	2	4d 5/2	5f 7/2	2 -[b]
60	Nd	147	5/2[a]		$[5f\ 7/2]^{-3}_{5/2}$	
61	Pm	147	7/2	[404] 7/2		
62	Sm	153	3/2		[651] 3/2 or [521] 3/2	3/2[c]
64	Gd	159	3/2		[521] 3/2	3/2 -[d]
65	Tb	160	3	[411] 3/2	[521] 3/2	3[e]
66	Dy	165	7/2		[633] 7/2	7/2 +[f]
		166	0			
67	Ho	166	0	[523] 7/2	[633] 7/2	0 -[g]
68	Er	169	1/2		[521] 1/2	1/2 -[h]
		171	5/2		[521] 5/2	5/2 -[i]
69	Tm	170	1	[411] 1/2	[521] 1/2	1 -[j]
		171	1/2	[411] 1/2		1/2 +[k]

[a] Also measured with the paramagnetic-resonance method (Ref. 41).
[b] Ref. 31
[c] Ref. 57
[d] Ref. 68
[e] Ref. 69
[f] Ref. 56
[g] Ref. 70
[h] Ref. 71
[i] Ref. 72
[j] Ref. 73
[k] Ref. 74

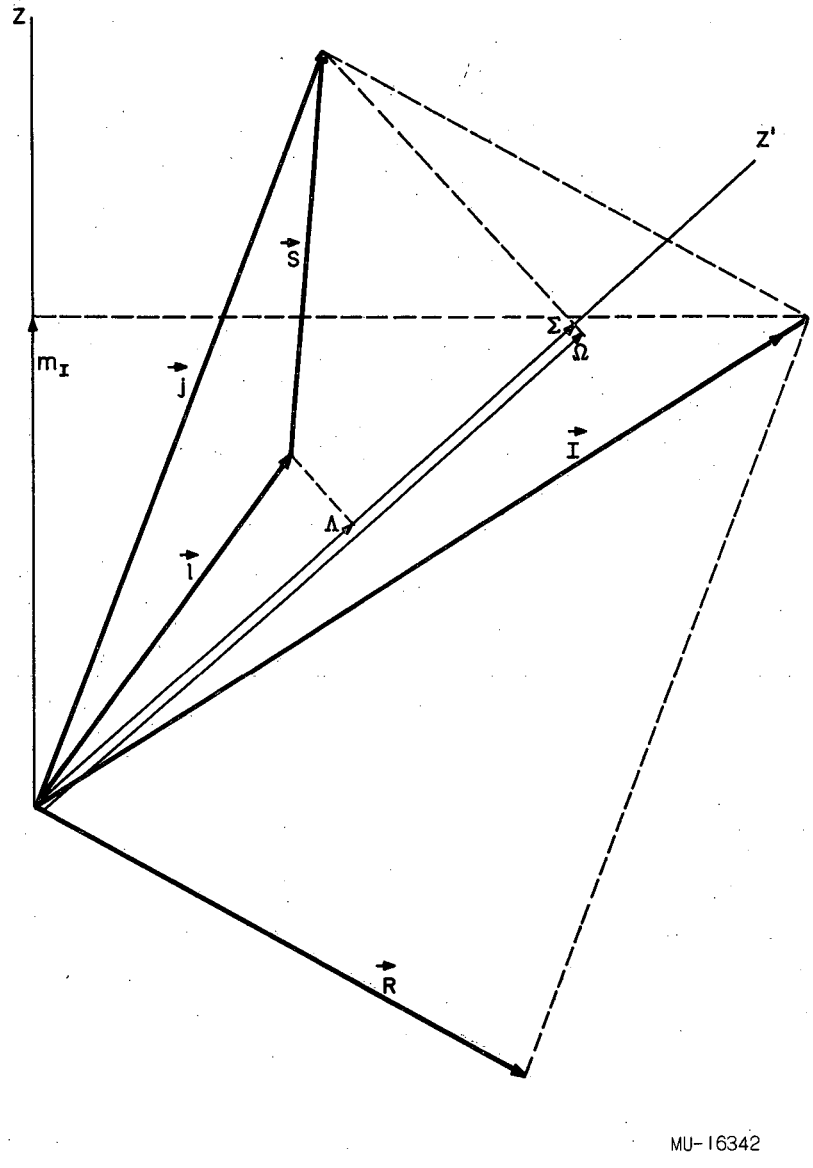

Fig. 48. Angular momenta in the collective model.

A large number of the observed spins in nature are successfully treated by this model. Also, we have found good agreement between our calculations of the nuclear moments of Pr^{142} from the hfs and the estimates based on this model.

B. Collective Model

In the region A ~25, 150< A < 190, and A >222, the nuclear shape is observed to deviate considerably from spherical symmetry. The collective-model theory has been introduced in order to attempt to explain many facets of these deformed nuclei.[75] This model assumes that the nuclear core has an ellipsoidal shape which undergoes surface vibrations and rotations about a nuclear symmetry axis usually labeled z'. The reflection-symmetry plane of the nucleus is perpendicular to this axis and passes through the center of the core. The energies due to surface vibrations are known to be high enough so that the ground state and first few excited states are not affected.

The rotation of the nuclear core is represented by the angular momentum $\vec{R}$ in Fig. 48. The resulting rotation energies are the so-called rotational bands. In the zero-order approximation, the nuclear Hamiltonian in this model contains a spherically-symmetric potential V(r) together with the kinetic energy. In order to include the departure of the nuclear shape from spherical symmetry, a term proportional to $r^2 Y_2^0 \delta$ is included, where δ is a deformation parameter and Y_2^0 is the second-order spherical harmonic. Also, the spin-orbit interaction $\vec{s}\cdot\vec{\ell}$ is included together with an orbit-orbit interaction $\vec{\ell}\cdot\vec{\ell}$ for nucleons with high ℓ.

The last odd nucleon is then assumed to move about this deformed core. The nucleon has angular momentum $\vec{j}$, where $\vec{j} = \vec{\ell} + \vec{s}$. The projections of the orbital and intrinsic spin angular momenta on the symmetry axis z' are denoted by Λ and $\sum$, respectively, and Ω is the projection of $\vec{j}$ on this axis.

In the "strong-coupling" approximation, where the spin-orbit coupling energy is treated as a perturbation, the good quantum numbers for the specification of a nuclear state are $[N\ n_z\ \Lambda]\ \Omega$, where N and n_z are the total oscillator quantum number and its component along z', respectively. The only degeneracy in each level is that due to $\pm\ \Omega$. It is seen from Fig. 48 that the resultant nuclear spin is $\vec{I} = \vec{j} + \vec{R}$. However, $\vec{R}$ is perpendicular to z' for the ground state so that the ground-state spin is $I_0 = \Omega$. For two odd nucleons coupling to a ground-state spin, Gallagher and Moszkowski have proposed the following coupling rules:[76] (a) The Ω's are added if the intrinsic spins are either both parallel or both antiparallel to their respective orbitals. That is, we have

$$I_0 = \Omega_p + \Omega_n$$

for

$$\Omega_p = \Lambda_p \pm 1/2 \qquad \text{and } \Omega_n = \Lambda_n \pm 1/2.$$

(b) The resultant spin is the difference between the Ω's if spin and orbit are parallel for one nucleon and antiparallel for the other nucleon. Then we have

$$I_0 = \left| \Omega_p - \Omega_n \right|$$

for

$$\Omega_p = \Lambda_p \pm 1/2 \quad \text{with} \quad \Omega_n = \Lambda_n \mp 1/2.$$

In the weak-coupling limit, the spin-orbit energy predominates and the nuclear energy levels, as expected, approach the levels in shell-model theory.

It is evident from Table XVIII that the nuclear spins of rare earth nuclei with $A > 150$ are successfully treated by this model. The measured spins indicate that the range of the deformation parameter in this region is $0.2 < \delta < 0.4$ (see Figs. 49 and 50).

ACKNOWLEDGMENTS

It is a pleasure for me to express my indebtedness to:

Professor William A. Nierenberg for his support and interest;

Dr. Richard Marrus for his guidance in countless numbers of experiments at the laboratory;

Dr. Ingvar Lindgren for the generous donation of much of his time and knowledge towards my general enlightenment;

Dr. Edgar Lipworth and Professor Howard Shugart for some very informative and pleasant conversations;

Dr. Joseph Winocur for his help in the early stages of the research;

Douglas B. MacDonald and G. G. Young for their expert engineering advice;

Mark Rubinstein and Burt Budick for their assistance in the runs;

The L. R. L. Health Chemistry Department --in particular, Homer Adams and R. McCracken--for their most efficient handling of the radioactive sources;

My parents, most of all, for their encouragement, understanding, and invaluable assistance.

This work was done under the auspices of the U. S. Atomic Energy Commission.

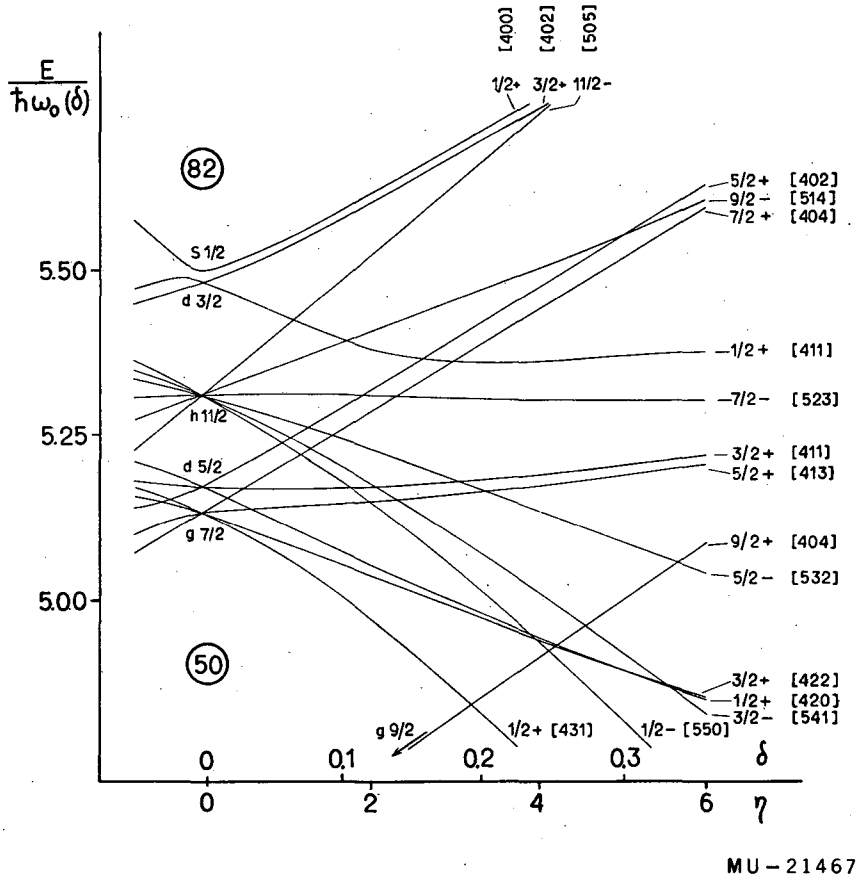

Fig. 49. Proton levels in the collective model for 50 < Z 82.

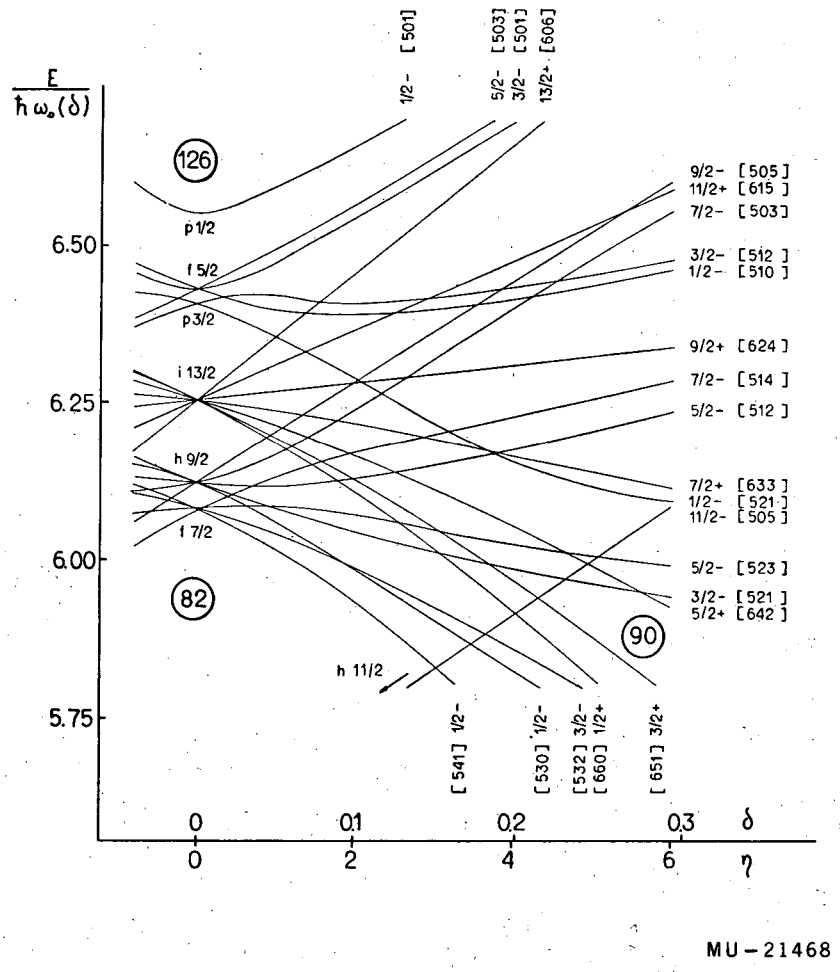

Fig. 50. Neutron levels in the collective model for $82 < N < 126$.

APPENDICES

A. Matrix Elements of $\Sigma(3\cos^2\theta_i - 1)$ in Tensor Form

The tensor C^k_q of rank k is defined by

$$C^k_q = (-1)^q [(k-q)!/(k+q)!]^{1/2} P^q_k(\cos\theta)\, e^{iq\phi}, \tag{67}$$

where the associated Legendre polynomials are

$$P^q_k(\cos\theta) = \sin^q\theta\, d^q/d(\cos\theta)^q \quad P_k(\cos\theta).$$

These tensors obey the following commutation relations:

$$\left[J_z,\ C^k_q\right] = qC^k_q$$

$$\left[J_\pm,\ C^k_q\right] = \left[k(k+1)-q(q\pm 1)\right]^{1/2} C^k_{q\pm 1}.$$

In the definition of C^k_q [Eq. (67)], set k = 2 and q = 0. This gives

$$C^2_0 = P_2(\cos\theta) = 1/2(3\cos^2\theta - 1).$$

Therefore, in tensor operator form, we have

$$(3\cos^2\theta_i - 1) \longrightarrow 2(C^2_0)_i\ . \tag{68}$$

Let us make the definition $Q^* \equiv \sum_i 2\,(C^2_0)_i$.

The matrix element of this tensor operator connecting the states indicated is

$$(\ell^n\, a\, SLJJ \mid Q^* \mid \ell^n\, a'\, S'L'J'J') = \begin{pmatrix} J & 2 & J' \\ -J & 0 & J' \end{pmatrix} (\ell^n\, aSLJ \| Q^* \| \ell^n a'S'L'J')$$

$$= \begin{pmatrix} J & 2 & J' \\ -J & 0 & J' \end{pmatrix} n\,\delta(S,S')(-1)^{S+J+L'+L+\ell} \left[(2J+1)(2J'+1)(2L+1)(2L'+1)\right]^{1/2}$$

$$\begin{Bmatrix} L & J & S \\ J' & L' & 2 \end{Bmatrix} \sum_{\bar\psi} (-1)^{\bar L} \begin{Bmatrix} \ell & L & \bar L \\ L' & \ell & 2 \end{Bmatrix} (\psi\{|\bar\psi)(\psi'\{|\bar\psi)(\ell \| Q^* \| \ell). \tag{69}$$

The selection rules observed by noting the triangular conditions on the first 6-j symbol in Eq. (69) are

$$\Delta L = 0, \pm 1, \pm 2 \qquad \text{and} \qquad \Delta J = 0, \pm 1, \pm 2.$$

The Kronecker delta $\delta(S,S')$ in Eq. (69) immediately imposes the condition $\Delta S = 0$ for the expression to remain non-zero. Thus there are no off-diagonal matrix elements in S for this operator.

Because of the small admixture from the two $^2H_{9/2}$ levels (-0.152 and 0.064), the selection rules above indicate that the only matrix element of interest is that which is diagonal in the ground level $^4I_{9/2}$. The contribution to the expectation value of Eq. (39) from (210)(21) $^2H_{9/2}$ enters as the square of the admixture coefficient (-0.152) multiplied by the diagonal matrix element of the state $^2H_{9/2}$.

The diagonal matrix element of Q^* is

$$(\ell^n \alpha SLJJ \,|\, Q^* \,|\, \ell^n \alpha SLJJ) = n(-1)^{S+J+2L+\ell}(2J+1)(2L+1) \tag{70}$$

$$\times \begin{pmatrix} J & 2 & J \\ -J & 0 & J \end{pmatrix} \begin{Bmatrix} L & J & S \\ J & L & 2 \end{Bmatrix} \sum_{\bar{\Psi}} (-1)^{\bar{L}} \begin{Bmatrix} \ell & L & \bar{L} \\ L & \ell & 2 \end{Bmatrix}$$

$$\times (\psi \{| \bar{\Psi})^2 \; (\ell \,\|Q^*\|\, \ell),$$

where

$$(\ell \,\|\, Q^* \,\|\, \ell) = (-1)^{\ell} (2\ell+1) \begin{pmatrix} 3 & 2 & 3 \\ 0 & 0 & 0 \end{pmatrix}.$$

Evaluating this for the ground level with $J_z = J$, we have

$$(f^3\, {}^4I_{9/2}\; 9/2 \,\Big|\, \sum_i (3\cos^2\theta_i - 1) \,\Big|\, f^3\, {}^4I_{9/2}\; 9/2) \tag{71}$$

$$= -(260/3) \begin{pmatrix} 9/2 & 2 & 9/2 \\ -9/2 & 0 & 9/2 \end{pmatrix} \begin{Bmatrix} 6 & 9/2 & 3/2 \\ 9/2 & 6 & 2 \end{Bmatrix} \left[2 \begin{Bmatrix} 3 & 6 & 3 \\ 6 & 3 & 2 \end{Bmatrix} + 7 \begin{Bmatrix} 3 & 6 & 5 \\ 5 & 3 & 2 \end{Bmatrix} \right]$$

$$= -28/121 = -0.2314.$$

This result is in agreement with Hin Lew's calculation based on the single-particle wave functions, and that obtained using Nierenberg's derivation [Eq. (15)]. The evaluated n-j symbols are listed in the following Appendix.

B. Definitions of the n-j Symbols

The kets $\left|\, \gamma SLJJ_z\right)$ may be expanded in terms of kets $\left|\, \gamma SLS_zL_z\right)$:

$$\left|\, \gamma SLJJ_z\right) = \sum_i (SLJJ_z \left|\, SS_zLL_z\right)_i \left|\, SLS_zL_z\right)_i$$

The Wigner 3-j symbol is defined in terms of this vector coupling coefficient, $(SLJJ_z \left|\, SS_zLL_z\right)$, also known as the Clebsch-Gordan coefficient, by

$$\begin{pmatrix} S & L & J \\ S_z & L_z & J_z \end{pmatrix} = (-1)^{S-L-J_z} (2J+1)^{-1/2} \; (SLJ-J_z \left|\, SS_zLL_z\right).$$

An even permutation of the columns leaves the value of the symbol invariant. An odd permutation corresponds to multiplication by $(-1)^{S+L+J}$.

Another notation used by Condon and Shortley is

$$(SS_zLL_z \left|\, SLJJ_z\right) = (-1)^{-S+L-J_z} \begin{pmatrix} S & L & J \\ S_z & L_z & -J_z \end{pmatrix}.$$

The six-j symbol

$$\begin{Bmatrix} a & b & e \\ d & c & f \end{Bmatrix}$$

is the same as Racah's W-function except for a phase factor:

$$\begin{Bmatrix} a & b & e \\ d & c & f \end{Bmatrix} = (-1)^{a+b+c+d} W(abcd;ef)$$

The numerical evaluation of these symbols by Rotenberg et al, uses Racah's formula for W. The many symmetry properties of this symbol are also discussed in the book by Rotenberg et al.[27]

This symbol is invariant under interchange of columns. Moreover, it is also unchanged if any two numbers in a row are interchanged with those directly above or below it.

The triangular conditions on the 6-j symbol are denoted by [77]

$$\left\{\begin{matrix} x & x & x \\ x & x & x \end{matrix}\right\} \quad \left\{\begin{matrix} x & x & x \\ x & x & x \end{matrix}\right\} \quad \left\{\begin{matrix} x & x & x \\ x & x & x \end{matrix}\right\} \quad \left\{\begin{matrix} x & x & x \\ x & x & x \end{matrix}\right\} . \tag{72}$$

The 6-j symbol usually occurs in the coupling of three angular momenta. For example, one coupling scheme for the angular momenta $\underset{\sim}{j}_1$, $\underset{\sim}{j}_2$, and $\underset{\sim}{j}_3$ is

$$\underset{\sim}{j}_1 + \underset{\sim}{j}_2 = \underset{\sim}{j}_{12}, \quad \text{then } \underset{\sim}{j}_{12} + \underset{\sim}{j}_3 = \underset{\sim}{j}.$$

This is represented by the state $|(j_1 j_2)\, j_{12} j_3\, j)$.

Another coupling scheme results in a state $|(j_1 j_3) j_{13}\, j_2\, j)$, namely,

$$\underset{\sim}{j}_1 + \underset{\sim}{j}_3 = \underset{\sim}{j}_{13} \quad \text{then} \quad \underset{\sim}{j}_{13} + \underset{\sim}{j}_2 = \underset{\sim}{j} .$$

The vector coupling coefficient between the two states is

$$\left((j_1 j_2) j_{12},\, j_3\, j \;\middle|\; (j_1 j_3) j_{13},\, j_2\, j \right)$$

$$= (-1)^{j_1+j_2+j_3+j} \left[(2j_{12}+1)(2j_{13}+1)\right]^{1/2} \left\{\begin{matrix} j_2 & j_1 & j_{12} \\ j_3 & j & j_{13} \end{matrix}\right\} .$$

The 9-j symbol may be defined in terms of a sum over products of 6-j symbols.

$$\left\{\begin{matrix} a & b & c \\ d & e & f \\ g & h & i \end{matrix}\right\} = \sum_x (2x+1)(-1)^{2x} \left\{\begin{matrix} a & i & x \\ h & d & g \end{matrix}\right\} \left\{\begin{matrix} h & d & x \\ f & b & e \end{matrix}\right\} \left\{\begin{matrix} f & b & x \\ a & i & c \end{matrix}\right\} . \tag{73}$$

Fano's $\bar{X}$-function[78] is exactly the 9-j symbol, so that Eq. (73) equals $\bar{X}(abc;def;ghi)$.

The symmetry properties of this symbol are such that an even permutation of rows or columns leaves the value unchanged. An odd permutation introduces the phase $(-1)^A$, where A is the sum of all the entries in the symbol. A reflection about either diagonal also leaves the value unchanged.

C. Evaluationsof the n-j symbols Used in the Calculations[27]

$$\begin{Bmatrix} 3/2 & 6 & 9/2 \\ 6 & 3/2 & 1 \end{Bmatrix} = -1/2(7/130)^{1/2} \qquad \begin{Bmatrix} 3 & 6 & 5 \\ 6 & 3 & 1 \end{Bmatrix} = -1/7(2/13)^{1/2}$$

$$\begin{Bmatrix} 6 & 9/2 & 3/2 \\ 9/2 & 6 & 1 \end{Bmatrix} = -1/2(21/715)^{1/2} \qquad \begin{Bmatrix} 3/2 & 1/2 & 1 \\ 1/2 & 1/2 & 1 \end{Bmatrix} = -1/3$$

$$\begin{Bmatrix} 6 & 9/2 & 3/2 \\ 1 & 3/2 & 9/2 \end{Bmatrix} = 3/10(3/22)^{1/2} \qquad \begin{Bmatrix} 6 & 3 & 5 \\ 3 & 5 & 2 \end{Bmatrix} = -17/7(1/2145)^{1/2}$$

$$\begin{Bmatrix} 6 & 6 & 2 \\ 1 & 1 & 6 \end{Bmatrix} = 1/2(11/273)^{1/2} \qquad \begin{Bmatrix} 6 & 3 & 3 \\ 3 & 5 & 2 \end{Bmatrix} = -1/2(1/66)^{1/2}$$

$$\begin{Bmatrix} 1/2 & 3/2 & 1 \\ 3/2 & 1/2 & 1 \end{Bmatrix} = 1/6(5/2)^{1/2} \qquad \begin{Bmatrix} 6 & 6 & 2 \\ 9/2 & 9/2 & 3/2 \end{Bmatrix} = 1/11(21/26)^{1/2}$$

$$\begin{Bmatrix} 3 & 6 & 3 \\ 6 & 3 & 2 \end{Bmatrix} = 5/2(1/858)^{1/2} \qquad \begin{pmatrix} 3 & 2 & 3 \\ 0 & 0 & 0 \end{pmatrix} = 2(1/105)^{1/2}$$

$$\begin{Bmatrix} 3 & 6 & 5 \\ 6 & 3 & 2 \end{Bmatrix} = -1/7(2/429)^{1/2} \qquad \begin{pmatrix} 9/2 & 1 & 9/2 \\ -9/2 & 0 & 9/2 \end{pmatrix} = 3(1/110)^{1/2}$$

$$\begin{Bmatrix} 3 & 6 & 3 \\ 6 & 3 & 1 \end{Bmatrix} -1/2(1/26)^{1/2} \qquad \begin{pmatrix} 9/2 & 2 & 9/2 \\ -9/2 & 0 & 9/2 \end{pmatrix} = (3/55)^{1/2}$$

$$\begin{Bmatrix} 3/2 & 3/2 & 1 \\ 6 & 6 & 2 \\ 9/2 & 9/2 & 1 \end{Bmatrix} = 3/110(7/26)^{1/2}$$

$$\begin{Bmatrix} 3/2 & 1/2 & 1 \\ 6 & 5 & 2 \\ 9/2 & 9/2 & 1 \end{Bmatrix} = 3/220(7/5)^{1/2}$$

D. The Electromagnetic Fields at the Nucleus due to Two Equivalent Electrons

1. Magnetic Field

Judd[79] has given the matrix element of a general tensor product $X^K = T^{k_1} U^{k_2}$, where T^{k_1} and U^{k_2} are tensor operators that act on parts 1 and 2 alone, respectively. We use his formula to calculate the spin part of the magnetic field first.

$$(\ell^2 SLJJ \,|\, \sum_i (\underset{\sim}{s}\underset{\sim}{C}^2) \,|\, \ell^2 S'L'JJ) = (-1)^{J-J}\begin{pmatrix} J & 1 & J \\ -J & 0 & J \end{pmatrix} 2(3)^{1/2}(2J+1)$$

$$\times \begin{Bmatrix} S & S' & 1 \\ L & L' & 2 \\ J & J & 1 \end{Bmatrix} (\ell^2 S \| \underset{\sim}{s} \| \ell^2 S')\,(\ell^2 L \| \underset{\sim}{C}^2 \| \ell^2 L') \tag{74}$$

For two equivalent electrons, it is seen from Eqs. (35) and (36) in reference 25 that

$$(\ell^2 S \| \underset{\sim}{s} \| \ell^2 S') = (-1)^S \left[(2S+1)(2S'+1)\right]^{1/2} \begin{Bmatrix} S & 1 & S' \\ 1/2 & 1/2 & 1/2 \end{Bmatrix} (1/2 \| s \| 1/2) \tag{75}$$

and

$$(\ell^2 L \| \underset{\sim}{C}^2 \| \ell^2 L') = (-1)^{L'} \left[(2L+1)(2L'+1)\right]^{1/2} \begin{Bmatrix} L+2+L' \\ \ell \quad \ell \quad \ell \end{Bmatrix} (\ell \| C^2 \| \ell') \tag{76}$$

with

$$(\ell \| \underset{\sim}{C}^2 \| \ell') = (-1)^{\ell} \left[(2\ell+1)(2\ell'+1)\right]^{1/2} \begin{pmatrix} \ell & 2 & \ell' \\ 0 & 0 & 0 \end{pmatrix}$$

and

$$(1/2 \| \underset{\sim}{s} \| 1/2) = (3/2)^{1/2}$$

The matrix elements of the orbit part of N are

$$(\ell^2 SLJJ \left| \sum_i \underset{\sim}{\ell}_i \right| \ell^2 S'L'JJ) = \begin{pmatrix} J & 1 & J \\ -J & 0 & J \end{pmatrix} \delta(S,S') (-1)^{S+L'+J+1}$$

$$\times (2J+1) \begin{Bmatrix} J & 1 & J \\ L' & S & L \end{Bmatrix} (\ell^2 L \| \sum_i \underset{\sim}{\ell}_i \| \ell^2 L'). \qquad (77)$$

The last reduced matrix element is

$$(\ell^2 L \| \sum_i \underset{\sim}{\ell}_i \| \ell^2 L') = (-1)^{L'+1} \left[(2L+1)(2L'+1)\right]^{1/2} \begin{Bmatrix} L & 1 & L' \\ \ell & \ell & \ell \end{Bmatrix}$$

$$\times (\ell \| \underset{\sim}{\ell} \| \ell).$$

Therefore the total electronic matrix element of the magnetic field operator $\underset{\sim}{N}$ is obtained by combining Eqs. (74) and (77) to give

$$(\ell^2 SLJJ \left| \underset{\sim}{N} = \sum_i \underset{\sim}{\ell}_i - (10)^{1/2} (\underset{\sim}{s} \underset{\sim}{C}^2)_i \right| \ell^2 S'L'JJ). \qquad (78)$$

If the dipole constant a is measured in the level J, μ_I is given by

$$\mu_I = \frac{a(J)\, I\, J \left\langle r^3 \right\rangle}{2\mu_0 (\ell^2 aJJ \left| \underset{\sim}{N} \right| \ell^2 aJJ),} \qquad (79)$$

where the matrix element in Eq. (79) may include off-diagonal as well as diagonal terms calculated from Eq. (78). The other quantum numbers necessary to specify the state are denoted by a.

2. Matrix Elements of $2\,\Sigma(C_0^2)_i$

Appendix A shows how $3\cos^2\theta_i - 1$ is converted to the tensor-operator form $2(C_0^2)_i$. For the configuration, ℓ^2, the matrix element of this operator is

$$(\ell^2 SLJJ \left| 2 \sum_i (C_0^2)_i \right| \ell^2 S'L'JJ) = 2\delta(S,S')(-1)^{S+L+J}(2J+1)$$
$$\times \begin{Bmatrix} J & 2 & J \\ L' & S & L \end{Bmatrix} (\ell^2 L \left\| \Sigma (C_0^2)_i \right\| \ell^2 L'), \qquad (80)$$

where the last reduced matrix element is given by Eq. (76).

Therefore the quadrupole moment for this system is

$$Q = \frac{-b(J)\,\langle r^3 \rangle}{e^2(\ell^2\, aJJ \left| \sum_i 2(C_0^2)_i \right| \ell^2\, aJJ)}\,, \qquad (81)$$

where the matrix element in Eq. (81) is calculated from Eq. (80) for the electronic eigenfunction, which may include higher levels perturbing the ground level.

E. Analytic Radial Wave Functions.

For numerical calculations it is very convenient to have an approximate analytic expression for the wave functions obtained by the SCF method. This also makes it possible to interpolate between such functions. A suitable form is the Slater-Löwdin approximation,[80] which for functions of the 4f type (single maximum) is

$$R(r) = r^n (c_1 e^{-a_1 r} + c_2 e^{-a_2 r} + c_3 e^{-a_3 r} + \cdots).$$

With three terms in this expansion, the agreement with the original wave function is extremely good. For our purpose, however, we prefer to use a two-parameter function and choose the symmetric form

$$R(r) = N\, r^n\, e^{-ar} \cosh \kappa\,(ar-n) = \frac{1}{2}\, Nr^n \left[e^{-\kappa n} e^{-a(1-\kappa)r} + e^{n} e^{-a(1+\kappa)r} \right] . \tag{82}$$

For this function, the position of the maximum depends only on a, and the other parameter, κ essentially determines the shape. A function of this type fitted to the SCF wave function for Tm^{+3} is shown in Fig. 51. Similarly, Fig. 52 shows the function for Pr^{+3}. One could easily determine both parameters in Eq. (82) by interpolation or extrapolation from existing SCF calculations, but we believe that more reliable wave functions are obtained if one of the parameters is determined from the experimental spin-orbit coupling constant. Since the shape of the wave function changes very little from element to element, we have determined κ by comparison with SCF wave functions and a from the spin-orbit coupling constant. In the latter case we have used the Thomas-Fermi potential, which is accurate enough for this purpose. This potential is particularly close to SCF potentials near the nucleus, where the main contribution to the spin-orbit coupling originates (see Fig. 53).

No SCF calculations are available for any rare earth atoms but some have recently been carried out for Pr^{+3} and Tm^{+3} ions. The difference in shape between the 4f wave functions for these ions is very small, and both correspond to a κ value slightly greater than 0.4. Since one would not expect the shape to differ much between the ions and the atoms, this should be a reasonable value also for the atoms. This is in agreement with the value obtained by extrapolation from heavier atoms like W and Hg. Figure 54 shows the radial wave functions for these isotopes.

For the wave function (82) the following formulae are easily verified (subscript hy indicates hydrogenic value):

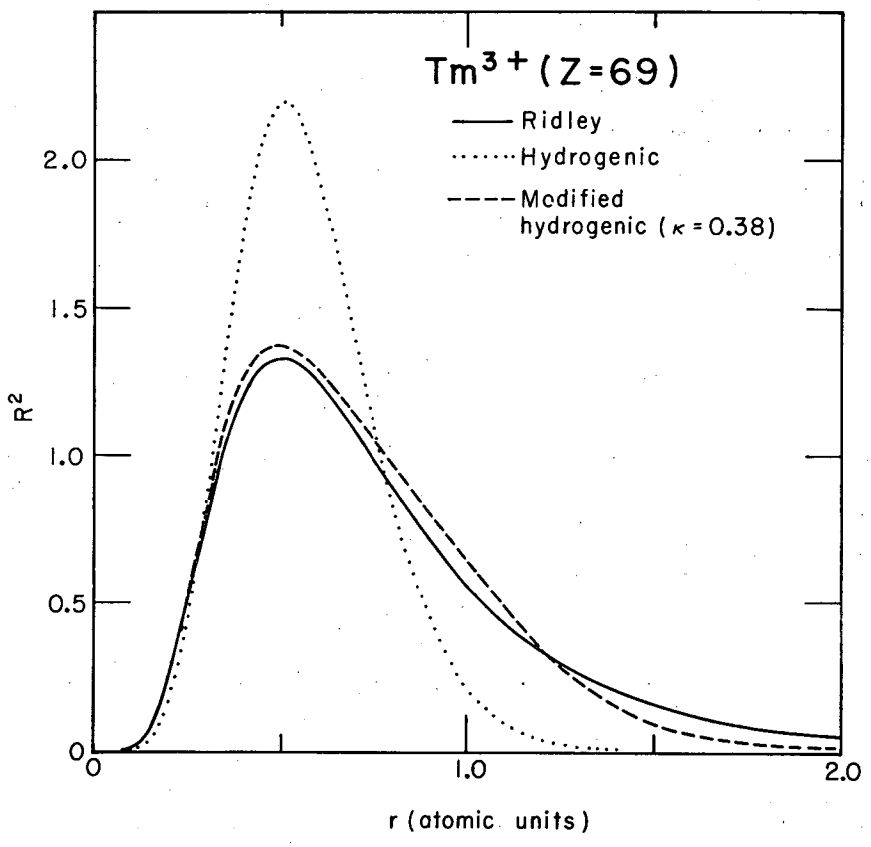

Fig. 51. Radial wave functions for Tm^{+3}.

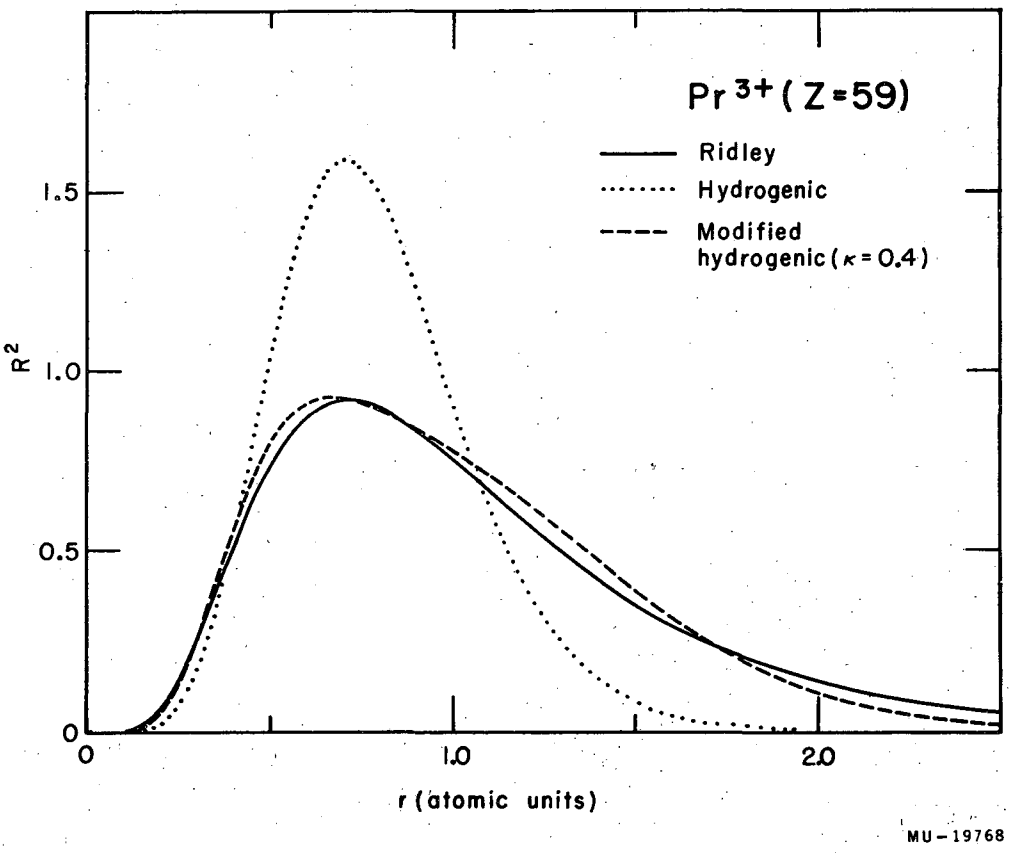

Fig. 52. Radial wave functions for Pr^{+3}.

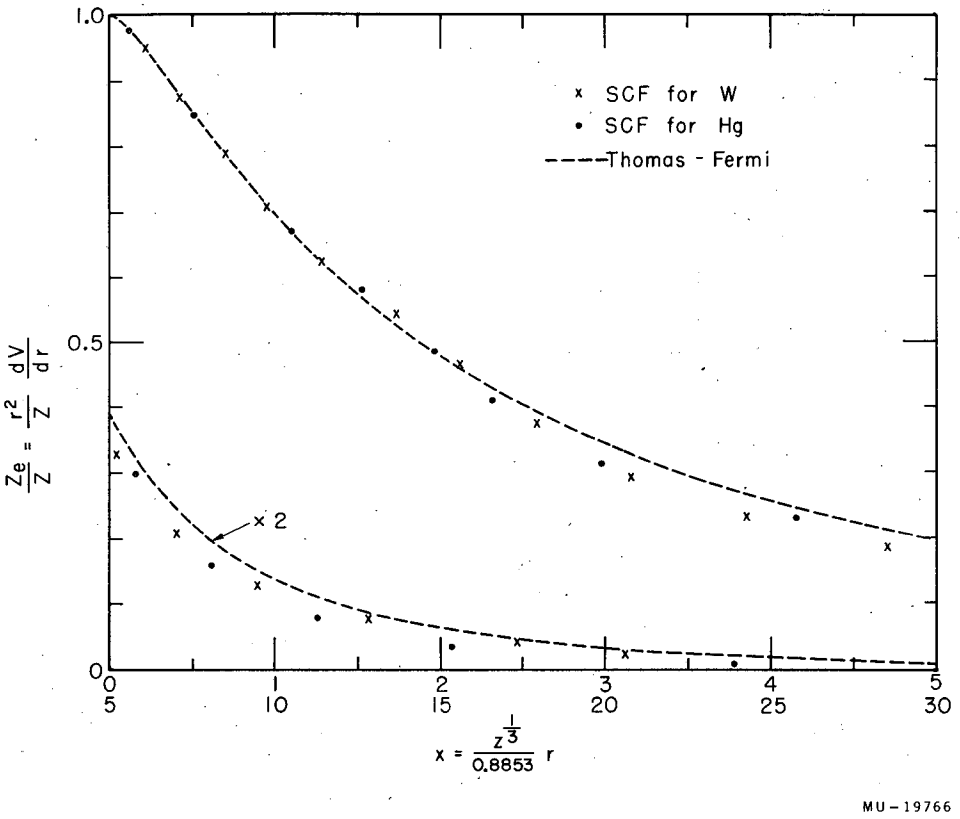

Fig. 53. Comparison between r^2 dV/dr from Thomas-Fermi and from self-consitent fields.

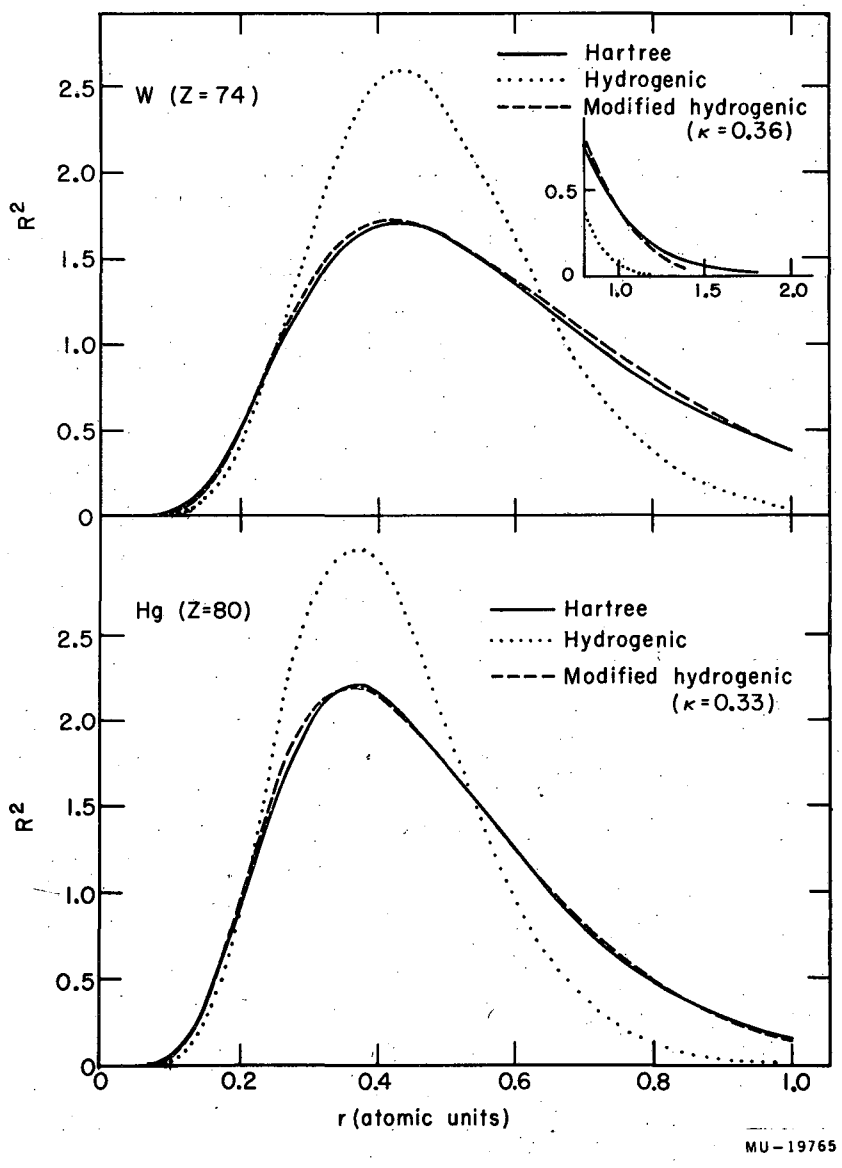

Fig. 54. Radial wave functions for tungsten and mercury.

$$N^2 = \frac{(2a)^{2n+1}}{(2n)!} \frac{1}{C_{2n+1}} = \frac{N_{hy}^2}{C_{2n+1}} \quad ,$$

$$\left\langle r^{-m} \right\rangle = \frac{(2a)^m (2n-m)!}{(2n)!} \frac{C_{2n+1-m}}{C_{2n+1}} = \left\langle r^{-m} \right\rangle_{hy} \frac{C_{2n+1-m}}{C_{2n+1}} \quad ,$$

$$\left\langle T \right\rangle = 1/2 \left[n(n-1) \left\langle r^{-2} \right\rangle - \left\langle \frac{1}{R} \frac{d^2R}{dr^2} \right\rangle \right] = 1/2\, a^2 \left[1 - \kappa^2 - 2\kappa \frac{D_{2n}}{C_{2n+1}} \right] ,$$

where

$$C_s = \frac{1}{4} \left[e^{-2n\kappa} (1-\kappa)^{-s} + 2 + e^{2n\kappa} (1+\kappa)^{-s} \right]$$

and

$$D_s = \frac{1}{4} \left[e^{-2n\kappa} (1-\kappa)^{-s} - e^{2n\kappa} (1+\kappa)^{-s} \right] .$$

REFERENCES

1. A. Cabezas, E. Lipworth, R. Marrus, and J. Winocur, Phys. Rev. 118, 233 (1960).
2. A. Cabezas and I. Lindgren, Atomic Beam Study of the Hyperfine Structure of Thulium-170, UCRL-9163, (to be published) May 9, 1960.
3. R. Marrus, A. Cabezas, E. Lipworth, and J. Winocur, Bull. Am. Phys. Soc. II, 4, 251 (1959).
4. A. Cabezas, E. Lipworth, R. Marrus, and J. Winocur, Bull. Am. Phys. Soc. II, 4, 354 (1959).
5. I. Lindgren, A. Cabezas, and W. A. Nierenberg, Bull. Am. Phys. Soc. II, 5, 273 (1960).
6. A. Cabezas, I. Lindgren, R. Marrus, and W. A. Nierenberg, Atomic Beam Investigations of Electronic and Nuclear Ground States in the Rare Earth Region, UCRL-9225, 1960.
7. A. Cabezas, I. Lindgren, and R. Marrus, Bull. Am. Phys. Soc. II, 5, 343 (1960).
8. A. Cabezas, I. Lindgren, R. Marrus, and W. A. Nierenberg, Hyperfine Structure of Praseodymium-142, UCRL-9224, 1960.
9. A. Cabezas, I. Lindgren, E. Lipworth, R. Marrus, and M. Rubinstein, Nuclear Spins of Neodymium-147 and Promethium-147, UCRL-9122, March 16, 1960.
10. L. S. Goodman, W. C. Childs, R. Marrus, I. Lindgren, and A. Cabezas, Bull. Am. Phys. Soc. II, 5, 344 (1960).
11. E. U. Condon and H. G. Shortley, Theory of Atomic Spectra (Cambridge University Press, Cambridge, England 1935).
12. N. F. Ramsey, Molecular Beams Clarendon Press, (Oxford, England, 1956).
13. O. Stern and W. Gerlach, Ann. Physik, 74, 673 (1924).
14. G. Racah, Phys. Rev. 62, 438 (1942).
15. C. Schwartz, Phys. Rev. 97, 380 (1955).

16. J. Winocur, Some Nuclear and Electronic Ground-State Properties of Pa^{233}, Am^{241}, and 16-hr Am^{242} (Thesis), UCRL-9174, April, 1960.

17. J. M. Blatt and V. F. Weisskopf, Theoretical Nuclear Physics (John Wiley and Sons, Inc., New York, 1952).

18. E. Fermi, Z. Physik 60, 320 (1930).

19. L. Davis, B. T. Feld, C. W. Zabel, and J. R. Zacharias, Phys. Rev. 76, 1076 (1949).

20. H. Kopfermann, Nuclear Moments, E. E. Schneider, Trans. (Academic Press, New York, 1958).

21. F. Hund, Linienspektren und periodisches System (Springer-Verlag, Berlin, 1927), p. 124.

22. G. O. Brink, J. C. Hubbs, W. A. Nierenberg, and J. L. Worcester, Phys. Rev. 107, 189 (1957).

23. H. B. G. Casimir, On the Interaction Between Atomic Nuclei and Electrons (Teyler's Tweede Genootschap, Haarlem, 1936).

24. W. A. Nierenberg, University of California, private communication.

25. B. R. Judd, Berkeley Notes (unpublished), University of California, 1960.

26. R. E. Trees, Phys. Rev. 92, 308 (1953).

27. M. Rotenberg, R. Bivins, N. Metropolis, and J. Wooten Jr., The 3-j and 6-j Symbols (The Technology Press, Massachusetts Institute of Technology, Cambridge Mass., 1959).

28. J. R. Zacharias, Phys. Rev. 61, 270 (1942).

29. G. O. Brink, Nuclear Spins of Thallium-197, Thallium-198m, Thallium-199, and Thallium-204 (Thesis), UCRL-3642, June 1957.

30. R. Marrus, Hyperfine-Structure Measurements on Some Transuranic Elements (Thesis), UCRL-8547, Nov. 1958.

31. A. V. Pohm, W. E. Lewis, J. H. Talboy Jr., and E. N. Jensen, Phys. Rev. 95, 1523 (1954).

32. M. A. Grace, C. E. Johnson, R. G. Scurlock, and R. T. Taylor, Phil. Mag. 3, 456 (1958).

33. M. G. Mayer and J. H. D. Jensen, Elementary Theory of Nuclear Shell Structure (John Wiley and Sons, Inc., New York, 1955).
34. P. F. A. Klinkenberg, Revs. Modern Phys. 24, 63 (1952).
35. R. Marrus, W. A. Nierenberg, and J. Winocur, Hyperfine Structure of Americium-241, UCRL-9207, May 1960.
36. I. Lindgren, Relativistic and Diamagnetic Corrections of Atomic g Values, UCRL-9184, May 9, 1960.
37. B. R. Judd and I. Lindgren, Theory of Zeeman Effect in the Rare-Earth Region, UCRL-9188, May 9, 1960.
38. Hin Lew, Phys. Rev. 91, 619 (1953).
39. R. Sternheimer, Phys. Rev. 86, 316 (1952); Phys. Rev. 95, 736 (1954).
40. R. J. Blin-Stoyle, Revs. Modern Phys. 28, 75 (1956).
41. R. W. Kedzie, M. Abraham, and C. D. Jeffries, Phys. Rev. 108, 54 (1957).
42. B. R. Judd, Proc. Roy. Soc. A 251, 127 (1959).
43. T. D. Lee and C. N. Yang, Phys. Rev. 104, 254 (1956).
44. C. S. Wu, E. Ambler, R. W. Hayward, D. D. Hoppes, and R. P. Hudson, Phys. Rev. 105, 1413 (1957).
45. B. R. Judd, Proc. Roy. Soc. (London) A 250, 562 (1959).
46. W. E. Albertson, Phys. Rev. 47, 370 (1935).
47. W. C. Rutledge, J. M. Cork, and S. B. Burson, Phys. Rev. 86, 775 (1952); P. R. Evans, Phil. Mag. 3, 1061 (1958); A. C. G. Mitchell, C. B. Creager, and C. W. Kocker, Phys. Rev. 111, 1343 (1958).
48. M. G. Mayer, S. A. Moszkowski, and L. W. Nordheim, Revs. Modern Phys. 23, 315 (1951).
49. K. F. Smith and I. Spalding, Cambridge University (private cummunication).
50. Ph. Schummans, Physica 11, 419 (1946).
51. B. R. Judd, Lawrence Radiation Laboratory (private communication).
52. J. E. Mack, Revs. Modern Phys. 22, 64 (1950).

53. B. Bleaney and W. Low, Proc. Phys. Soc. (London) 68 A, 55 (1955).

54. H. N. Russell, J. Opt. Soc. Am. 40, 550 (1950).

55. S. Penselin and K. Schlüpmann, University of Heidelberg (private communication).

56. W. C. Jordan, J. M. Cork, and S. B. Burson, Phys. Rev. 92, 1218 (1953).

57. V. S. Dubey, C. E. Mandeville, and M. A. Rothman, Phys. Rev. 103, 1430 (1956).

58. E. U. Condon and H. G. Shortley, Phys. Rev. 37, 1025 (1931).

59. G. Racah, Physica 16, 655 (1950).

60. H. N. Russell and W. F. Meggers, Bur. Standards, J. Research 9, 625, R. P. 497 (1932).

61. S. Singer, Lawrence Radiation Laboratory, (private communication).

62. W. F. Meggers, Revs. Modern Phys. 14, 96 (1942).

63. E. C. Ridley, Proc. Cambridge Phil. Soc. 56, 41 (1960).

64. K. H. Lindenberger, Z. Physik 141, 476 (1955).

65. G. Breit, Nature 122, 649 (1928).

66. H. Margenau, Phys. Rev. 57, 383 (1940).

67. A. Abragam and J. H. Van Vleck, Phys. Rev. 92, 1448 (1953). More general treatments are given by K. Kembe and J. H. Van Vleck, Phys. Rev. 96, 66 (1954) and F. R. Innes and C. W. Ufford, Phys. Rev. 111, 194 (1958).

68. N. Marty, Compt. rend. 241, 385 (1955).

69. C. E. Johnson, J. F. Schooley, and D. A. Shirley, Nuclear Orientation of Tb^{160}, UCRL-9267, June 15, 1960.

70. A. W. Sunyar, Phys. Rev. 93, 1345 (1954).

71. E. N. Hatch and F. Boehm, Bull. Am. Phys. Soc., Ser. II, 1, 390 (1956).

72. F. P. Cranston, M. E. Bunker, J. P. Mize, and J. W. Starner, Bull. Am. Phys. Soc., Ser. II, 1, 389 (1956).

73. R. L. Graham, J. L. Wolfson, and R. E. Bell, Can. J. Phys. 30, 459 (1952).

74. W. G. Smith, R. L. Robinson, J. H. Hamilton, and L. M. Langer, Phys. Rev. 107, 1314 (1957).

75. S. G. Nilsson, Klg. Danske Videnskab. Selskab. Mat.-fys. Medd. 29, No. 16 (1955); A. Bohr, Phys. Rev. 81, 134 (1951); A. Bohr, Klg. Danske Videnskab. Selskab. Mat.-fys. Medd. 26, No. 14 (1952); A. Bohr and B. R. Mottelson, Klg. Danske Videnskab. Selskab. Mat.-fys. Medd. 27, No. 16 (1953); D. L. Hill and J. H. Wheeler, Phys. Rev. 89, 1102 (1953); and K. W. Ford, Phys. Rev. 90, 1929 (1953).

76. C. J. Gallagher, Jr., and S. A. Moszkowski, Phys. Rev. 111, 1282 (1958).

77. A. R. Edmonds, Angular Momenta in Quantum Mechanics, (Princeton University Press, Princeton, N. J., 1957).

78. U. Fano, National Bureau of Standards Report 1214 (unpublished), Washington, D. C. (1951).

79. B. R. Judd, Berkeley Notes, (unpublished) University of California, 1960, p. 22.

80. J. C. Slater, Phys. Rev. 42, 33 (1932); P. O. Löwdin, Phys. Rev. 90, 120 (1953).